Beitr. Paläont., **31**:299–343, Wien 2009

The Late Miocene Mammal Faunas of the Mytilinii Basin, Samos Island, Greece: New Collection

13. Giraffidae

by

Dimitris S. Kostopoulos*)

Kostopoulos, D.S., 2009. The Late Miocene Mammal Faunas of the Mytilinii Basin, Samos Island, Greece: New Collection. 13. Giraffidae. — Beitr. Paläont., **31**:299–343, Wien.

Abstract

The study copes with the systematic review of the giraffid assemblage(s) from the late Miocene fossil sites of Samos Island (Greece). Newly discovered and old material from several collections across the world is described and compared. The data analysis allows recognizing *Palaeotragus rouenii*, *Palaeotragus quadricornis*, *Samotherium boissieri*, *Samotherium major* and *Helladotherium duvernoyi*. Discussion on long-lasting taxonomic and phylogenetic questions implies that *P. quadricornis* remains as a distinct species, as well as upholding the ancestor-descendant relationships between the sexually bimodal *S. boissieri* and *S. major*, following phyletic growth procedures. The chronostratigraphic occurrence of the Samos giraffids is updated and their significance for the biochronology and palaeogeography of the SE European region is restored.

Keywords: Late Miocene, Samos, Greece, Mammalia, Giraffidae, Systematics.

Zusammenfassung

Die Studie beschäftigt sich mit einer systematischen Revision der Giraffiden-Vergesellschaftung der miozänen Fundstellen der Insel Samos (Griechenland). Neu entdecktes Material, wie auch Funde aus älteren Aufsammlungen, die über die ganze Welt verteilt sind, werden beschrieben und verglichen. Die Analyse erlaubt eine Bestimmung von: *Palaeotragus rouenii*, *Palaeotragus quadricornis*, *Samotherium boissieri*, *Samotherium major* und *Helladotherium duvernoyi*. Die Diskussionen über taxonomische und phylogenetische Fragen, machen das Beibehalten von *P. quadricornis* als eigene Art notwendig, und nach dem Wachstumsmuster nimmt sie eine Mittelstellung zwischen den sexuell bimodalen *S. boissieri* und *S. major* ein. Das chronostratigraphische Vorkommen der Samos Giraffiden wird neu aufgenommen und ihre Bedeutung für die Biochronologie und Palaeogeographie Südosteuropas wird diskutiert.

Schlüsselworte: Obermiozän, Samos, Griechenland, Mammalia, Giraffidae, Systematik.

1. Introduction

One hundred and twenty years after the expatriate English botanist Forsyth-Major (1888) announced the famous Late Miocene mammal fauna of Samos (Greece) and its poster child *Samotherium*, considerable giraffid material from numerous fossil sites on the island is still waiting for publication, being housed at several Natural History Museums and institutions across the world. Indeed, giraffids appear to be one of the less studied mammal groups of the Samos fauna, even though one of the best represented. Paradoxically, most of the available information on the Samos giraffid assemblage(s) comes from indirect sources, mainly comparisons and discussions on material from other Eurasian and African Neogene sites (e.g. Bohlin, 1926; Borissiak, 1914; Churcher, 1970; de Mequenem, 1924; Geraads, 1974, 1978, 1979, 1994; Godina, 2002; Hamilton, 1978; Kostopoulos & Saraç, 2005; Kostopoulos & Koufos, 2006; Lydekker, 1890; Ozansoy, 1965; Pilgrim, 1911; Senyürek, 1954). Worse yet, the old Samos collections suffer from absence of stratigraphic credibility, allowing mixing of the material and long-lasting taxonomic confusion. As a consequence, little is really known about the original chronological distribution of Samos giraffids and much less about their taxonomic and intraspecific variability (Table 1).

The 1994-2006 paleontological expedition of the Aristotle University of Thessaloniki on Samos Island (Koufos et al., 1997), brought to light important new and well-stratified

*) Dr. Dimitris S. Kostopoulos, Aristotle University of Thessaloniki, Department of Geology, Laboratory of Geology and Palaeontology, GR-54124 Thessaloniki, Greece. e-mail: dkostop@geo.auth.gr

Table 1: The giraffid assemblage(s) from Samos according to several authors.

Qx, Q1-6: Barnum Brown's sites; S: Stefano of Forsyth-Major; A: Adriano of Forsyth-Major; S2,3: Solounias (1981) sites; OMB: Old Mill Beds, WB: White Beds, MBB: Main Bone Beds of Weidmann et al. (1984).

Author	Bohlin, 1926	Geraads, 1976	Solounias, 1981										Bernor et al., 1996		
Site/species			**Qx**	**Q4**	**S**	**Q2**	**S2**	**S3**	**Q5**	**A**	**Q1**	**Q6**	**OMB**	**WB**	**MBB**
Palaeotragus rouenii	+	+	+		+					+	+				+
Palaeotragus coelophrys					+		+			+	+			+	
Palaeotragus quadricornis	+													?	
Samotherium boissieri	+	+		+		+	+	+	+	+	+	+	+		
Samotherium major	+														
Samotherium sp.														+	+
Helladotherium duvernoyi	+									+	+				+
Helladotherium sp.		+													?
Bohlinia speciosa															?
Bohlinia attica														?	

giraffid material, leading to a fresh and certainly more accurate overview. Giraffid remains have been collected from nearly all new sites and especially Mytilinii-4 (MLN), Mytilinii-1A (MTLA) and Mytilinii-1B (MTLB), the first from the south slopes of Potamies stream and the last two from Adrianos ravine (for local stratigraphy and fossil-site location see Solounias, 1981; Kostopoulos et al., 2003; Kostopoulos et al., this volume). A few additional specimens previously collected (1963, 1983) from Adrianos ravine by professor J. Melentis (Melentis, 1969a) and labeled PMMS have also been included in this study. Both collections are stored at the Aegean Museum of Natural History, Zimalis Foundation (NHMA), on Samos. The description of the new material would, however, be meaningless without reference to the old one. Thus, the present analysis involves unpublished giraffid remains from the American Museum of Natural History (AMHN, B. Brown's collection), and the Natural History Museum of Paris (MNHNP, Braillon collection) and reviews of the Samos giraffid-collections at the Natural History Museum of London (NHML, Forsyth-Major collection), the Paleontological Institute of Münster (PIM), the Natural History Museum of Vienna (NHMW), the Department of Geology of the Lausanne University (MGL) and the Natural History Museum of Basel (NHMB). Some more specimens mentioned by Bohlin (1926) from the Bayrische Staatssammlung für Paläontologie und historische Geologie-München (BSPM), the Senckenbergisches Naturhistorisches Museum-Frankfurt (SMF), and the Staatliches Museum für Naturkunde-Stuttgart (SMNS) are also described and discussed.

The study tries to synthesize the available and dispersed data concerning Samos giraffids, giving special attention to unresolved taxonomic and phylogenetic questions as well as on their chronostratigraphic significance.

Abbreviations:

LGPUT: Laboratory of Geology & Paleontology of Thessaloniki University; nn: absence of catalogue number; nl: absence of locality indication; TD: transverse diameter; APD: anteroposterior diameter; L: length; W: width; H: height; b: base; prox: proximal; dia: diaphysis dis: distal; art: articular; st: sustentaculum tali; tro: trochlea; max: maximum; min: minimum; lat: lateral; med: medial. Capital letters (P, M, D) on tooth specimens represent upper toothrow samples and lower case letters (p, m, d) lower toothrow samples (premolars, molars and milk teeth respectively). All measurements are given in millimeters (mm). Frontal appendages of late Miocene giraffids are called „ossicones" even though their origin is still debatable.

2. Systematic Paleontology

Palaeotragini Pilgrim, 1911

Genus *Palaeotragus* Gaudry, 1861

***Palaeotragus rouenii* Gaudry, 1861**
(Plate 1, Tables 1-5)

Localities & Ages:

Mytilinii-4 (MLN), Potamies ravine; late early Turolian (MN11), 7.6-7.4 My

Mytilinii-1A, 1B (MTLA, MTLB), Adrianos ravine; middle Turolian (MN12), 7.1-7.0 My

Quarry 2 (Q2), Potamies ravine; late early Turolian (MN11), 7.6-7.4 My

Quarry A (Qa), Adrianos ravine; middle Turolian (MN12), 7.1-7.0 My

Quarry 1 (Q1), Adrianos ravine; middle Turolian (MN12), 7.1-7.0 My

Quarry 5 (Q5), Limitzis; early late Turolian (MN13), 6.9-6.7 My

MGLS-Stefano, Stefana hill, late early Turolian (MN11), 7.6-7.4 My

MGLS-Adriano, Adrianos ravine, middle Turolian (MN12), 7.1-7.0 My

The material from the NHMW, SMF, SMNS has no locality indication.

Material:
NHMA: MLN86, part of m3 sin; MLN48, proximal radius; MLN75, proximal metatarsal plus scaphocuboid; MLN74, part of astragalus; MLN71, part of calcaneum. MTLA261, right ossicone; MTLA157, distal humerus; MTLA197 proximal metacarpal; MTLA452, distal femur; MTLA246, metatarsal.
MTLB52, left D3-M1; MTLB170, right D3-M1; MTLB128, left P2-M3; MTLB160a, right P2-M3; MTLB226 part of left mandible with p2-m3; MTLB165, scapula; MTLB156, radius; MTLB155, metacarpal.

AMNH: AMNH22813, left m1-m3, Q2
AMNHN86588, right D2-M1, Qa (=Q1); AMNH nn-Box35, D2-D4 Q1,
AMNH86507, right D2-M1, nl;
AMNH86584, left D2-D4 (M1), Q5; AMNH20574, left M1-M3, Q5; AMNH86520, left d3-m2, Q5; AMNH22944, right p2-m3, Q5; AMNH86373, left p3-m3, Q5;

MGL (all postcranials without indication are coming from the Stefano site):
MGL S1237, M3, nl; MGL S279, right p4-m3, Andriano; MGL S1214, distal humerus; MGL S790, S910, radius; MGL S781 metacarpal; MGL S858, proximal metacarpal; MGL S778, distal tibia Andriano; MGL S682 distal tibia; MGL S492, astragalus; MGL S1067, proximal metatarsal; MGL S1110, MGL S1111 first phalanx.

NHMW: A476, skull; 1911-Samos-V76, left P2-M3; nn-radius (from Geraads, 1994)

SMF: part of female skull with no further indication (Bohlin, 1926:pl. IV, figs. 11, 12).

SMNS: SMNS44240 part of female skull.

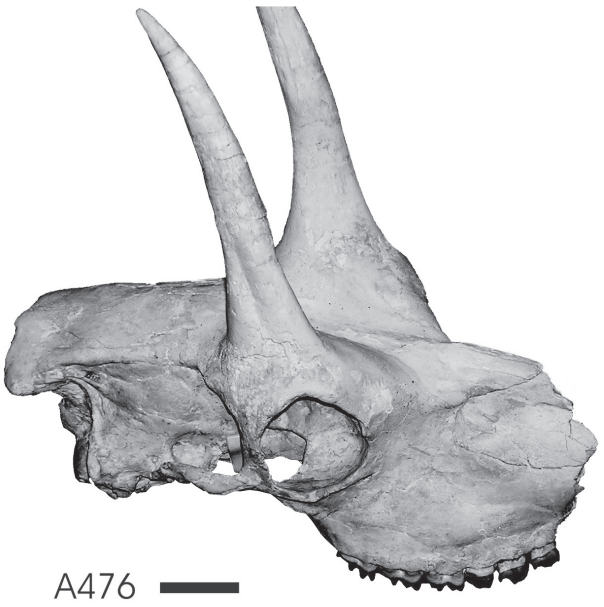

Figure 1: *Palaeotragus rouenii*, cranium NHMW A476, dorsolateral view. Scale-bar 4 cm.

Measurements	NHMW A476	MNHNP PIK1670
Length from the midpoint above anterior margin of the orbits to the nuchal crest	201	215
Anteroposterior diameter of orbit	55	52
Supraorbital width	102	106
P2-M3	115	120.6
APD at ossicone's base	44	41*

Table 2: Metrical comparison between the *P. rouenii* crania NHMW A476 from Samos and MNHNP PIK1670 from Pikermi. *: MNHNP PIK1680 according to Geraads (1974).

Description:
The new Samos expedition did not provide any new cranial material of *P. rouenii*. Thus, the only cranial specimens from Samos known so far are still the skull-fragment stored in SMF (Frankfurt) and figured by Bohlin (1926: pl. IV, figs. 11, 12), the almost complete skull NHMW A476 in Vienna and the female skull SMNS44240 in Stuttgart. The SMF specimen preserves only a part of the face and the palate with both toothrows extensively worn. The anterior margin of the orbit is placed above M3. The lachrymal fossa is shallow and wide, limited ventrally by a well developed facial tuber which is replaced anteriorly by a blunt crest that rises above the infraorbital foramen. The latter opens in front of P2. A thin elongated ethmoidal fissure is present above the premolars. The premolar/molar ratio is 81 with P2-M3 length of 104 mm (according to Bohlin, 1926). Both the Frankfurt skull and SMNS44240 appear to be 'hornless', indicating female individuals. The much more well-preserved skull specimen NHMW A476 belongs to a mature male (Fig. 1, Table 2). Judging from dental measurements it appears to be 10% larger than the Frankfurt cranium. The anterior margin of the orbit is placed above the middle of M3. The ossicones are inserted on the lateral edges of the posterior part of the orbital roof, leaving a wide and weakly concave frontal area in between them. Pneumatization seems to be well expressed in the supraorbital area. The face is high with a well developed facial tuber and a wide, moderately shallow lachrymal fossa. The basicranial angle is low (~20°). The frontoparietal region is flat, limited laterally by rather strong parietal crests that run parallel to each other. The nuchal crest is also strong and projects horizontally to the rear, but this might have partly been the result of dorsoventral deformation. In lateral view, the occipital condyles are directed downwards. The ossicones are moderately long, weakly curved posteriorly and strongly compressed mediolaterally. The premolar/molar ratio is about 71 with P2-M3 length of 115 mm.
The ossicone MTLA261 (Pl. 1, fig. 6) is about 170 mm long. It curves weakly posteriorly and it is slightly mediolaterally compressed in its basal part (TDb=42.5mm; APD=51.5mm). The cross-section is spindle-shaped at the base and becomes almost rounded towards the tip. A rubbing surface is present on the posterior face of the apex. Dental material of *P. rouenii* is known from MLN and

Table 3: Upper and lower toothrow measuremens and proportions of *Palaeotragus* from Samos.

*: data from Bohlin (1926).

P. rouenii	L P2-M3	L P2-P4	L M1-M3	Index P/M
SMF skull *	104.0	47.0	58.0	81.0
NHMW A476	115.0	48.0	67.0	71.6
MTLB160a	115.1	50.3	67.1	75.0
MTLA128	120.2	51.4	68.3	75.3
AMNH20574			67.6	
NHMW1911 v76	109.8	50.7	63.3	80.1
P. quadricornis *	155.0	67.0	91.0	73.6
P. quadricornis b*	132.0	61.0	74.0	82.4
Palaeotragus **sp.** MTLA374			77.6	
P. rouenii	L p2-m3	L p2-p4	L m1-m3	Index p/m
MGL S279			82.7	
MTLB226	133.0	51.7	79.0	65.4
AMNH22944 Q5	124.6	49.5	73.6	67.3
AMNH86373 Q5			71.7	
AMNH22813 Q2			79.2	
Palaeotragus **sp.** PIM 293			[90]	

MTLB, whereas the old collections at the NHMW and AMNH offer some additional samples. The length of the upper milk toothrow (D2-D4) ranges from 57.2 to 58.6 mm. The styles become bulbous toward the crown's base. D2 is elongated and trapezoidal-shaped with a weakly divided lingual wall (Pl. 1, fig. 3). The parastyle is strong but less so than the paracone, which has a flat posterior flange and is obliquely placed, merging at its base with the parastyle. The metastyle is weak, but in most cases it is associated with a strong basal cingulum which prolongs anteriorly onto the crown's base and forms an additional more (AMNH86507) or less (AMNH86588) developed labial style (Pl. 1, fig. 3). The anterior lobe of D3 is not fully molariform and rather trapezoidal-shaped (Pl. 1, fig. 3). The parastyle is stronger than the mesostyle; the paracone is much heavier than the metacone. The posterior flange of the protocone and the anterior flange of the hypocone merge slowly with wear. The D4 is fully molariform and, similarly to D3, it has a strong paracone and parastyle and well developed mesostyle. The protocone is angular lingually and its posterior flange slightly curves to the front. A feeble hypoconal spur is present in most specimens and in two out of four D4 a lingual cingulum develops between the lobes. In the specimens MTLB128, MTLB160 and NHMW 1911-Samos-V76 preserving the entire P2-M3 series (Table 3), the premolars represent 75.3%, 74.9% and 80.1% of the molars respectively. P2 is sub-squarish with a strong parastyle and paracone that fuse together at the base (Pl. 1, fig. 4). A well developed enamel fold can occur on the posterior part of the central cavity (MTLB128, NHMW-1911-V76; Pl. 1, fig. 4). The metastyle varies considerably from strong (MTLB160, NHMW-1911-V76) to almost absent (MTLB128). On the lingual wall the protocone and the hypocone are barely distinguished by a shallow groove. P3 is very similar to P2 but more rounded lingually. P4 is also similar to them but the paracone is placed more centrally on the labial wall and the enamel fold on the central cavity is significantly reduced. The M1 and M2 have a more developed metastyle than the D4, their mesostyle is stronger than the parastyle and points to the front, and an additional protoconal fold might occur at first stages of wear (MTLB170, MTLB52). The most anterior point of both the protocone and the hypocone points in anterior direction and is constricted (Pl. 1, fig. 4). M3 is smaller than M2, with a vertically oriented mesostyle and a strong metastyle that is directed labially. There is no available lower milk dentition in the new collection.

Scapula	**Lmax**	**TDart**	**APDart**	
MTLB165	410.0	107.4	76.5	
Humerus	**TDdia**	**TDdis**	**Hkeel**	
MTLA157	40.3	77.5	45.2	
MGL S1214		79.0		
Radius	**L**	**TDprox**	**TDdia**	**TDdis**
MLN48		79.7	52.5	
MTLB156	520.0	77.5	49.7	67.1
NHMWnn	480.0	74.0	48.0	
MGL S790	465.0	81.7	42.6	74.0
MGL S910	470.0	85.0	43.0	70.0
NHML M4313	370.5	82.6	40.1	75.0
MLN44	473.0	85.0	55.7	
Femur	**TDtro**	**Ltro**	**TDbi-condyle**	
MTLA452	38.4	78.0	74.0	
Tibia	**TDdis**	**APDdis**		
MGL S778 Andriano	64.5	52.0		
MGL S682	[60]	55.0		
Scaphocuboideum	**TDmax**	**APD max**		
MNL75	54.4	64.2		
Calcaneum	**Hmax**	**Hmin**	**TDst**	**APDst**
MLN71		74.0	41.9	61.9
Astragalus	**Llat**	**Lmed**	**TDdis**	
MLN74	76.6		47.2	
MGL S492	73.5	65.0	47.0	

Table 4: Post-cranial measurements of *Palaeotragus rouenii* and *Palaeotragus* sp. (NHML M4313, MNL44) from Samos.

Metacarpal	L	TDprox	APDprox	TDdia	APDdia	TDdis	APDdis
MTLA197		62.3	42.1				
MTLB155	434.0	60.6	43.3	38.3	35.7	61.6	39.4
MGL S781	410.0	63.2	45.1	37.4	39.4	61.2	39.2
MGL S858		56.0	42.8				
Metatarsal	**L**	**TDprox**	**APDprox**	**TDdia**	**APDdia**	**TDdis**	**APDdis**
MLN75		54.3	57.5	32.5	36.8		
MTLA246	445.0	55.0	55.5	32.8	32.4	59.2	36.5
MGL S1067		50.0	42.4	30.0	36.5		
P. quadricornis *	404.0	62.0	61.0	42.0	42.0	73.0	42.0
MGL S1241		60.0	59.0				

Table 5: Metacarpal and metatarsal measurements of *Palaeotragus rouenii* and *Palaeotragus* sp. (MGL S1241) from Samos.

*: *P. quadricornis* metatarsal reported by Geraads (1974).

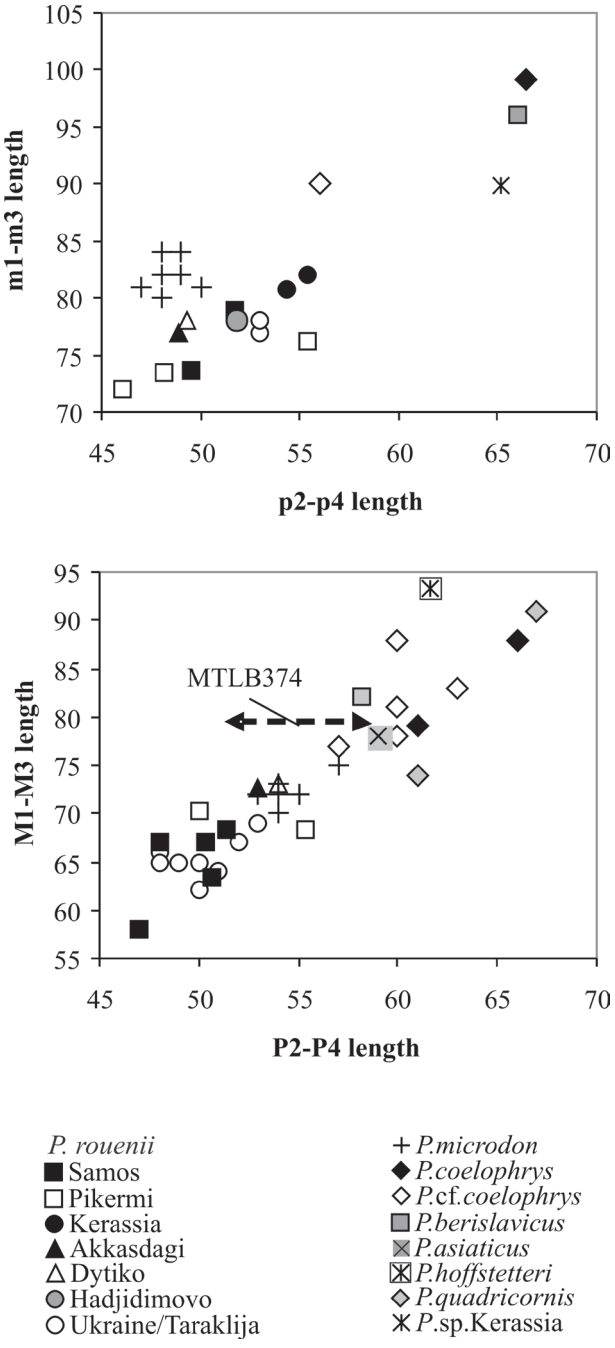

Figure 2: Scatter diagram comparing the premolar/molar ratio on the lower (up) and upper (down) toothrow of *Palaeotragus rouenii* from several sites (Samos, Pikermi, Kerassia, Akkaşdağı, Hadjidimovo, Dytiko, Taraklija, Ukraine) and other *Palaeotragus* species (sources: Bohlin, 1926; Geraads, 1974; Geraads et al., 2005; Godina, 1979; Iliopoulos, 2003; Korotkevich, 1988; Kostopoulos & Saraç, 2005 and pers. data).

The specimen AMNH86520 from Q5 bears, however, the posterior part of the d3 and the complete d4. The talonid of d3 is similar to that of p3 with an oblique and elongated entoconid independent from the rest of the tooth and a long endostylid that reaches the lingual wall. The d4 has a squarish anterior lobe, strong basal pillars between the lobes, rather angular middle and posterior labial crescents and ostensibly convex lingual ribs.

The left mandibular ramus MTLB226 and the partial right mandible AMNH22944 from Q5 give some information on the mandible shape and bear the entire p2-m3 series (Table 3). The horizontal ramus is low ranging from 33 mm in front of p2 to 56 mm behind m3. The posterior profile of the vertical ramus is weakly concave, ending downwards into a visibly convex mandibular angle that prolongs ventrally. The premolar row represents 65.4% of the molars in MTLB226 and 67.2% in AMNH22944. On p2 the paraconid is missing and a wide valley separates the well developed parastylid from the anteroposteriorly expanded metaconid. The entoconid and the entostylid fuse together from the middle of the crown's height, forming a closed valley. The p3 shows some variability in the development of the metaconid, affecting the closing of the anterior valley. The specimen AMNH22944 (Pl. 1, fig. 1) shows an extensively molarized p3, following the typical *P. rouenii* pattern: a fully molariform trigonid and moderately developed talonid. In the specimens AMNH86373 and MTLB226 (Pl. 1, figs. 2, 5) the independent and anteroposteriorly oriented metaconid elongates towards the crown's base where it finally fuses with both the strong and posteriorly curved paraconid and the elliptical entoconid. The p4 is typically giraffid with well-developed parastylid and hypoconid and almost anteroposteriorly settled entoconid (Pl. 1, figs. 1, 5). The lower molars (AMNH86373, AMNH22813, MTLB226) bear a strong metastylid, increasing from m1 to m3 and a well-developed parastylid and entostylid. The hypoconid rests independently until advanced wear. A small basal pillar can occur on m1, which additionally shows a clear notch on the posterior flange of the protocone (Pl. 1, figs.

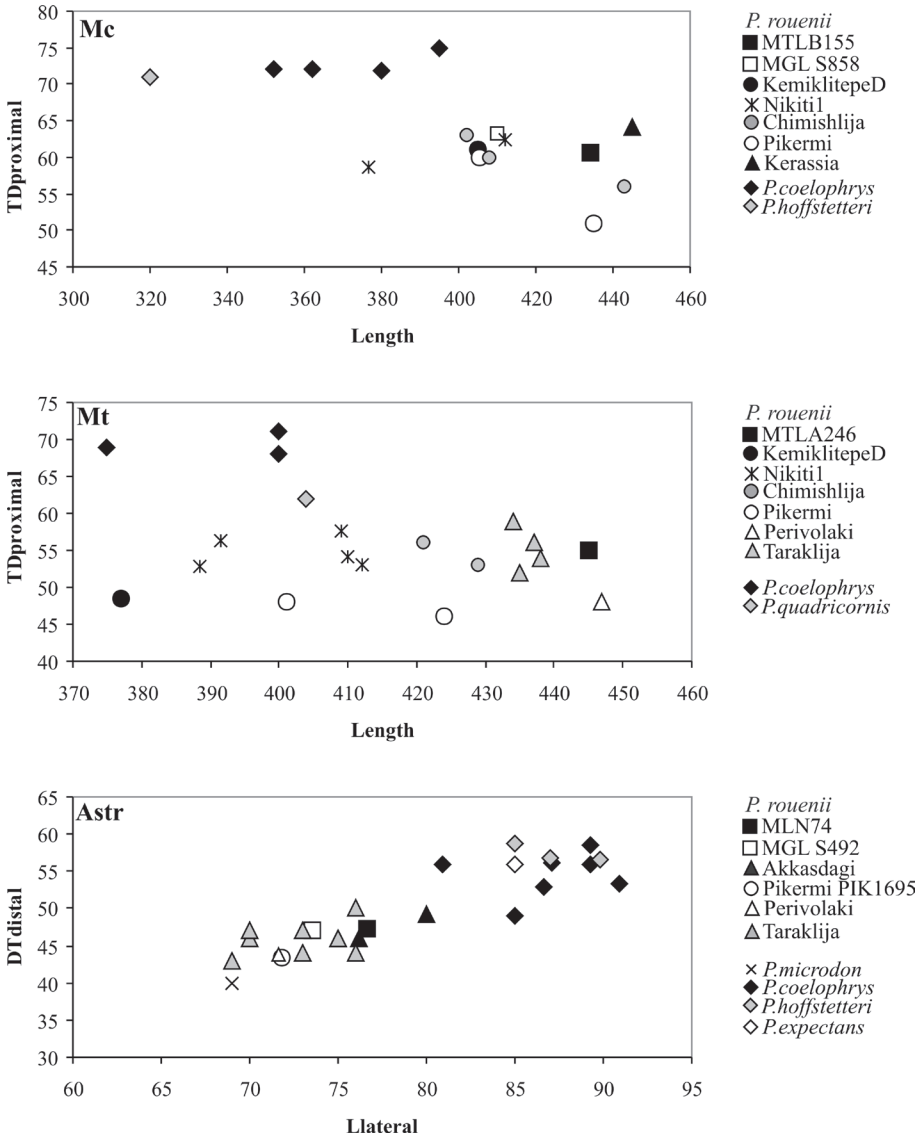

Figure 3: Scatter diagrams comparing limb proportions of *Palaeotragus rouenii* from several sites (Samos: MLN, MTLA, MTLB, MGL, Pikermi, Nikiti-1, Kerassia, Perivolaki, Kemiklitepe D, Akkaşdağı, Taraklija, Chimishlija) and other *Palaeotragus* species (sources: Bohlin, 1926; Geraads et al., 2005; Godina, 1979; Iliopoulos, 2003; Korotkevich, 1988; Kostopoulos et al., 1996; Kostopoulos & Saraç, 2005; Kostopoulos & Koufos, 2006 and pers. data).

Mc = metacarpal; Mt = metatarsal; Astr = astragalus

1, 2, 5). The third lobe of m3 is single-cuspid and rounded. A posterior part of m3 from MLN (MLN86) is also morpho-metrically compatible with the m3 of MTLB226 and AMNH22813. A few postcranials are preserved from MLN, MTLA and MTLB; some additional specimens are known from Stefano (MGL) (Tables 4, 5). The right scapula MTLB165 (Pl. 1, fig. 8) is sub-triangular-shaped with narrow neck. The spine is moderately developed. The glenoid cavity is oval-shaped and rather shallow separated from the highly positioned supraglenoid tuber by a semicircular articular surface limited distally by a strong crest. This morphology is identical to that of *P. rouenii* from Taraklija (Godina, 1979:fig.4a).

The humerus (MTLA157, MGL S1214) shows an elongated olecranon fossa and a long and shallow radial fossa. The lateral and medial epicondyles are almost equally developed and the distal trochlea is rather symmetrical since the lateral condyle reaches the same level proximally as the medial one. The distal keel is wide and blunt.

The radius (MTLB156, MGL S790, S910) is long and slender (Table 4). The medial articular facet of the capitular fossa is squarish, the lateral protuberance is positioned highly and the radial tuberosity is weak. In the distal part, the groove for the extensor carpi radialis tendon is wide and flat, defined by a strong lateral crest, ending distally into a tuber and by an equally long but weaker medial crest. The groove for the common extensor tendon is well-defined and rather short (Pl. 1, fig. 9). A well-developed medial tuberosity occurs 2 cm above the distal articulation. The scaphoid facet is rounded with prominent borders, of which the caudal one forms a strong crest that runs parallel to the caudal edge of the lunar facet. The lunar facet is oval-shaped and significantly smaller than that of the scaphoid (Pl. 1, fig. 9).

The metacarpal (MTLB155, MTLA197, MGL S781, MGL S858) is long and slender (Pl. 1, fig. 7; Table 5). The robusticity index "TD shaft/length" is 8.82 in MTLB155 and 9.12 in MGL S781 and the ratio "length of radius/length of mc*100" for the MTLB specimens is about 120. On the proximal articular surface, the sinovial fossa is closed caudally. The facet for the magnum is sub-quadrangular shaped and the unciform facet is sub-triangular with a strongly convex lateral border (Pl. 1, fig. 7). In anterior view, the vascular

groove is invisible in the lower ⅔ of the metacarpal and the distal epiphysis projects moderately from the shaft. The right distal part of the femur MTLA452 has a rather symmetrical and gently oblique trochlea with bulbous medial rim. The lateral condyle is shorter than the medial one. The supracondyloid fossa faces caudally and is rather short and wide with a weak lateral crest. The scaphocuboid (MLN75; Pl. 1, fig. 10) has a strong and thin posteromedial protuberance that, however, does not raise to the peak of the medial astragalar facet, which is highly elevated; the calcanear facet prolongs behind the lateral peak and the furrow between the two peaks is wide and shallow. The astragalus (MLN74, MGL S492) is slightly asymmetrical distally with a well expressed distal notch. The calcaneum MLN71 has a moderately projected sustentaculum, whereas the cranial and caudal borders of the body run parallel to each other. The deformed metatarsal MTLA 246 and the preserved proximal parts of the metatarsal (MLN75, MGL S1067) indicate an elongated and slender bone (robusticity index = 7.3) slightly longer than the metacarpal; on the plantar side of the proximal epiphysis both the medial and lateral tubercles are strongly developed and close to each other (Pl. 1, fig. 11; Table 5).

Discussion:
Small-sized palaeotragines appear to be much less frequent in the Samos faunal assemblages than large-sized ones. According to Bernor et al. (1996), *P. rouenii* occurs only in the upper fossiliferous horizons (Samos Main Bone Beds member), while Solounias (1981) mentions the species from the sites Qx, MGLS-Stefano, MGLS-Adriano and Q1, suggesting a much wider time distribution (Table 1). The data exposed in this work shows that the species certainly occurs in three successive fossil-levels but there is no proof of its presence in the earliest known level represented by the Qx and Vryssoula sites in the Brown- and NHML-collections.
The skull specimen NHMW A476 from Samos shows a good morpho-metrical fit with the type specimen of *P. rouenii* MNHNP PIK1670 from Pikermi (Table 2), as well as with the skull specimens from Taraklija (Godina, 1979:Pl. I, fig. 1), Nova Elisavetovka (Korotkevich, 1988: fig. 6) and Tchobroutchi (Pavlow, 1913:Pl. I, fig. 3). The ossicone morphology of *P. rouenii* shows weak posterior curvature, slight mediolateral compression and rather regular slimming towards the apexes. The specimen MTLA261, however, shows that a rubbing surface equivalent to that seen in *P. microdon* from China (Bohlin, 1926:figs. 2, 3) can also occur in some individuals. The skulls from Frankfurt and Stuttgart are also similar to 'hornless' specimens from Taraklija, and Nova Elisavetovka (Godina, 1979; Korotkevitch, 1988), representing females, but Geraads (1994) showed that females of *P. rouenii* can occasionally(?) bear ossicones (e.g., Dytiko, Kemiklitepe D samples).
The upper and lower toothrow proportions of Samos samples are well within the known range of *P. rouenii* (Fig. 2), having at average a shorter molar row than *P. microdon* from China. Although dental morphology of *P. rouenii* from Pikermi indicates a relatively high variability in the development of accessory features such as cingula, tubercles, spurs etc., Kostopoulos & Saraç (2005) imply a probable structural smoothening with time. Accessory dental elements are minor in the available Samos toothrows.
Identified postcranials of small late Miocene palaeotragines are generally rare; as a result their anatomy and dimensional ranges are barely known (Fig. 3). The radius from MLN (NHMA) and Stefano (MGL) appears to be slightly shorter and wider than those from the MTLB and NHMW collection. This is well expressed by the index "DTproximal * 100/length" which is 17.5-18.1 in the first group instead of 15.0-15.5 in the second. The same index is 17.5 for the Kemiklitepe-D, Turkey (KTD46) specimen, 14-16 in Pikermi (Greece; n=3), and 16-18 (n=3) in the Taraklija-Chimishlija sample (Ukraine), while it averages or is larger than 20 in *P. coelophrys* from Maragheh (Iran) and related forms. Similarly, the "DTdistal * 100/length" index varies from 15 to 16 in the MGLS-Stefano sample, while it appears slightly smaller in MTLB (12.9); the same index is 15.5 for KTD46, between 12.5-14.0 in Pikermi (n=4) and between 15.0-15.6 in Chimishlija-Taraklija (n=3), while it appears larger than 18.5 in *P. coelophrys*.
The metacarpal robusticity is rather stable, ranging from 6.2(?)-9.5 in *P. rouenii* (n=9) instead of 9.8-13.3 in *P. coelophrys* (n=4). The same value is 8.8 in MTLB155 and 9.1 in MGL S781. The metatarsal MTLA246 is metrically close to the larger values of *P. rouenii* especially regarding its length. The Nikiti-1 and Kemiklitepe-D samples show relatively shorter metatarsals than the Taraklija, Chimishlija and Perivolaki samples, with the two specimens from Pikermi having an intermediate position (Fig. 3). The astragalus from MLN and MGLS-Stefano are well within the range of *P. rouenii* (Fig. 3) being significantly smaller than those of *P. coelophrys* and *P. hoffstetteri* Ozansoy, 1965 from Turkey. Although inadequate for statistically reliable conclusions some limb proportions of *P. rouenii* might indicate an increase of lengthening and slenderness with time.

Palaeotragus quadricornis Bohlin, 1926

Studied Material:
SMNS: SMNS44242, part of skull, nl.

Reference Material:
BSPM: part of nn skull and related right mandible with p2-m3 figured by Bohlin (1926:fig. 53, 55, 56); part of nn skull figured by Bohlin (1926:fig. 54).
SMNS: P2-M3 and two isolated upper teeth figured by Bohlin (1926:Pl. IV, fig. 13-15).

Description & Discussion:
Two partially preserved crania and a lower toothrow from the Munich collection (BSPM), as well as some isolated teeth and an upper toothrow from Stuttgart (SMNS) are the basis on which Bohlin (1926:42, figs. 53-56) erected *P. quadricornis*. The taxonomic value of this species is, ho-

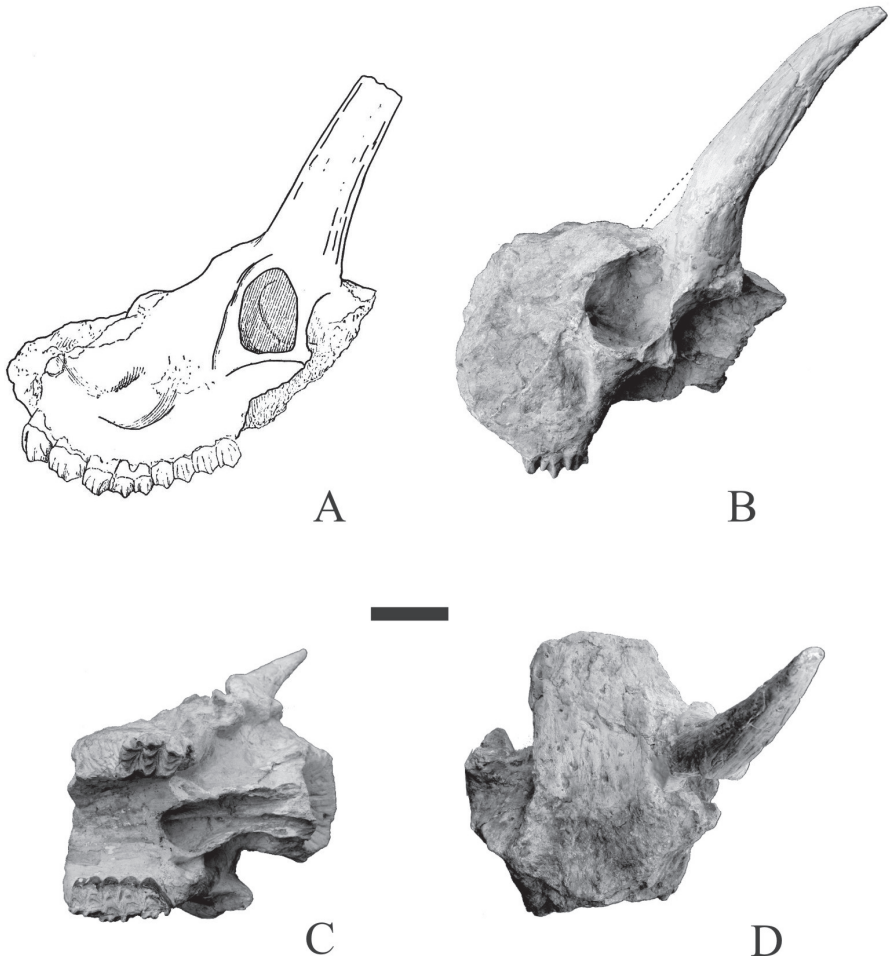

Figure 4: *Palaeotragus quadricornis*, cranium in Munich (A) reproduced from Bohlin (1926) and cranium SMNS44242 in lateral (B) ventral (C) and dorsal (D) view (by courtesy of SMN Stuttgart). Scale-bar 6 cm.

wever, frequently questioned; Bosscha-Erdbrink (1977), Geraads (1986) and Gentry & Heizmann (1996) regard *P. quadricornis* as synonymous with *P. coelophrys* (Rodler & Weithoffer, 1890), while Geraads (1978) and Hamilton (1978) consider it as valid mainly because of the supposed presence of two pairs of ossicones (fide Bohlin, 1926). The same feature allows Solounias (2007) to assign the species to *Shansitherium* Killgus, 1922. Evidently, the fragmentary character of the material and its origin from scattered localities and from unknown levels of Samos cannot allow thorough comparison and confident conclusions. Let alone when the type series of *P. quadricornis* described by Bohlin (1926) has been permanently lost during 2nd World War (Solounias, pers. comm. 1995; Heizmann, pers. comm. 2007).

According to the descriptions and drawings of Bohlin (1926), the female skull of *P. quadricornis* has a wide and rather long opisthocranium and bears straight ossicones that appear to be conical and parallel to each other. The male skull of the species (Fig. 4A) is characterized by a sub-quadrangular orbit placed just behind the M3 and rather high in relation to the alveolar level. The face is also high. The antero-ventral margin of the orbit is marked by a jugo-maxillary swelling. The ossicone is placed above the orbit and curves slightly backwards; longitudinal furrows are probably present on its postero-basal surface. Just above the anterior margin of the orbit, Bohlin (1926:fig. 53) recognizes a hump that he interprets as the position of a second pair of ossicones. The upper toothrow, P2-M3, is ~132 mm long with a premolar/molar ratio of about 69 (Bohlin, 1926:fig. 55). Bohlin (1926:44-45; Pl. IV, fig. 15) also assigns another P2-M3 series from Stuttgart to *P. quadricornis* which belongs to a young adult individual and is 155 mm long with a premolar/molar ratio of 73.6. According to Bohlin's illustrations, the upper molars have a moderately thin and anteriorly oriented mesostyle, a strong paracone and weak metacone, a simple central cavity, and a rounded hypocone and protocone. The P2 is trapezoidal-shaped with a strong parastyle and flat posterior flange of the paracone, whereas the central cavity bears a strong posterior fold. The P3 and P4 are quite similar to the P2 but the protocone is much more developed lingually. The development of the hypocone increases from P2 to P4.

The lower dentition of *P. quadricornis* is known by a single p2-m2 row figured by Bohlin (1926: fig. 56); the lower premolar row is about 56 mm long. The p2 is short compared to the p3 with a weakly developed metaconid. The p3 has a moderately developed paraconid and free metaconid that probably prolongs to the rear. The p4 is molarized and of *P. rouenii*-type; the molars show an angular protoconid and hypoconid.

Bohlin (126:42, 125) assigns another skull from the Stuttgart collection (SMNS44242) to the same species, which has previously been ascribed to "*Palaeotragus vetustus*" by Forsyth-Major (1901). It is a badly preserved and extremely fragmentary specimen (Fig. 4B-D) including part

of the face and cranial roof, on which the ossicone is not necessarily correctly attached (according to Heizmann, pers. comm. 2007, there is no real bone contact between the frontal and the ossicone). SMNS44242 shows, indeed, several morphological similarities to the male skull of *P. quadricornis* such as the sub-rounded orbit placed relatively backwards (above the posterior lobe of M3) and far up from the alveolar level, the presence of a jugo-maxillary swelling, the weakly curved ossicones bearing posterior longitudinal furrows, and the simple molar pattern. The palate is 73 mm wide at the posterior lobe of M3; the M1-M3 length is estimated at 96 mm; the ossicone is 240 mm long and its basal APD is 70 mm; the internal distance between the ossicones is larger than 100 mm.

The presence of an additional pair of ossicones on the male skull of *P. quadricornis* is not certain at all. Bohlin (1926: fig. 53) arrived at this conclusion based on the presence of a hump just above the anterior margin of the orbit. This feature may, however, be the effect of an advanced pneumatization, such as seen in the broken supraorbital region of the specimen SMNS44242 and in the type skull of *Samotherium boissieri* (NHML M4215; Bohlin, 1926: figs. 135, 136). On the other hand, the implantation and orientation of the *P. quadricornis* main ossicone does not seem to be related to the condition seen on the *Shansitherium* holotype skull (cast AMNH32502).

Arambourg & Piveteau (1929) and Geraads (1974) provisionally attribute the Maragheh 'horn-core' of de Mequenem's figure 9-left (1924) to *P. coelophrys*. This ossicone is rather short, wide at its base and curves gently posteriorly; its anteroposterior diameter is 63 mm (fide Geraads, 1974). Both its morphology and size are comparable with those of male *P. quadricornis* (APD ~60 mm from Bohlin's, 1926: fig. 53 and 70 mm in SMNS44242).

Apart from the type specimen of Rodler & Weithoffer (1890) from Maragheh, *P. coelophrys* skulls are known from Ravin de la Pluie (RPl, Greece) and China. Nonetheless, all specimens are 'horn-less' suggesting that they most probably belong to females. On the other hand Bohlin (1926) determines the 'horned' skull of his fig. 54 from Samos as a female *P. quadricornis*. Of course, the presence of ossicones on females cannot be considered a safe criterion for taxonomic distinction between these two species, since ossicones appear to be occasionally present on females of *P. rouenii* (see Bohlin, 1926; Geraads, 1978, 1994; Godina, 1979; Korotkevitch, 1988) and *Samotherium* (see below). The main skull difference between *P. quadricornis* from Samos and *P. coelophrys* from Maragheh and China is the relative position of the orbit, which, in the latter species, is placed lower and more anteriorly (its front margin is above M2-M3). The same feature distinguishes the Ravin de la Pluie (RPl-91) cranium from the Maragheh one (Geraads, 1978), suggesting that this feature is independent of sex and age, as both crania belong to adult females. On the *P. coelophrys* face from Maragheh and China a crest originating from the middle of the anterior margin of the orbit prolongs sub-horizontally until above P4-M1. This feature is replaced in *P. quadricornis* by a jugo-maxillary swelling in a more ventral position. The posterior edge of the maxilla is less inclined in *P. coelophrys* and its upper point ends at the level of the postorbital bar, whereas in *P. quadricornis* the same border slopes abruptly with its upper point ending at the middle of the lower orbital margin. According to these features, the RPl-91 cranium and *P. asiaticus* Godina, 1979 appear to be closer to *P. quadricornis* than to *P. coelophrys*, whereas *P. expectans* Borissiak, 1914 better meets the condition expected for males of *P. coelophrys*.

Dentally, small differences, especially in the premolar morphology, between all above-mentioned species cannot be appreciated, because of the limited available material. The trapezoidal shaped P2 with reduced parastyle and flat posterior flange of the paracone of *P. quadricornis* from Samos strongly recalls that of *P. hoffstetteri,* but less like RPl-91 and *P. asiaticus* (Godina, 1979: fig. 6), while it differs from the well-developed and more symmetrical P2 by a strongly concave posterior flange of the paracone seen in *P. expectans*, *P.* cf. *coelophrys* from China and *P. coelophrys* from Maragheh [the skull figured by Rodler & Weithoffer (1890) and the maxilla figured by de Mequenem, 1924: MNHNP MAR 670]. Both P3 and P4 of *P. quadricornis*, as well as those of *P. hoffstetteri* show an incipient lingual bilobation, which is absent from *P. coelophrys* specimens figured by de Mequenem (1924) and Bohlin (1926) and *P. expectans* from Sebastopol (Borissiak, 1914, 1915). On the other hand, the p2 of *P. quadricornis* is wider and less advanced in the stylid development than the p2 of *P. coelophrys* figured by de Mequenem (1924; MNHNP MAR669) and *P. expectans* (Borissiak, 1914: Pl. I, fig. 7) but the p3 and p4 are quite similar considering the actual morphological variability seen in these teeth.

Evidently, the comparison between *P. quadricornis* and *P. coelophrys* cannot allow a definite systematic decision. Based on the available material the two species look similar but not identical, being different in several cranial and dental features, whose credibility unfortunately cannot be checked. Hence, it seems preferable to retain their taxonomic distinction for the moment, waiting for new and more informative material.

Palaeotragus sp.

Localities & Ages:

Mytilinii-4 (MLN), Potamies ravine; late early Turolian (MN11), 7.6-7.4 My

Mytilinii-1B (MTLB), Adrianos ravine; middle Turolian (MN12), 7.1-7.0 My

Quarry x (Qx), Mytilinii village; early Turolian (MN11), 8.0-7.6 My

The material from the PIM, MGL, NHML has no locality indication.

Studied Material:

NHMA: MLN44 radius, MTLB374, P4-M3 dex

AMNH: AMNH20773, frontlet Qx; AMNH22807 (D2) D3-M1sin, nl;

PIM: PIM293, p3-m3 sin, nl
MGL: MGL S1241, Adriano?, proximal metatarsal
NHML (from Iliopoulos, 2003): NHML M4313, radius.

Description & Discussion:
The presence of small palaeotragines which differ from *P. rouenii* is also documented by scarce specimens from various sites on Samos, described here as *Palaeotragus* sp. That, however, does not imply that they necessarily represent a homogeneous sample, i.e., a single species.
The frontlet AMNH20773 from Qx (Fig. 5), assigned by Solounias (2007:fig. 21.4A) to *P. coelophrys*, is wide (external distance at the ossicone base = 200 mm; internal distance at the ossicone base = 116 mm; distance between the supraorbital pits = 94 mm) with a concave frontal area between the ossicones. The supraorbital pits are situated medially in relation to the ossicone's longitudinal axis and prolong anteriorly through wide grooves. Pneumatization seems to be advanced in the supraorbital area. The ossicones are straight, weakly divergent towards the tips, not very long (~190 mm) and rather thin (TDbase = 40, APDbase = 44 mm) with an oval to rounded cross-section. Morphologically, the frontlet AMNH20773 looks very similar to the female specimen of *P. quadricornis* figured by Bohlin (1926:fig. 54) but also is not significantly different from the type skull of *P. rouenii* (MNHNP PIK1670), except for the straighter ossicones and the rather wider and certainly more concave interfrontal area. Bohlin (1926) gives few measurements of the two *P. quadricornis* skulls from which it can be deduced that in the females of this species the internal distance between the ossicones is much larger than in the males, evidently because of the larger mediolateral development of the ossicones in the latter. The ratio of "external distance/internal distance at the ossicone bases" is, therefore, 3.2 for the male skull and 1.9 for the female of *P. quadricornis*. The same ratio in AMNH20773 is 1.7, probably implying a female individual. The gracility and straightness of the ossicones could also be related to the sex of the individual, just as the condition seen in *P. rouenii* (Geraads, 1978, 1994) but individual age could also be responsible for differences in the ossicones.
The upper milk dentition AMNH22807 with (D2)D3-M1 is supposed to be originating from Q5 but according to the associated matrix and the type of fossilization, the locality indication is probably incorrect. D2 and D3 appear to be wider than those of *P. rouenii* from Samos. In D3, the fusion between the two lobes is much more intense than in *P. rouenii*; the hypocone is less extended lingually; the anterior and posterior flange of the paracone form an obtuse angle instead of an acute angle in *P. rouenii*, and the metacone is less developed. Moreover, a rather robust basal pillar occurs between the protocone and the hypocone, whereas a short but strong anterolingual cingulum is present. Different from *P. rouenii*, the D4 of AMNH22807 has no constricted protocone, there is no mark of an anterior fold on the hypocone and the metacone is weakly developed, whereas a strong anterolingual cingulum is also present here. The morphological characteristics

Figure 5: *Palaeotragus* sp., frontlet AMNH20773 from Qx in anterior view. Scale-bar 2 cm.

of D3 and D4 of AMNH22807 are close to those of the specimen AMNH26362 from Shansi (Pao-Te-Chu, Chi-Chia-Kou-43), China, ascribed to *P.* cf. *coelophrys*. The right P4-M3, MTLB374, is slightly larger than that of *P. rouenii* from the same locality (the molar length is 77.6 mm instead of 58-68 in *P. rouenii* from Samos; Fig. 2). The parastyle of P4 is weaker than in *P. rouenii*, the lingual lobes of the molars are more rounded and their mesostyle is thicker. Dimensionally, MTLB374 is among the minimum values for *P. quadricornis*, *P. asiaticus* and *P. coelophrys*. Its wider than long P4 with traces of an hypoconal spur is closer, however, to *P. hoffstetteri* and *P. quadricornis* than to *P. coelophrys*.
PIM293 is a p3-m3 row with advanced wear (m1-m3 ~90 mm). The dental morphology looks completely compatible with that of Bohlin's *P. quadricornis* but the paraconid and the parastylid of the p3 have been fused by wear, the m1 bears a basal pillar, m2 and m3 show a weak anterolabial cingulum and the m3 has strong parastylid and well developed paraconid. Furthermore, the presence of an important parastylid on the m3 of PIM 293 and the occurrence of an anterior cingulum on the m2 and m3 of the same specimen distinguish it from MNHNP MAR669 of *P. coelophrys*.
The radius MLN44 is badly preserved. In comparison with the radius of *P. rouenii* from Samos it appears to be slightly shorter and wider (Table 4). The medial facet of the capitular fossa is more elongate than in *P. rouenii* and the lateral protuberance is weaker. The groove for the extensor carpi radialis is concave, defined by a strong medial crest and a weaker lateral one. The groove for the common ex-

tensor tendon appears as a depression without well defined limits. The scaphoid facet is squarish with less developed margins than in *P. rouenii*. Its caudal edge does not form a crest as in *P. rouenii* and converges with the caudal edge of the lunar facet, which runs sub-horizontally. One more radius from the NHML collection (M4313) is shorter than MLN44 but proportionally closer to it than to *P. rouenii* (Table 4). Size comparison between the Samos specimens and those of *P. rouenii* from Pikermi and Samos and *P. coelophrys* from Maragheh, show that the Samos radius is shorter than that of *P. rouenii* and less robust than that of *P. coelophrys*. The proximal metatarsal MGL S1241 is relatively wider than that of *P. rouenii* from Samos (Table 5) and close to the dimensions reported for *P. quadricornis* (Geraads, 1974).

Genus *Samotherium* Forsyth-Major, 1888

Samotherium boissieri Forsyth-Major, 1888

(Plate 2, figs. 3, 11, 16; Tables 6-16)

Localities & Ages:
Mytilinii-4 (MLN), Potamies ravine; late early Turolian (MN11), 7.6-7.4 My
Quarry x (Qx), Mytilinii village; early Turolian (MN11), 8.0-7.6 My
Quarry 2 (Q2), Potamies ravine; late early Turolian (MN11), 7.6-7.4 My
MGLS-Stefano, Stefana hill, late early Turolian (MN11), 7.6-7.4 My
NHML-Vryssoula, early Turolian (MN11), 8.0-7.6 My
The material from the MNHNP, SPGM, SMF has no locality indication.

Studied Material:
NHMA: MLN25, 46, radius; MLN76 distal radius; MLN9, 80, metacarpals; MLN32, proximal metacarpal; MLN57, 76, distal metacarpal; MLN47, tibia; MLN21, 24, 60, 78, distal tibia; MLN34, 64, 65, 68, astragalus; MLN10, 69, 70, 72, calcaneum; MLN35, 66, 73, scaphocuboid; MLN22, 31, 33, 43, 77, 79, metatarsals
AMNH: Exchange with NHML: AMNH15876(M4230), D3-M1, Qx?; AMNH nn, distal radius; AMNH(M4267), metacarpal; AMNH15876, metacarpal; AMNH M4283, astragalus; AMNH(M4289)a & b, metatarsal
Exchange with Munich: AMNH9863a, D3-D4, nl; AMNH9863b d2-d4, nl.
Q2: AMNH22829, humerus; AMNH22808, radius; AMNH22820, radius; AMNH22828a, metacarpal; AMNH28825, tibia; AMNH22828b, metatarsal.
AMNH nn, left mandible with p2-m3, nl.
MNHNP: SMS2, left mandible with p2-m3.
NHML: NHML M4215, young-adult male skull (holotype); NHML M4216, adult female skull; NHML M4226b, milk maxilla; NHML M4227, M4229, right upper milk dentition; NHML M4228, left upper milk dentition; NHML M4226, M4219, palate; NHML M4221, M4223, M4225, left upper dentition; NHML M4238, left lower milk dentition; NHML M4239, right lower milk dentition; NHML M4224, P2-M3 and left mandible with p2-m3; NHML M4234, M4235, M4236, right mandibles; NHML M2336, atlas; NHML M4243, scapula; NHML M4252, humerus; NHML M4255, M4256, M4257, distal humerus; NHML M4259, M4260, M4262, radius; NHML M4264, four distal radius; NHML M4268, metacarpal; NHML M4267, nine metacarpals; NHML M4275a&b, M4278, tibia; MBNH M4283, five astragali; NHML M4284, five scaphocuboids; NHML M4282, five calcanei; NHML M4289, twelve metatarsals; NHML M4290, two first phalanges; NHML M4299, nine first phalanges; NHML M4300, five first phalanges.
MGL: (all the material except MGL S12, is coming from Stefano)
MGL S202, part of skull; MGL S12, p2-m2, Potamies; MGL S450, radius; MGL S789, S787, metacarpals; MGL S1240, proximal metacarpal; MGL S452, Snn, tibia; MGL S937, distal tibia; MGL S601, S586, S864, S1014, S1015, astragalus; MGL S690, scaphocuboid; MGL S458, S382, metatarsals; MGL S1074, first phalanx.

Reference Material:
BSPM (from Bohlin 1926): SPGM nn-a & b, upper milk dentition; BSPM nn-1 & 2, P2-M3
SMF (from Bohlin 1926): SMF nn, lower milk dentition; SMFa & b, P2-M3

Description:
Bohlin (1926) gives a brief description of the species based mainly on material in London (NHML) and Lausanne (MGL). Although there is no precise stratigraphic information, the material comes from several sites (Stefana, Vryssoula, Potamies) of the lower fossil-levels, excavated by Forsyth-Major in 1887 and 1889 (see also Solounias, 1981). As already mentioned by Geraads (1994), the study of the NHML *Samotherium* sample indicates that it represents a single species, namely *S. boissieri* Forsyth-Major, 1888. Exceptions are a *Samotherium* astragalus mentioned by Bohlin (1926:89) but not relocated into the collection and a tibia labeled NHML M4299 that appears to be larger than the rest of the sample and should be ascribed to *S. major*. Iliopoulos (2003) also mentions another large *Samotherium* tibia plus tarsals NHML M5432. It is quite possible that these specimens disturbing the NHML *Samotherium* homogeneity came from exchanges with other institutions or that they represent occasional findings. There is also no apparent reason to contest the taxonomic homogeneity of the MGL *S. boissieri* sample labeled "Stefano", to which the mandible MGL S12 from Potamies should also be ascribed. Bohlin (1926:89) attributed the cranium MGL S202 from Stefano to a female individual of *S. major*, but its dimensions are significantly smaller than the female skulls MGL S15 and NHMB Sam29 of *S. major* (cf. measurements in Bohlin, 1926: table, p. 89). The AMNH includes additional unpublished material of *S. boissieri* from B. Brown's excavations (Q2 sample), as well as specimens purchased by exchange from the NHML and the BSPM. Another un-numbered left

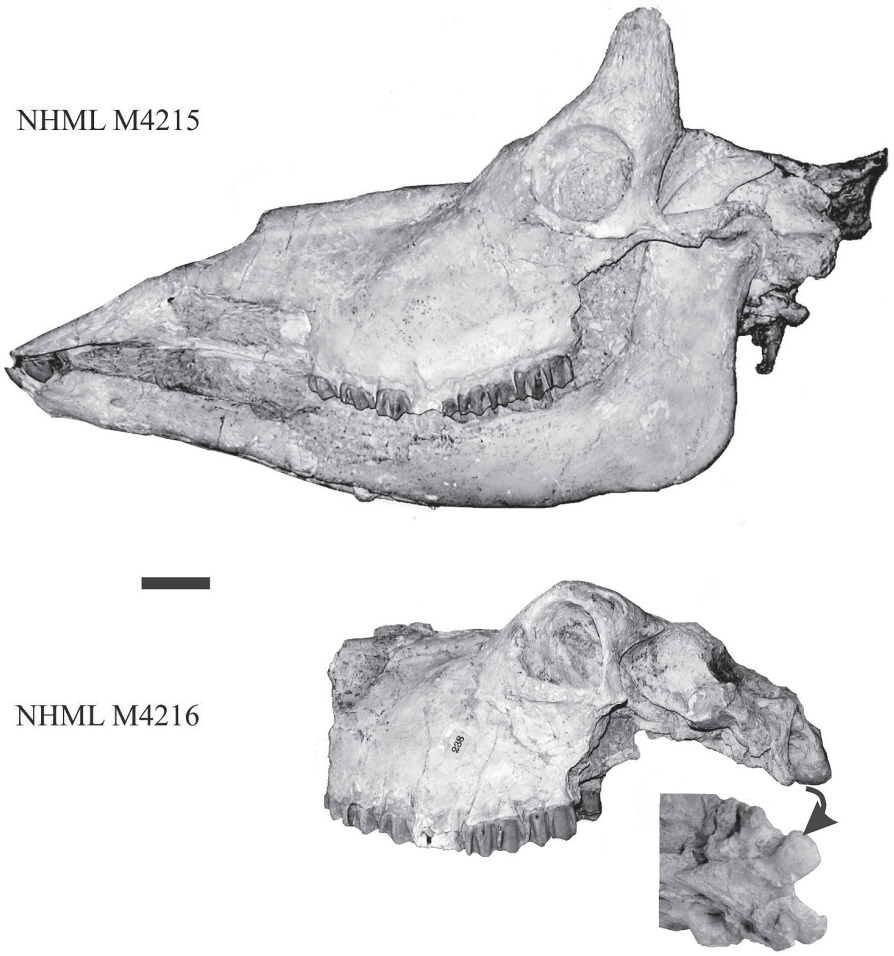

Figure 6: *Samotherium boissieri*, NHML M4215, holotype in lateral view; NHML M4216 in lateral view and detail of the basioccipital. Scale-bar 5 cm.

mandible with p2-m3 from the AMNH is supposed to be from Q1 but its red coating rather suggests Q2 as the site of origin. Finally, a left, unpublished mandible from Samos housed at the MNHNP also belongs to the present species.

Skull. One male (NHML M4215) and two female skulls (NHML M4216, MGL S202) are known (Lydekker, 1890; Forsyth-Major, 1891:fig. 1; Forsyth-Major, 1902:fig. 65; Bohlin, 1926:figs. 135, 136). Although notably compressed laterally, the skull NHML M4215 preserves most of its morphometrical features (Fig. 6, Table 6). The opisthocranium is rather short. In dorsal view, the parietals are bulbous anteriorly and the parietal crests are rather strong defining an almost flat cranial roof between them. They converge up to the level of the external auditory meatus, from where they diverge to meet the strongly posteriorly projecting and fan-shaped nuchal crest, which is interrupted by a median wide notch. The upper margin of the external auditory meatus is placed just below the lower orbital level. A rather strong temporal foramen is present. The zygomatic arches run parallel to the sagittal plane. The fronto-parietal suture is not visible. The frontals are wide and slightly concave between the ossicones. The ossicones are placed above the posterior part of the orbits. They diverge towards the tips and are barely curved backwards. Their cross-section is constantly rounded and they could be long and probably pointed. In lateral view the frontals slope rather abruptly in front of the ossicones. Extended lachrymal sinuses form a characteristic hump placed in the antero-dorsal part of the orbit and just at the level of the fronto-lachrymal suture. The fronto-nasal suture is placed above M2 and is "m"-shaped. The nasals are elongated, thin and weakly convex in lateral view. A thin, elongated ethmoidal fissure is defined by the nasal, lachrymal and maxillary bones. The fronto-lachrymal area forms a blunt crest that prolongs obliquely on the face up to above P3/P4, defining the nasals a triangular-shaped and short depression with an open anterior limit (lachrymal depression) (Fig. 6). The infraorbital foramen opens just in front of P2. A weak facial crest prolongs up to M1. The orbit is round, placed rather high (its upper half is above the nasal level) and anteriorly (its anterior margin is placed above the middle of M3) (Fig. 6). There possibly is no contact between the premaxillae and the nasals. The premaxilla is long and its suture with the maxilla forms a convex line (unlike the restoration of Bohlin, 1926: fig. 135). The muzzle is elongated and rather oval shaped anteriorly. The horizontal ramus of the mandible is moderately shallow, forming a gentle obtuse angle with the vertical ramus. The angle of the mandible is rounded with a weak vascular impression (Fig. 6).

The skull NHML M4216 (Fig. 6) is 'hornless' with a smooth supraorbital region. On the contrary, the adult skull MGL S202 shows a rough supraorbital region and a small 'horn'-like exostosis (TDb = 15 mm; APDb = 12 mm) on the right side. Solounias (1988) also described this specimen as a "female *Samotherium* with adult dimensions

	Samotherium boissieri			*Samotherium major*						
	MGL S202	NHML 4215	NHML 4216	MGL S15	MGL S17	AMNH 22786	MTLA 540	NHMB Sam30	NHMB Sam29	MNHNW nn
L-OrNc		160				315	305	[277]	[292]	
W-BR	110			120.5	125	122.0	118.6			
W-Or	235.5	[240]		242	240				[235]	260
W-bCo			75	97.3	100	110	112.4	95	113	108
W-bMa						181.0	178.5	173	[138]	
L-M3Ba			~170			245	[280]	211	226	[250]
L-P2Ba			340			435	425	436	410	445
W-pTu			41	50.3		56.9	56.5	55	[55]	
W-aTu			20	29.0			27.5			
TD-HCb	15.0	32.5+			59		47.2			
APD-HCb	12.0	48.5			80	132.5	42.5			
H-Occ	[65]			77	90		116.3			
W-Nc	97			114	107		141.1			
L-BaCh							300	[302]	[279]	
TD-Or		67.0	66.0				87.5	76	[75]	
L-Hor		525					560			
H-Ver		230					270			

	L-Fr	L-CN	L-Na	W-Or	WBR	W-bCo
PIM298	140	121		~200	117	89.3
PIM299	144	119.4	116	210	116	

Table 6: Skull measurements of *Samotherium* from Samos.

L-OrNc: length from the midpoint between the anterior margin of the orbits to the nuchal crest; W-BR: width of the braincase; W-Or: maximum width at the posterodorsal corner of the orbits; W-bCo: bi-condyle width; W-bMa: bimastoid width; L-M3Ba: length from basion to the back of M3; L-P2Ba: length from basion to the front of P2; W-pTu: width at the posterior tuberosities of the basioccipital; W-aTu: width at the anterior tuberosities of the basioccipital; TD-HCb: transverse diameter at the ossicone base; APD-HCb: anteroposterior diameter at the ossicone base; W-Occ: max width of the nuchal crest; L-BaCh: length from basion to the anterior margin of the choane; TD-Or: horizontal diameter of the orbit; L-Hor: length of the horizontal ramus of the mandible from i1 to the back of the angle; H-Ver: maximum height of the vertical ramus of the mandible. L-Fr: length of the frontals; L-CN: length from the frontoparietal suture to the nuchal crest; L-Na: length of the nasals. Additional specimens in Bohlin (1926).

and small ossicones of irregular shape". Regarding these two specimens it seems that females of *S. boissieri* can bear thin ossicones, such as seen in *P. rouenii*. The supraorbital processes of the frontals are strongly extended (Fig. 6). The thickness of the frontals at the orbital region is about 20 mm in MGL S202. The parietal crests are similar to those of the male skull, but probably less converging and the nuchal crest is less projected and more square-shaped. The placement of the orbit is totally comparable to that of the male (i.e., periscopic with the anterior orbital margin above M2-M3 limit). The lachrymal depression is slightly shorter than in the male. The basicranial angle is about 30° and possibly stronger than in the male. The occipital condyles are strong and point postero-ventrally. The basioccipital is short (Fig. 6), with thin, crest-like anterior tuberosities and small posterior ones; the anterior tuberosities converge to the front, while the posterior ones are almost vertical to the sagittal plane and merge with the ventral edges of the condyles, giving the basioccipital a rhomboid look. The tympanic bulla is small and the paroccipital processes are placed clearly in front of the condyles.

Dentition. The upper milk dentition D2-D4 ranges from 80.2 to 87.8 mm (Table 7). The styles and pillars are strong except the metacone which, however, increases from D3 to M1. The anterolingual face of D2 is almost flat or bears a shallow and wide groove, while another weaker groove can also occur in central position. The anterior lobe of D3 is fully molariform and the two lobes tend to converge lingually (NHML M4227, M4229, AMNH15876); an additional tubercle appears in postero-labial position. The length of the lower milk dentition d2-d4 is not well known; Bohlin (1926:91) gives a length of 75 mm for a

Table 7: Upper and lower milk-toothrow measurements of *Samotherium* and *Helladotherium* from Samos.

*: data from Bohlin (1926).

	L D2-D4	LD2	WD2	LD3	WD3	LD4	WD4
S. boissieri							
NHML (n=4)	80.2-87.8						
AMNH15876				30.0	21.0	36.6	27.4
BSPM nn-a*	82.0	26.0	18.0	32.0	22.0	32.0	20.0
BSPM nn-b*	83.0	24.0	19.0	27.0	24.0	32.0	28.0
S. major							
MTLB94	88.1	24.8	19.5	31.5	24.6	34.1	30.0
MTLB95	85.9	24.2	18.1	29.6	23.0	33.8	28.3
MTLB373	88.9	25.8	19.5	31.3	24.5	34.7	30.2
AMNH nn Q5					23.9	34.8	31.9
AMNH22795a Q5						30.5	25.0
MGL S5				26.5	20.0	33.1	26.3
MGL S4	89.0	23.3	18.5	30.7	23.3	36.0	28.0
MGL S6	89.6	24.5	18.5	31.7	24.0	35.2	28.4
MGL S3				31.5	24.0	36.0	28.6
PIM298	89.0	24.0	17.0	30.0	22.0	34.0	28.0
PIM299	92.0	26.0	20.0	31.0	25.0	35.0	30.0
PIM467	91.5	26.0	19.0	34.0	23.0	36.0	27.0
PIM465	94.5	26.0	19.0	34.0	25.0	37.0	30.0
PIM468	90.7	25.0	18.0	32.0	23.0	35.0	28.0
NHMB Sam28a	88.0						
NHMB Sam28b	91.0						
H. duvernoyi							
AMNH22795b Q5	94	26.1	20.2	34.5	23.7	[32]	30.4
SMF2440-421	[99]	28.0	19.0	35.0	26.0	36.0	30.0
SMF24431	108.0	29.0	25.0	37.0	30.0	40.0	39.0
	L d2-d4	**Ld2**	**Wd2**	**Ld3**	**Wd3**	**Ld4**	**Wd4**
S. boissieri							
AMNH9863b				25.4	13.9	40.1	20.7
SMF nn*	75.0	17.0	9.0	21.0	12.0	38.0	16.0
S. major							
MTLA495	94.6	19.2		28.0	13.7	48.0	17.4
MTLB227	88.0	19.6	10.6	27.2	14.6	43.3	20.3
MTLC12				27.0	15.8	43.5	23.0
AMNH nn,nl	99.0	23.0	9.7	28.5	13.3	45.0	19.5
AMNH22885 Q4				25.7	13.0	44.7	20.5
MGL S1A	86.7	19.7	9.9	24.0	13.4	43.0	20.6
MGL S1B	85.2	18.5	9.7	25.2	13.1	42.7	20.0
H. duvernoyi							
AMNH95120	101.2	19.9	9.8	29.8	16.5	50.5	23.4
NHMWnn*	92.0	23.0	13.0	30.0	18.0	45.0	24.0

milk mandible in Frankfurt but the mean length of the species should certainly be higher. The d2 is simple, long with an elongated cuspid (metaconid+entoconid) that points backwards, reaching the postero-lingual angle of the tooth. The d3 has a moderately developed hypoconid, an anteriorly curved metaconid and posteriorly pointing paraconid. The latter two cuspids touch each other, forming a closed anterior valley. The anterior lobe of d4 is squarish and flat lingually; an accessory fold can also occur (Table 7).

The P2-M3 length ranges between 162.7 and 180.5 mm with a mean premolar/molar ratio of 69.6 (Table 8). The upper permanent teeth are characterized by variably strong styles and pillars; the posterior flange of the paracone always slopes more gently than the anterior one (Fig. 7). The parastyle and the paracone of the premolars are equally strong and sometimes bulbous; the metastyle varies from strong (NHML M4215, M4219, M4226, M4223) to feeble (NHML M4216, M4225) (Fig. 7). The P2 and P3 are rounded lingually, while 2 out of 5 P4 have a flat and oblique lingual wall. A weak labial groove is present in the paracone of most P4 and some of the P3. A feeble hypoconal fold can be present in some P3, P4 and freshly erupted M1. The presence of a cingulum varies considerably from strong to almost absent. A rudimentary basal tubercle attached to the posterior lobe of the molars is also frequently present. The protocone of the molars is always narrower and more projected lingually than the hypocone.

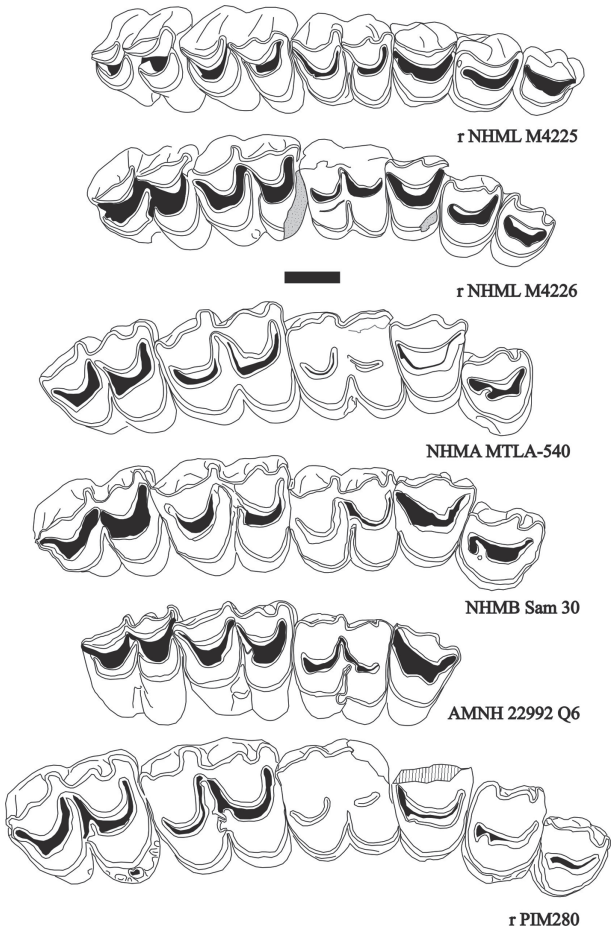

Figure 7: Upper toothrow of *S. boissieri* (NHML M4225, M4226) and *S. major* (NHMA MTLA540, NHMB Sam30, AMNH22992, PIM280) from Samos. r = left toothrows shown as if they were from the right side. Scale-bar 2 cm.

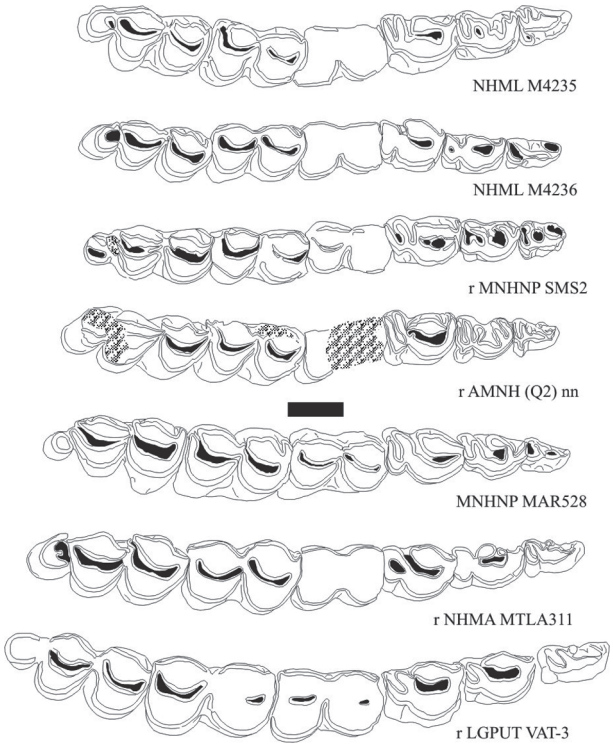

Figure 8: Lower toothrow of *S. boissieri* (NHML M4235, M4236, MNHNP SMS2, AMNH (Q2) nn) and *S. major* from Samos (NHMA MTLA311) and Vathylakkos (LGPUT VAT3; Axios valley Greece), as well as of *S. neumayri* (MNHNP MAR528) from Maragheh. r = left toothrows shown as if they were from the right side. Scale-bar 2 cm.

The mandibular rami NHML M4224 and M4234 most probably belong to the same individual. The p2-m3 length ranges between 177.5 and 189.1 mm with a premolar/molar ratio from 61.4 to 65.6 (n=3; Table 8). The p2 always has a basal tubercle in posterolabial (hypoconal) position (Fig. 8); the parastylid is strong; in 4 out of 6 specimens the metaconid is undeveloped and the hypoconid is incipient but clear while in the rest of the specimens (MNHNP SMS2, NHML M4235), the hypoconid is not developed, but a thin metaconid points backwards, closing the valley with the entoconid. The p3 of MGL S12, NHML M4224, M4234 and M4236 shows advanced molarization with a well developed but narrow hypoconid and an anteroposteriorly oriented metaconid in contact with a relatively strong and posteriorly curved paraconid (Fig. 8). The p3 of NHML M4235, MNHNP SMS2 and AMNH nn is less molarized with a posteriorly pointing metaconid that fuses with or overlaps the entoconid; the anterior valley remains open; the paraconid is variably developed and can curve posteriorly; the hypoconid is weakly developed and a basal tubercle occurs in posterolabial position (Fig. 8). The p4 has a more stable morphology with a fully molarized anterior lobe and strong parastylid. The reduced posterior lobe is formed either by an obliquely placed entoconid and a sigmoid hypoconid + entostylid complex (NHML M4224, M4234) or by a rather primitive elongated entoconid-entostylid pattern and a well individualized hypoconid with or without a small postero-labial tubercle (AMNH nn, MGL S12, MNHNP SMS2, NHML M4235, 4236) (Fig. 8). The molars are simple with a weakly marked paraconid, and a moderately developed metastylid that disappears towards the crown's base. The parastylid is moderate to strong and the third lobe of m3 is single-cuspid and sub-squarish-shaped.

Postcranials. Measurements are given in the tables 9-16, while morphological data is discussed below together with those of *S. major*.

Samotherium major Bohlin, 1926

(Plate 2, figs. 1-2, 4-10, 12-15, 17-18; Tables 6-16)

Localities & Ages:

Mytilinii-3 (MYT), Potamies ravine; early middle Turolian (MN12), ~7.3 My

Mytilinii-6 (MTN), Tholorema; early middle Turolian (MN12), 7.4-7.3 My

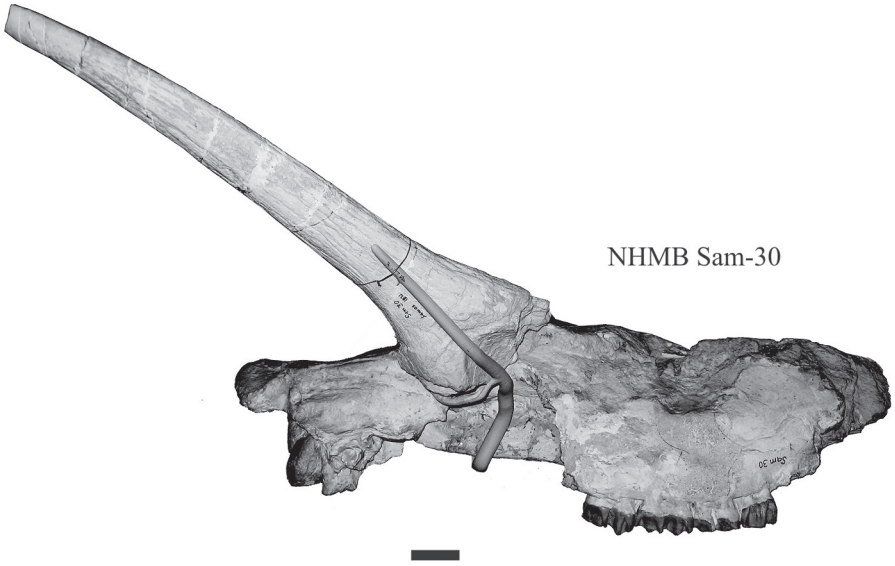

Figure 9: *Samotherium major*, cranium NHMB Sam30 in lateral view (by courtesy of NHM Basel). Scale-bar 5 cm.

Mytilinii-1A, 1B, 1C (MTLA, MTLB, MTLC), Adrianos ravine; middle Turolian (MN12), 7.1-7.0 My
PMMS, Adrianos ravine; middle Turolian (MN12), 7.1-7.0 My
Quarry 4 (Q4), Potamies ravine; early middle Turolian (MN12), ~7.2 My
Quarry 6 (Q6), Tholorema; early middle Turolian (MN12), 7.4-7.3 My
Quarry 1 (Q1), Adrianos ravine; middle Turolian (MN12), 7.1-7.0 My
Quarry 5 (Q5), Limitzis; early late Turolian (MN13), 6.9-6.7 My
MGLS-Adriano, Adrianos ravine, middle Turolian (MN12), 7.1-7.0 My
The material from NHML, NHMW, NHMB, PIM, SMNS, SMF has no locality indication.

Studied Material:
NHMA:
MYT: MYT14, radius; MYT37, proximal radius; MYT120, 121, carpals; MYT6, 41, metacarpals; MYT7, distal metacarpal; MYT42, 89, astragalus; MYT42, calcaneum; MYT5, proximal metatarsal; MYT60, first phalanx
MTN: MTN1, astragalus.
MTLA: MTLA540, skull; MTLA546, P2sin; MTLA281, P2dex; MTLA195, i1; MTLA311, mandible; MTLA495, d2-d4 dex; MTLA420, atlas; MTLA252, humerus; MTLA137, 335, 482, 483, 535a, part of humerus; MTLA137, 241, 335, 482, radius; MTLA86, 120, 198, 482, part of radius; MTLA263, 291, magnum; MTLA40, 71, 75, 76, 117, 398, 399, 431, 450, metacarpal; MTLA256, pelvis; MTLA255, femur; MTLA59, 549, part of femur; MTLA81, 253, tibia; MTLA82, 170, 343, 353, 448, 449, distal tibia; MTLA41, 47, 426, 463, 484, 547a, astragalus; MTLA547c, 247, 279, 396, 470, 524, scaphocuboid; MTLA268, 547b, 341, 406, v5, calcaneum; MTLA72, 84, 210, 247, 279, 342, 352, 386, 387, 400, 401, 470, 550, metatarsal; MTLA377, 551, first phalanx.
MTLB: MTLB94, D2-M1dex; MTLB95, D2-M1sin; MTLB373, D2-M1sin; MTLB227, d2-m1dex; MTLB141, proximal radius & distal humerus; MTLB172 proximal femur; MTLB342, distal femur; MTLB349, distal tibia-young; MTLB375, 380, 400, astragalus; MTLB379, 386, 405, calcaneum; MTLB395, 403, scaphocuboid; MTLB249, metatarsal; MTLB345, 401, part of metatarsal; MTLB103, 378, phalanx I;
MTLC: MTLC12, d3-d4sin; MTLC17, 37, part of radius; MTLC14, 20, 21, 28, astragalus; MTLC13, 31, part of calcaneum
MTLD: nn postcranial specimens (old quarry leftovers)
PMMS: PMMS68, metacarpal; PMMS67, 76, 77 astragalus; PMMS76, 77, calcaneum.

AMNH:
Q4: AMNH22885, mandible with d3-d4 dex and d2-d4sin; AMNH20758, metacarpal; AMNH nn, astragalus; AMNH20753, scaphocuboid; AMNH20753, calcaneum; AMNH22845a & b, metatarsal.
Q6: AMNH22992, P4-M3; AMNH nn, metacarpal (see comment)
Q1: Skull AMNH 22786 (Q1 or Q5); AMNH20596, atlas; AMNH 20630, radius; AMNH20595, 95121, 20614, 95122, metacarpal; AMNH20688, 20680, 20595, tibia; AMNH23008, 2*nn, 95122 astragalus; AMNH20595, 20633, 20615, 20636, metatarsal.
Q5: AMNH nn D3-M1; AMNH22795a, D3-M1; AMNH22970, 22971, 22969, 22973, metacarpal; AMNH nn, astragalus; AMNH nn, scaphocuboid; AMNH nn, calcaneum; AMNH22968, 22966, 22967, metatarsal.
AMNH Nn, d2-d4, nl.

NHML: NHML M4299, tibia, nl.

MNHNP: MNHNP SMS3, astragalus

NHMW: NHMWnn, female skull with attached mandible;

NHMB: NHMB Sam29, female skull; NHMB Sam30, male skull; NHMB Sam28, D2-D4 (two specimens)

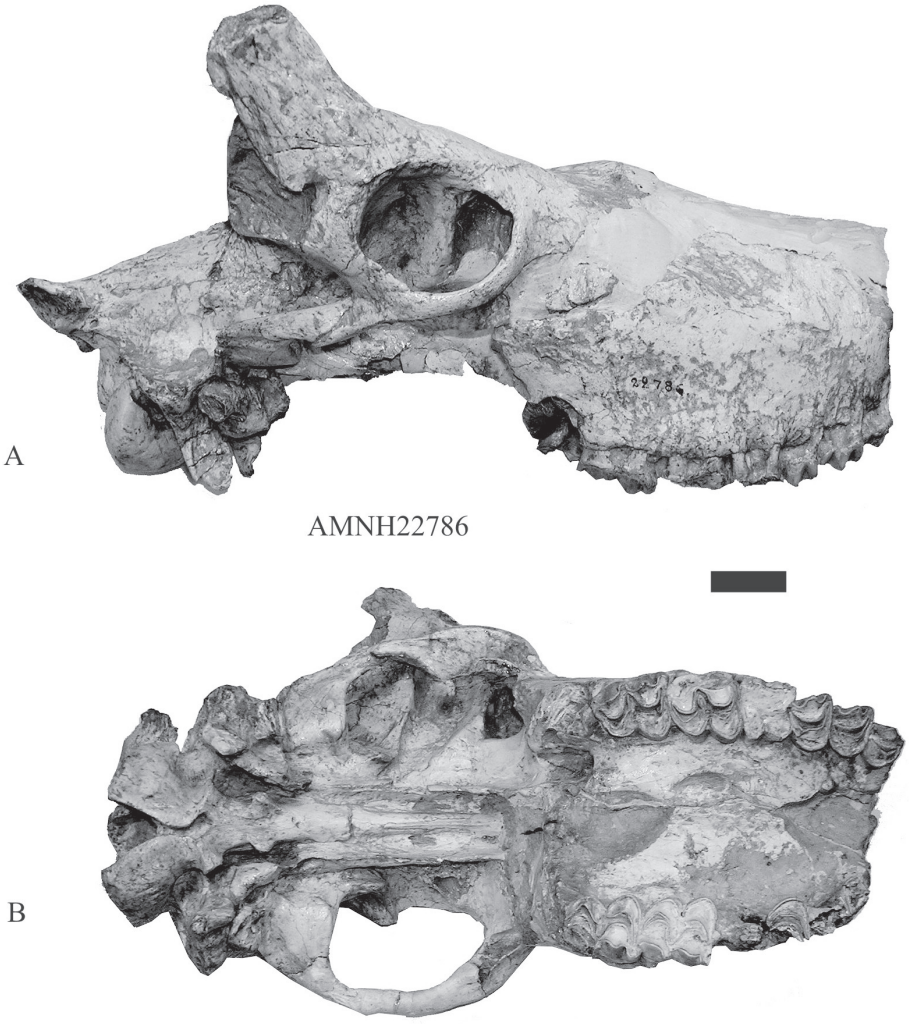

Figure 10: *Samotherium major*, cranium AMNH22786 from Q1 or Q5 in lateral (A) and ventral (B) view. Scale-bar 5 cm.

MGL: MGL S17, part of male skull; MGL S15, part of female skull; MGL S5, D3-M1; MGL S4, D2-M1; MGL S6, D2-D4; MGL S3, D3-D4; MGL S517, D2; MGL S10, M1-M3; MGL S495, S496, P3; MGL S14, P2; MGL S997, M3; MGL S1a,b, d2-d4; MGL S13, p2-m3; MGL S230, humerus; MGL S835, S850, distal humerus; MGL S349, S536, S947, radiocubitus; MGL S229, S574, S946, radius; MGL S32, S535, metacarpal; MGL S387, S898, S1058, S1239, proximal metacarpal; MGL S533, femur; MGL S838, S836, S453, distal femur; MGL S534, tibia and tarsals; MGL S853, distal tibia; MGL S231, S236, S329, S330, S383, S530, S531, S565, S592, S594, S598, S1066 astragalus; MGL S563, calcaneum; MGL S575, S727, scaphocuboid; MGL S94, S95, metatarsal; MGL S382b, S1063, proximal metatarsal; MGL S217, S335, S566, S1261 phalanx I; MGL S1021, S1050, phalanx II;

PIM: PIM286, ossicone; PIM299, PIM298, young ?female skull; PIM1013, female skull; PIM465, 467, 468, D2-D4; PIM271, PIM269, P4-M3sin; PIM296, P3-M3 dex; PIM280, P2-M3 sin; PIM295, P2-M3sin; PIM364, distal humerus; PIM379, 380, radius; PIM324, 326, 327, 328, 329, 330, 336, 337, 340 metacarpal; six astragalus without number indication; PIM48, 344, 346, 350, 352, 355, 359, 360 metatarsal.

Reference material:
NHMW (from Bohlin, 1926): NHMWnn, radius (2 specimens)
SMNS (from Bohlin, 1926): SMNS nn, skull with mandible
SMF: female skull illustrated by Bohlin (1926: Pl. IX, figs. 8-10); SMF3600, illustrated by Solounias (2007: fig. 21.4B); SMF2439, p2-m3.
NHML (from Iliopoulos, 2003): NHML M5432, tibia + tarsals

Description:
Few facts are known about the morphology and variation of *Samotherium major*. Bohlin (1926) offers a concise overview of most European skull and dental specimens attributable to this species without, however, entering into details. Some additional data on *S. major* comes from continental Greece and Turkey (Senyürek, 1954; Geraads, 1978, 1994) but species variation is still unknown. As a total, *S. major* is represented in the Samos fossil sites by four male (NHMB Sam30, MGL S17, AMNH22786, SMF3600) and seven female adult skulls (NHMB Sam29-lectotype, MTLA540, MGL S15, NHMW nn, PIM1013, SMF nn and SMNS-nn, the latter two referred to by Bohlin, 1926 but not seen). Two more 'hornless' skull-specimens are known from PIM

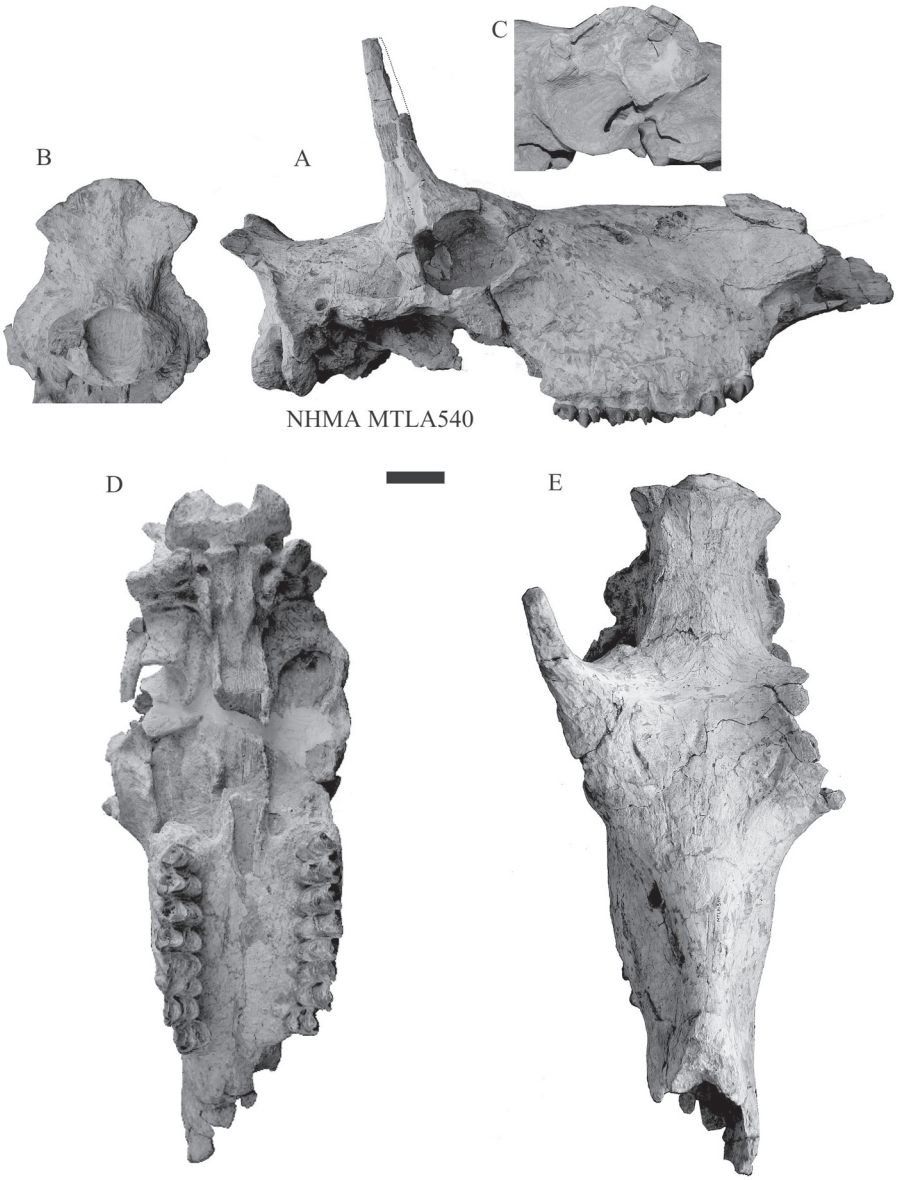

Figure 11: *Samotherium major*, NHMA MTLA540 in lateral (A), occipital (B), ventral (D) and dorsal (E) view and detail of left orbital area (C). Scale-bar 5 cm.

(PIM298, PIM299). Bohlin (1926:89) refers to one of them as belonging to a female of *S. boissieri*. Obviously it is about PIM 299 (the only one of the three PIM skull-specimens on which Bohlin could take the measurements he gives), which, however, belongs to a young individual (M1 is just erupted), justifying its smaller dimensions. **Skull**. NHMB Sam30 (Fig. 9) and AMNH22786 (Fig. 10) belong to individuals of comparable ontogenetic age (M3 in moderate to advanced wear stage); MGL S17 does not retain its maxilla but it could belong to a younger – still adult – individual. The ossicone is placed above the posterior part of the orbit, as in *S. boissieri* but its development and orientation appear to be notably different. The ossicone extends posteriorly up to the notch between the temporal crest and the mastoid process. Its length exceeds 450 mm in NHMB Sam30 and is about 350 mm in MGL S17 (preserved length = 330 mm) and less than 200 mm in SMF3600; the apices are pointed in NHMB Sam 30 but they look polished in MGL S17 and SMF3600 (Solounias, 2007: fig. 21.4B). In SMF3600 and MGL S17 the ossicone is robust (59 x 80 mm in MGL S17), barely curved to the rear in its upper part and weakly inclined backwards and laterally. In AMNH22786 and NHMB Sam30 the ossicone is even sturdier (79 x 133 mm in NHMB Sam30 and -*132.5 in AMNH22786), straight and points posterolaterally but not horizontally as Bohlin (1926:88) implies (Fig. 9). The basal cross-section of the ossicone varies from elongated elliptical in MGL S17 to elongated triangular in NHMB Sam30 and AMNH22786. All the known female skulls of *S. major* appear to be 'hornless' except for MTLA540, which on the right side preserves a moderately short (preserved length 140 mm), thin (TD x APDbase = 47.2 x 42.5 mm), straight and almost uprightly inserted ossicone with a sub-squarish cross-section (Fig. 11A); in lateral profile, its anterior face is slightly concave and its posterior face slightly convex; the posterior margin of the ossicone's basal part is well in front of the notch between the temporal crest and the mastoid process (Fig. 11A). The notably smaller size and the different pattern and placement of the MTLA540 ossicone in comparison to those of MGL S17, SMF3600, AMNH22786 and NHMB Sam30 implies that it is the first 'horned' female of *S. major* ever

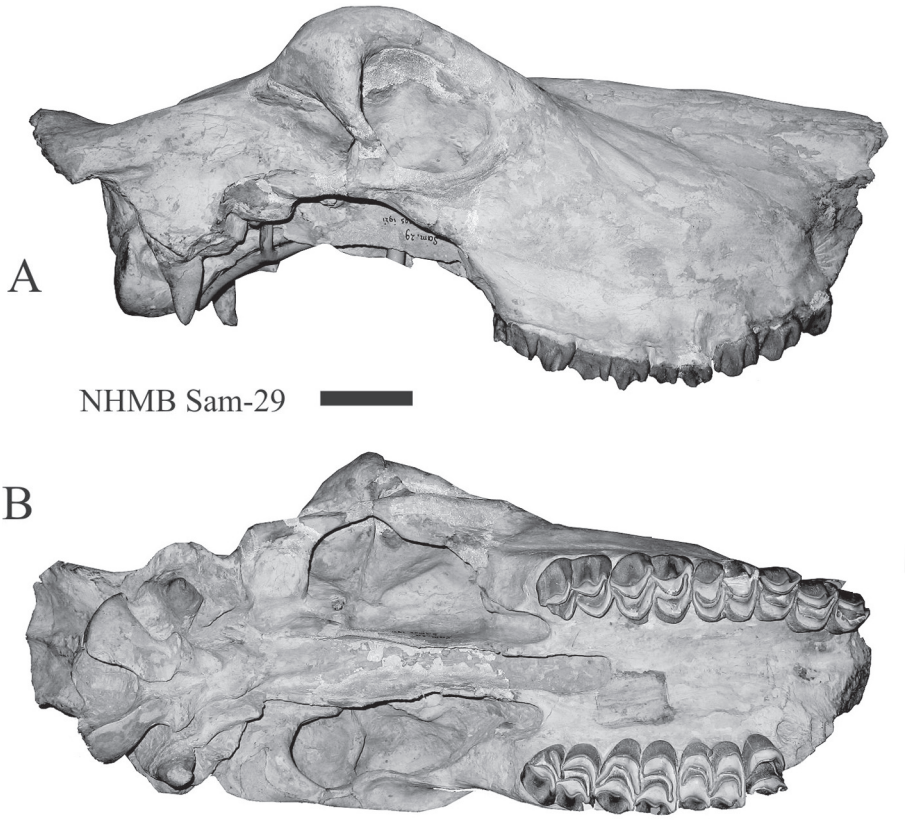

Figure 12: *Samotherium major*, NHMB Sam29, lectotype, in lateral (A) and ventral (B) view (by courtesy of NHM Basel). Scale-bar 5 cm.

known, since the rest of the cranial features between these specimens are almost identical. On the other hand, the ossicone of MTLA540 is probably analogous to the thick, protruding hollowed postero-dorsal orbital region seen in all the rest of *S. major* female skulls (Figs. 12, 13). A second *Samotherium* specimen with fully compatible morphology to MTLA540 is exhibited in the Paleontological Museum of Kiev. The occasional presence of ossicones on females of *S. major* follows the endowment of *S. boissieri* (i.e., the MGL S202 skull) as well as *Palaeotragus rouenii* and other large *Samotherium* species such as *S. sinense* and *S. eminens*.

The basic skull structure of the male skull of *S. major* is similar to that of *S. boissieri* (Table 6). The basicranial angle is very low and the alveolar level is parallel to the naso-parietal one. In lateral aspect, the braincase roof appears undulated: the postero-dorsally raised nuchal crest is followed anteriorly by the concave posterior part of the parietal and then by a hump in fronto-parietal position. This profile is less intense in the 'hornless' female skulls (Fig. 12, 13) but does not differ from the profile seen in MTLA540 (Fig. 11). On the other hand, the parietal crests are strong and show a similar sexual bimodality as in *S. boissieri*, with MTLA540 being closer to the males (Fig. 11E). Evidently both features (undulated lateral profile and convergent parietal crests) are not strictly related to the sex but they constitute the mechanical response of the skull to the presence of ossicones.

The zygomatic arches run parallel to the sagittal plane. The opisthocranium is short in relation to the face and relatively shorter than in *S. boissieri* (Figs. 9-12). The occipital condyles are large and, similar to *S. boissieri*, they point in postero-ventral direction, having an almost upright position. The foramen magnum is large and quadrangular. In posterior view, the occiput fans out dorsally and significantly projects to the rear, leaving the semicircular mastoid level behind it (Fig. 11B); in 'hornless' females this distinction is much less pronounced and the occiput looks more rectangular (Fig. 12B). The nuchal crest is strong, interrupted in its median part by a small notch. The external occipital protuberance is weak followed downwards by a short and blunt median occipital crest. The mastoid faces posteriorly. The paroccipital processes have a more vertical position than in *S. boissieri* and they exceed below the condyle level. As in *S. boissieri*, the auditory bulla is bean-shaped, relatively small compared to the skull size and is restricted between the tuberosities of the basioccipital. The basioccipital is more elongated than in *S. boissieri* but with similar structure; the posterior tuberosities are strong, crest-like and almost perpendicular to the sagittal plane, while the anterior tuberosities run parallel to the sagittal plane, forming tubercles in females but strong wings in males and MTLA540 (Figs. 10B, 11D, 12B). A wide groove runs along the central body of the basioccipital between its tuberosities. The foramen ovale is small and opens in front of the anterior tuberosities of the basioccipital.

Both in males and females the choane is "U"-shaped and prolongs much more anteriorly than the lateral indentations, reaching the M2-M3 border (Figs. 10-12). Nevertheless, the male choane is wider than the female one. In *S. boissieri* (NHML M4216) the choane is rather

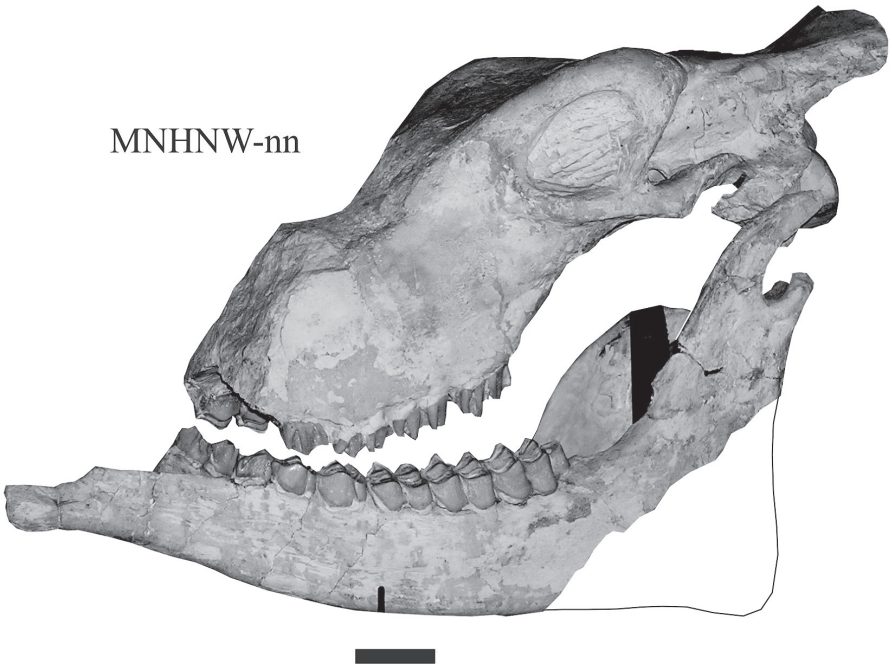

Figure 13: *Samotherium major*, skull NHMW- nn in lateral view. Scale-bar 5 cm.

	LP2-M3	LP2-P4	LM1-M3		Lp2-m3	Lp2-p4	Lm1-m3
S. boissieri							
NHML M4215	180.5	76.9	111.0	**NHML M4224**	189.2	72.2	119.0
NHML M4216	176.0	70.6	104.5	**NHML M4234**			
NHML M4225	172.0	72.6	104.3	**NHML M4235**	182.2	72.4	110.4
NHML M4226	175.0	76.1	105.5	**NHML M4236**	177.5	70.2	109.7
NHML M4219	176.5	72.0	105.9	**MGL S12**		67.6	
NHML M4223	162.7	72.6	91.8	**MNHNP SMS2**	182.0	70.0	114.0
NHML M4224	173.1	72.6	103.8	**AMNHnn.n***	183.7	71.0	112.0
NHML M4221			111.3				
MGL S202 dex			110.0				
BSPM-nn1*	180.0	71.0	115.0				
BSPM-nn2*	171.0						
SMF-a*	176.0	74.0	105.0				
SMF-b*	176.0	73.0	105.0				
S. major							
MTLA540 dex	193.0	80.0	121.0	**MTLA311**	205.5	77.5	132.1
AMNH22786 Q1/5	189.7	81.4	116.3	**MGL S13**	202.5	72.6	128.0
AMNH22992 Q6			112.5	**NHMW nn***	213.0		
NHMB Sam30	208.0		128.0	**SMF M24391**	201.0	74.0	130.0
NHMB Sam29	197.0	84.0	121.0	**SMF Skull***	217.0	84.0	133.0
NHMW nn*	205.0		125.0	**SMNS nn***	198.0	71.0	132.0
SMNSnn*	198.0	85.0	122.0				
MGL S10			124.0				
PIM271			109.1				
PIM280	195.0	83.5	117.6				
PIM295		80.0	121.0				
PIM269			108.7				
PIM296			120.3				

Table 8: Upper and lower permanent toothrow measurements of *Samotherium* from Samos.

*: data from Bohlin (1926).

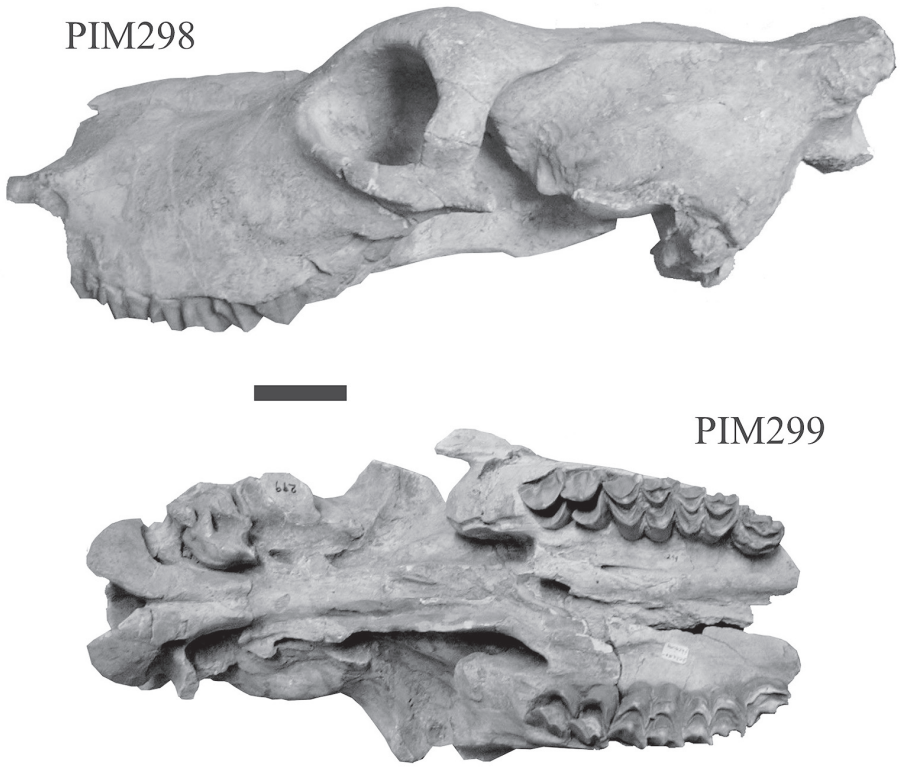

Figure 14: *Samotherium major*, young crania PIM 298 in lateral view and PIM 299 in ventral view. Scale-bar 5 cm.

"open-V" shaped and goes slightly more forward than the lateral indentations, reaching the posterior lobe of M3. According to Solounias (2007), the anteriorly positioned indentation of the soft palate could be related to the verticality of the distal neck, suggesting a more upright neck condition for *S. major*.

The 'periscopic' position of the orbit is less intense than in *S. boissieri*. Independent of sex, half of the orbit is placed above the level defined by the upper surface of the nasals in *S. boissieri*, whereas in *S. major* only ⅓ of the orbit surpasses this level (Figs. 10-13), but deformation might exaggerate the characteristic in *S. boissieri*. Furthermore, the orbit is much more posteriorly placed in *S. major* than in *S. boissieri*, with its anterior margin well behind M3 (Figs. 10-13). The humps seen on the anterodorsal orbital margin of the *S. boissieri* male skull are much weaker or they are completely missing from *S. major*. The general orbital shape of *S. major* males is similar to that of *S. boissieri* but 'hornless' females of the larger species have a more elliptical orbit with a thick posterior border (Fig. 12, 13 and Senyürek, 1954; Geraads,1994). The supraorbital foramens are placed into elongated grooves on the frontals. The entire supraorbital region is strongly pneumatized; the frontals are 29 mm thick in the specimen MGL S15 (that means ~45% more than in *S. boissieri* MGL S202). In MTLA540 the left supraorbital region shows at least one large and two smaller aerial chambers (Fig. 11C).

The nasals are thin and elongated with their widened posterior part above M2-M3 (Fig. 11E). The lachrymal depression is much wider and longer in *S. major* than in *S. boissieri*, reaching the P2 level. The ethmoidal fissure of *S. major* is defined by the same bone elements as in *S. boissieri* but is much smaller and "tear-drop" shaped (Fig. 11A). Its posterior margin is placed above M3 instead of above M1-M2 in *S. boissieri*. The infraorbital foramen opens into a bone-pocket in front of and above P2. The interalveolar margin of MTLA540 forms a strong arch (Fig. 11A), clearly more accentuated than that seen in the male of *S. boissieri* (Fig. 6). The narial opening is lower and wider than in *S. boissieri*.

The young skulls PIM298 and PIM 299 are usually assigned to females because of the absence of ossicones but since the age of ossicone fixation/emergence on the *Samotherium* skull is not known, their sex is rather questionable (Fig. 14). According to the previously described differences between males and females of *Samotherium* it is quite possible that PIM299 represents a young male and PIM298 a young female of *S. major*. The anterior margin of the choane reaches the middle of M1; the anterior margin of the orbit is placed behind M1 and the orbits are situated completely below the nasal level (Fig. 14); the parietal and occipital crests are already well developed; the ethmoidal fissures are thin but much longer than in the adults (Fig. 14); a short facial crest is present, while absent in the adults; the crest-like temporal lines are much clearer than in the adult skulls.

The general profile of the adult mandible MTLA311 is similar to that of *S. boissieri*, but the coronoid process is shorter and less curved backwards and the back border of the vertical ramus is less concave. The height of the horizontal ramus increases considerably with age; in the specimen MTLA495 with not fully erupted d2, the height of the mandible between d2-d3 is just 25.5 mm, becoming 40 mm in MTLC12 with unworn milk dentition, 49.9 mm in MTLB227 with worn milk dentition and finally 58 mm between p2-p3 in the adult mandible MTLA311.

	L	TDprox	TDdia	APDdia	TDdis
S. boissieri					
AMNH22829 Q2	420.0	[100]	56.0	69.0	
NHML M4252	406.0	122.0	56.5	70.4	105.7
NHML M4255			56.5	66.0	97.8
NHML M4256			56.0	59.5	99.6
NHML M4257			46.0	61.0	
S. major					
MTLA252	465.0		73.0	70.3	143.7
MTLA137			74.9	76.6	143.9
MTLA335			75.6	70.6	134.7
MTLA482			73.8	74.4	141.0
MTLA483			75.0	75.1	140.0
MTLA535					148.2
MTLB141			75.9	74.5	132.4
MGL S230	420.0	150.0			
PIM364			65.0	69.0	
H. duvernoyi					
MTLA312			84.6	83.0	150.2
MTLA315			87.7		158.5
MTLA462				83.1	157.0
MGL S570	475.0	158.0	76.5	72.5	134.0
MGL S834					148.1
PIM400					131.5

Table 9: Humerus measurements of *Samotherium* and *Helladotherium* from Samos.

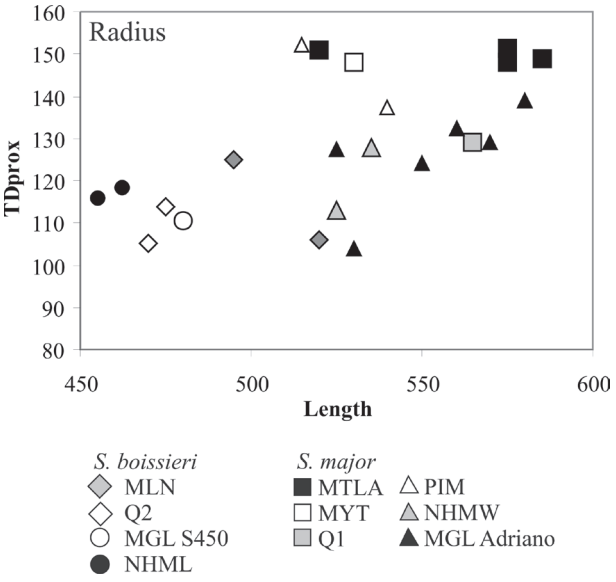

Figure 15: Scatter diagram comparing the radius proportions of *Samotherium* from various Samos sites and collections (sources: pers. data). *S. boissieri*: MLN, Q2, NHML, MGL S450; *S. major*: MYT, MTLA, Q1, PIM, MGL-Adriano, NHMW.

Dentition. There are no significant morphological differences in the milk dentition between *S. major* and *S. boissieri*, except for the more advanced structure of d2 on which an incipient paraconid is present and the metaconid is clearly distinguishable from the entoconid. Furthermore, the metaconid is much longer than in *S. boissieri* and the trigonid appears closed from the first stage of wear. The anterior lobe of D3 is fully molariform. The D2-D4 length ranges from 85.9 to 91.5 mm and that of d2-d4 from 85.2 to 99.0 mm (Table 7).

The P2-M3 length ranges between 189.7 and 208.0 mm, being on average 13.5% larger than that of *S. boissieri* but with a similar premolar/molar ratio of 68.7% (66.1-71.0, n=6) (Table 8). The upper toothrow of *S. major* is also very similar to that of *S. boissieri* (Fig. 7). P2 is asymmetrically rounded with an incipient antero-lingual notch. The paracone is more projected labially than the strong parastyle, whereas the metastyle is always weak. On the central cavity, a posterior fold is present in 1 out of 4 specimens. P3 is more symmetrical lingually, with a stronger parastyle and metastyle than on P2. A posterior fold is present in 5 out of 6 specimens. P4 is like P3 but much wider. A postero-lingual tubercle is occasionally present on some P3 and P4 (PIM296, MTLA540; Fig. 7). The molar morphology does not differ from that of *S. boissieri* but a buccal cingulum and basal pillars are more frequent and in some specimens (AMNH22992, M3 of PIM296) exceptionally strong (Fig. 7). The i1, i2 (MTLA195, MTLA311) are shovel-shaped and long and jut rather forward. The lower premolar/molar ratio ranges from 53.8 to 63.1 (mean=57.8, n=5), suggesting a relatively shorter premolar row than in *S. boissieri* (mean=63.6) (Table 8). The p2-m3 length is 198.0-217.0 mm, being on average 12.7% larger than in *S. boissieri*. Apart from p2, the premolar morphology appears to be more stabilized than in *S. boissieri* (Fig. 8). The p2 hypoconid is well-developed in MTLA311 and NHMW nn but not individualized labially in MGL S13. The entoconid and entostylid are always strong, the parastylid is well-developed and the metaconid is rounded, independent and centrally placed; the paraconid is very thin is MTLA311 and absent from NHMW nn. The p3 shows advanced molarization with a well-developed but narrow hypoconid, a well-marked parastylid and continuous lingual wall on the trigonid. In early stages of wear the elongated and anteroposteriorly oriented metaconid is just in contact with the posteriorly directed paraconid, but they fuse together quickly afterwards. The strong, elongated entoconid is obliquely placed. The p4 looks like a large version of p3 (Fig. 8). The lower molar morphology is comparable with that of *S. boissieri*.

Postcranials. Limb-bone morphology of *S. major,* mainly from the NHMA and AMNH is compared with that of *S. boissieri* (NHML, MLN, Q2) as well as with an *Helladotherium duvernoyi* sample from the NHMA, Pikermi (NHML, MNHNP) and Perivolaki (LGPUT).

Two atlases, MTLA420 and AMNH20596 from Q1 can be attributed to *S. major*. Their description is given in comparison with the specimen PMMS82 of similar size, which is assigned to *Helladotherium duvernoyi*. In dorsal view, the atlas of *S. major* (Pl. 2, fig. 1) looks more symmetrical than that of *H. duvernoyi* (Pl. 3, fig. 8), in which the width and the height decrease to the rear (MTAL420: H=102.6 mm, TDprox = 124.4 mm, TDdis = 132.8 mm;

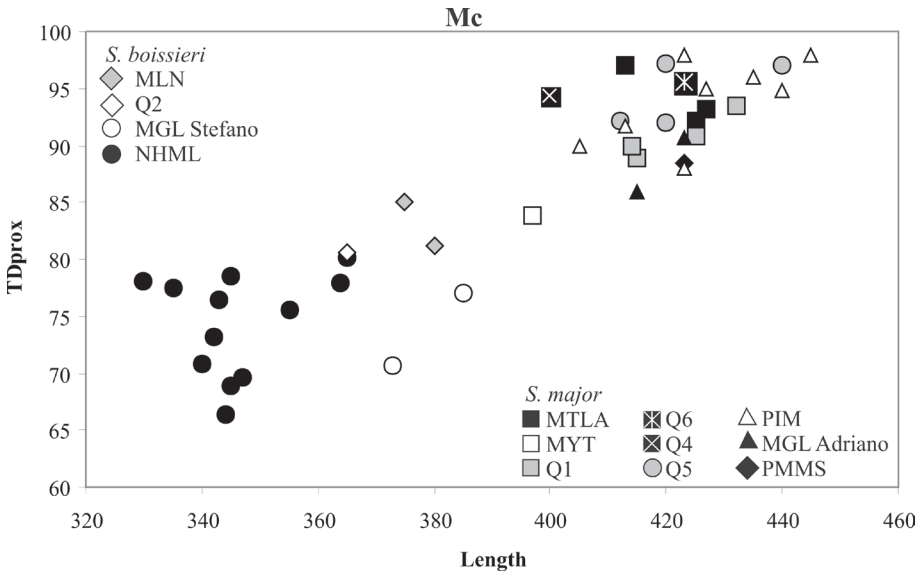

Figure 16: Scatter diagram comparing the metacarpal proportions of *Samotherium* from various Samos sites and collections (sources: pers. data).

S. boissieri: MLN, Q2, NHML, MGL-Stefano; *S. major*: MYT, MTLA, PMMS, Q4, Q6, Q1, Q5, PIM, MGL-Adriano.

PMMS82: H=94.4 mm, TDprox = 135.3 mm, TDdis = 120.0 mm). The dorsal anterior lobes of the wings are well rounded in both species but somewhat ventrally curved in *H. duvernoyi*. The anterior rim of the dorsal anterior arch forms a deep "V"-shaped notch in *S. major* (Pl. II, fig. 1), instead of an open "U"-shaped indentation in *H. duvernoyi* (Pl. 3, fig. 8). The anterior rim of the ventral anterior arch is semicircular-shaped in *S. major* with weakly developed anterior lobes, whereas in *H. duvernoyi*, the lobes are stronger and the central part of the anterior rim is straight, interrupted by a small tubercle. In *S. major*, the dorsal tubercle is much more prominent, slopes gently to the front and is hump-like with a weak longitudinal crest. In *H. duvernoyi*, the dorsal tubercle slopes more steeply and is rather flat with a well-developed central crest. The dorsal view of the alar foramen faces more laterally in *H. duvernoyi* and is teardrop-shaped instead of oval in *S. major*. The posterior angular processes are weakly developed in *S. major*; they are broken in PMMS82. In ventral view, a strong longitudinal crest runs along the sagittal plane of the *S. major* atlas (Pl. 2, fig. 1), whereas in *H. duvernoyi* it is replaced by a blunt, elongated hunch. The ventral mark of the alar foramen is smaller in *S. major* and faces rather laterally, whereas it is larger, triangular-shaped and facing ventrally in *H. duvernoyi*. The posterior wing depression is deep and localized in *H. duvernoyi* while in *S. major* it is shallower, wider and divided in two parts by a weak crest.

The humerus length is on average 14% longer in *S. major* than in *S. boissieri* (Table 9) while the increase of transverse diameters appears much more enlarged, reaching 40%. Apart from the size, there are minor morphological differences between the humerus of *S. boissieri* and *S. major*. In both species the deltoid tuberosity is placed laterally, being smaller than in *H. duvernoyi* (MTLA 312, 315, 462) and the radial fossa is well developed and larger than in *H. duvernoyi*. Also different from *H. duvernoyi*, the humerus torsion is weaker in *S. boissieri* and *S. major* (Pl. II, fig. 15), the distal trochlea is more symmetrical in cranial view, the lateral epicondyle projects strongly laterally and the lateral surface of the distal part of diaphysis faces mainly laterally, instead of anteriorly as in *Helladotherium*. The olecranon fossa is wide and shallow in *H. duvernoyi*, instead of narrow and deep in *S. boissieri*; in *S. major* the olecranon fossa appears wider and shallower than in *S. boissieri* but still narrower than in *Helladotherium*. In distal view, the upper edge of the distal trochlea of *H. duvernoyi* slopes gently to the lateral side, while in *S. boissieri* and but less in *S. major*, the same edge slopes more steeply because of the greater development of the medial epicondyle (Pl. 2, fig. 15). In lateral view, the angle between the horizontal plane and the main longitudinal axis of the lateral condyle is much larger in *H. duvernoyi* than in *S. boissieri*, with *S. major* having an intermediate position.

The ulnar diaphysis is much more developed (especially anteroposteriorly) in *S. boissieri* than in *S. major*, where its distal part, below the middle of radius height, appears like a longitudinal crest upon the radius (Pl. 2, fig. 18). The average increase of radius length from *S. boissieri* to *S. major* is 15% (Fig. 15; Table 10), whereas the increase of transverse enlargement ranges from 20-30%. On the other hand, the morphological differences between the radius of *S. boissieri* and *S. major* do not exceed observed variability within each species. As in *S. boissieri*, the radiocubitus of *S. major* is less concave in lateral view than that of *H. duvernoyi* and it has a shallower olecranon and a much less developed shaft of the ulna (MTLA534, 535; Pl. 3, fig. 3). In contrast to *H. duvernoyi*, the distal radial epiphysis of *S. boissieri* and *S. major* projects stronger mediolaterally in relation to the shaft (Pl. 2, fig. 18 and Pl. 3, fig. 3; Table 10). In proximal view, the medial facet of the capitular fossa is well-rounded in *H. duvernoyi* with a strong peripheral lip instead of a sub-quadrangular one in *S. boissieri* and *S. major*. The lateral facet of the capitular fossa is deeper and more oblique in *S. boissieri* and *S. major* than in *H. duvernoyi*. The caudal indentations for the attachment of the ulna are much better-marked in *Helladotherium* than in *Samotherium*. The lateral protuberance is strong and highly positioned in *S. boissieri* and *S. major* but weak and

low in *H. duvernoyi*. The radial tuberosity is stronger in *S. major* than in *S. boissieri*. The distal epiphysis of both *S. boissieri* and *S. major* is identical; it differs from that of *H. duvernoyi* by the shorter but deeper grooves for the extensor carpi radialis and the common extensor tendon, the stronger but shorter medial crest in comparison to the lateral one and the acute and parallel crests that define the lunar facet.

One left (MTLA291: TD=67.9 mm, APD=65.9 mm; Pl. 2, fig. 2) and one right (MTLA263: TD=71.1 mm, APD=65.3 mm), magnum are preserved and compared with MTLA292 of *H. duvernoyi* (DT=72.7 mm, APD=75.7 mm). The magnum of *S. major* is almost quadrangular and low comparatived to the magnum of *H. duvernoyi*. In *H. duvernoyi* the medial side bears two unequal protuberances separated by a relatively deep groove, extending distally; in *S. major* the medial wall is straight. In proximal aspect, the articular facet for the lunar is much narrower than in *H. duvernoyi*, especially in its posterior part. The back of the scaphoid facet is flat in *S. major* instead of concave in *H. duvernoyi*, in which the crest separating the two facets is much more elevated and sharp.

S. boissieri and *S. major* metacarpals differ from those of *H. duvernoyi* (MTLA248, 249) in the more slender diaphysis comparatived to the epiphyses, especially regarding the distal one, the closed sinovial fossa, the semicircular proximal articular surface without posteromedial and palmar tubercles and the much less developed crests along the palmar rims of the diaphysis (Pl. 2, figs. 9-12; Pl. 3, fig. 5; Table 11). On the proximal epiphysis, the anteromedial tuberosity is barely recognizable in *S. boissieri* but well-marked on the metacarpal of *S. major*, allowing the medial articular facet towards a more rounded anterior rim (Pl. 2, fig. 12). A lateral tubercle comparable to that of *H. duvernoyi,* but less developed, is also present in *S. major*, while it is missing from *S. boissieri*. The size increase from *S. boissieri* to *S. major* reaches 17% in the metacarpal length and about 22% in the transverse diameters (Fig. 16). The robusticity index does not change from *S. boissieri* (10.4-13.6; mean=12.45; n=12) to *S. major* (10.3-13.8; mean=12.48; n=22), always being smaller than in *H. duvernoyi* (13.2-17.4; mean=15.4; n=15). The ratio between the transverse diameter at the middle of the diaphysis and at the distal articulation ranges from 50.7 to 61.1 (n=12) in *S. boissieri* and from 47.8-59.5 (n=19) in *S. major*, always being larger than 60 in *H. duvernoyi* (60.9-69.6; n=14). Apart from size the metacarpals of *S. major* differ from those of *S. boissieri* in the more developed plantar tubercles of the proximal epiphysis, the less oblique crest dividing the proximal articular facets and the blunter keel of the distal trochleas.

An almost complete *S. major* pelvis, MTLA256 (Pl. 2, fig. 14), is preserved. In lateral aspect the shaft of the ilium and the shaft of the pubis are placed on the same plane (180°) and the shaft of pubis forms an acute angle with the ischium. In *H. duvernoyi* (MTLA469) the shaft of the ilium forms an obtuse angle with the shaft of the pubis, whereas the angle between the shaft of the pubis and the ischium is almost right. The lateral and medial borders of the ilium diverge moderately in *S. major* (115°) instead of strongly (140°) in *H. duvernoyi*. The shaft of the ilium is much more robust in *S. major* than in *H. duvernoyi*. The obturator foramen is oval in *S. major* but more elliptical in *H. duvernoyi*. In ventral view, the depression for the median tendon of the rectus femoris is stronger in *H.*

	L	TDprox	TDdia	TDdist
Samotherium boissieri				
MLN25	520.0	105.8	60.1	98.0
MLN46	495.0	125.0	60.6	98.6
MLN76				91.0
AMNHnn				89.4
AMNH22808 Q2	470.0	105.2	57.5	95.0
AMNH22820 Q2	475.0	114.0	43.2	95.4
NHML M4259	462.0	118.3	63.2	98.0
NHML M4260	455.0	116.0	57.5	93.5
NHML M4262	452.0		54.8	91.5
NHML M4264A			65.4	99.6
NHML M4264B				87.8
NHML M4264C				94.3
NHML M4264D				93.0
MGL S450	480.0	110.6	60.0	91.0
Samotherium major				
MYT14	530.0		72.0	109.2
MYT37		148.2		
MTLA137	585.0	149.0	82.0	125.0
MTLA241	575.0	151.5	83.1	125.7
MTLA335	575.0	148.0	72.5	118.6
MTLA482	520.0	150.8	81.0	128.6
MTLA86				117.8
MTLA198		140.4		
MTLB141		142.3		
MTLC17		140.0	75.0	
MTLC37			77.5	122.5
AMNH20630 Q1	565.0	129.0	65.0	115.6
MGL S536	570.0	129.0	75.5	105.0
MGL S947	530.0	104.0	66.5	
MGL S229	580.0	139.0	91.0	128.0
MGL S349	560.0	132.5	74.7	115.6
MGL S946	525.0	127.5	71.0	100.0
MGL S574	550.0	124.0	66.0	101.2
PIM379	515.0	152.0	62.6	121.0
PIM380	540.0	137.5	72.0	109.5
NHMWnn*	525.0	113.0	65.0	
NHMWnn-b*	535.0	128.0	78.0	
Helladotherium duvernoyi				
MTLA534	590.0	149.5	92.3	132.6
MTLA535b	560.0	147.0	86.0	
MTLA278		175.6	100.6	
MTLA461				150.0
PIMnn*	610.0	150.0	79.0	138.0

Table 10: Radius measurements of *Samotherium* and *Helladotherium* from Samos. *: data from Bohlin (1926).

	L	TDprox	APDprox	TDdia	APDdia	TDdis	APDdis
Samotherium boissieri							
MLN9	375.0	85.1		51.0	39.0	88.5	42.5
MLN80	380.0	81.2	48.8			90.2	41.7
AMNH22828 Q2	365.0	80.6	44.6	48.7	37.0	84.2	40.0
AMNH(M4267)	343.0	76.4	48.0	45.0	37.0	80.5	38.7
AMNH15876	345.0	68.9	37.2	44.8	29.7	75.2	40.5
NHML4268	344.0	66.4		44.0	34.0	72.0	
NHML M4267	347.0	69.6	42.6	38.7	36.5	71.0	
“	345.0	78.5	40.5			78.5	41.0
“	364.0	78.0	51.5	42.2	38.3	82.7	43.5
“	355.0	75.5	50.7			74.5	44.1
“	342.0	73.2	44.3				
“	335.0	77.5	45.0	42.0	37.0	76.0	43.0
“	330.0	78.1	44.8	43.0	33.5	78.0	41.4
“	340.0	70.8	51.0	42.0	38.5	77.0	41.5
“	365.0	80.2	47.0	45.5	37.5	89.7	46.0
MGL S789	373.0	70.6	49.3	39.0	42.6	73.2	45.3
MGL S787	385.0	77.0	54.0	50.2	40.0	84.0	46.6
Samotherium major							
MYT6	395.0			50.3	45.0	90.8	50.8
MYT41	397.0	83.8	53.3	52.4	43.2	88.0	47.6
MYT7						105.7	54.0
MTLA40		100.8	55.6				
MTLA75	413.0	97.1	61.3	56.3	48.0	99.6	55.7
MTLA76	425.0	92.2	59.3	58.7	46.1	105.5	55.0
MTLA117				57.3	44.4	106.8	55.8
MTLA398		91.0	62.6	51.0	42.1		
MTLA399				55.3	42.5	106.9	55.7
MTLA450	427.0	93.2	61.4	54.2	43.7	97.4	52.4
PMMS68	423.0	88.4	58.5	50.4	46.0	94.4	51.5
AMNH20758 Q4	400.0	94.3	60.2	53.5	44.8	100.6	55.6
AMNH nn Q6	423.0	95.6	59.6	57.5	53.4	107.4	55.1
AMNH20595 Q1	425.0	90.8	61.0	54.1	45.0	99.3	55.0
AMNH95121 Q1	415.0	88.9	56.8	53.4	46.0	97.1	52.2
AMNH20614 Q1	432.0	93.5	55.8	49.3	43.9	94.2	55.6
AMNH95122 Q1	414.0	90.0	56.3	52.0	40.5	99.3	52.1
AMNH22970 Q5	420.0	97.2	58.0	43.2	49.8	100.1	54.5
AMNH22971 Q5	440.0	97.0	59.0	57.2	48.0	106.9	55.2
AMNH22969 Q5	412.0	92.1	54.5	55.6	45.3		51.8
AMNH22973 Q5	420.0	92.0		54.0	41.9	95.2	50.0
MGL S32	415.0	86.0	54.0	47.6	43.8	104.3	49.3
MGL S535	423.0	90.7	57.0	50.3	45.7	100.0	53.3
PIM324	427.0	95.0	50.0	47.0	45.5	98.2	54.0
PIM328	440.0	94.8	56.3	55.0	50.0	104.5	56.5
PIM330	445.0	98.0	61.5	52.0	48.0	100.3	53.5
PIM336	413.0	91.7	55.0	51.7	45.0	97.0	49.3
PIM337	405.0	90.0	53.8	49.3	39.1	92.0	49.3
PIM327	435.0	96.0		55.0		98.0	
PIM340	400.0			55.0			
PIM326	423.0	98.0		58.0		102.0	
PIM329	423.0	88.0		50.0		99.0	
Helladotherium duvernoyi							
MTLA248	425.0	123.0				108.5	61.8
MTLA249	438.0	113.0	70.3	70.0	50.0	105.7	61.2
AMNH20610	447.0	107.1	69.6	64.2	52.6	98.3	58.8
MGL S322		103.5	63.5				
PIM339		114.5	77.5				
PIM338						105.0	72.0
SMF2436*		[120]					

Table 11: Metacarpal measurements of *Samotherium* and *Helladotherium* from Samos.

*: data from Bohlin (1926).

Table 12: Femur and tibia measurements of *Samotherium* and *Helladotherium* from Samos.

*: data from Iliopoulos (2003).

FEMUR	**L**	**Lhead**	**APDhead**	**TDdia**	**TDdis**	
Samotherium major						
MTLA255	540.0	78.5	83.7	67.8	131.4	
MTLA59				60.5	150.4	
MTLA549		85.9	88.5			
MTLB172		91.0	83.3			
MTLB342					144.5	
MGL S533	520.0	88.0	76.5	60.8	142.0	
MGL S838					148.0	
MGL S836					140.2	
MGL S453					148.5	
Helladotherium duvernoyi						
MTLA73	550.0	90.2	74.3	71.8	164.4	
MTLA320				62.7	136.3	
PMMS103	500.0	86.0	75.0		144.5	
TIBIA	**L**	**TDprox**	**TDdia**	**APDdia**	**TDdist**	**APDdis**
Samotherium boissieri						
MLN47	[430]		50.9	42.0		
MLN21					89.0	
MLN24			59.0	41.0		
MLN60				40.7	95.0	
MLN78			52.9	42.3	81.5	65.5
AMNH28825	448.0	127.8	61.2	49.4	76.5	68.2
NHML M4275	455.0	107.3			77.2	62.8
NHML M4275B	457.0		63.5		86.6	61.4
NHML M4278	455.0	135.1	60.3		75.7	62.2
MGL S452	[460]	129.0			88.0	
MGL Snn	507.0	132.0	58.6	50.0	85.5	70.0
MGL S937					81.0	63.7
Samotherium major						
MTLA81	518.0	140.0	74.0	54.0	96.0	77.7
MTLA253	543.0		72.3		102.8	86.0
MTLA82			77.8	53.2	106.3	70.0
MTLA343					108.0	71.0
MTLA449			78.0	60.4	109.7	84.0
MTLA353					95.5	77.0
MLA170					104.6	82.0
MTLB349-young					87.0	
AMNH20688 Q1	500.0	152.7	68.5	53.9	103.5	75.9
AMNH20680 Q1	510.0		61.5	50.6	102.5	75.1
AMNH20595 Q1	545.0	156.5	72.9	58.9	100.6	81.7
NHML M4299	510.0	134.8	70.5			
NHML M5432*	521.0					
MGL S534	550.0	156.0	73.0	55.0		106.5
MGL S853					95.5	75.0
Helladotherium duvernoyi						
MTLA74	565.0	181.0	74.7	56.0	116.0	81.2
MTLA313	525.0	165.3	78.9	53.4	116.6	83.3
MTLA83					113.9	81.8
MTLA254					116.4	82.5

duvernoyi than in *S. major*. In dorsal view and between the ischiatic spine and the acetabulum there is a wide depression in *S. major*; in *H. duvernoyi* it is narrower and shallow. The acetabulum is round in *S. major* (129.6 x 112.0 mm) instead of elliptical in *H. duvernoyi* (129.6 x 102.0 mm; Pl. 3, fig. 4). No *S. boissieri* femur is known from the NHML collection or other Samos lower fossil-levels. The femur head of *S. major* is spheroid-shaped (MTLA255, Pl. 2, fig. 6; Pl. 3, fig. 7b) and it appears less elongated than the head of *H. duvernoyi* in proximal view (MTLA73, PMMS103; Pl. III, fig. 7a, b); the femoral head proportions (L_{head} x 100/APD_{head}) is 94-97 in *S. major* versus 114-122 in *H. duvernoyi* from Samos (Table 12). In medial aspect, the neck deviation from the central longitudinal axis of

	Llat	Lmed	TDdis
Samotherium boissieri			
MLN34	90.8	78.5	57.6
MLN64	96.5	82.3	59.7
MLN65	97.5	85.1	58.4
MLN68	89.2	78.6	59.3
AMNH(M4283)	89.0	79.2	58.0
NHML M4283A	88.4	78.0	59.0
NHML M4283B	86.8	73.7	56.4
NHML M4283C	85.6	75.0	56.8
NHML M4283D	89.3	76.2	61.0
NHML M4283E	84.4	76.5	53.5
MGL S601	88.8	77.6	55.0
MGL S586	89.0	75.8	59.0
MGL S864	86.0	77.2	55.7
MGL S1014	90.0	76.6	56.0
MGL S1015	92.2	81.0	62.3
Samotherium major			
MYT42	98.6	87.7	65.6
MYT89	100.8	88.4	66.5
MTN1	91.4	83.9	65.8
MTLA41		94.5	69.0
MTLA47		98.0	69.0
MTLA426	109.6	95.3	71.3
MTLA463	110.5		
MTLA484	109.8		
MTLA547a	113.6	102.2	73.7
MTLB375	104.3	95.7	70.0
MTLB380	106.4	95.7	72.0
MTLB400	105.7	94.1	70.4
MTLC14	103.2	95.0	70.4
MTLC20	104.5	95.5	72.0
MTLC21	97.7	88.5	

	Llat	Lmed	TDdis
Samotherium major continued			
MTLC28	96.5		
PMMS67	105.3	92.8	71.3
PMMS76	99.8	94.3	67.5
PMMS77	95.6	85.2	59.7
AMNH nn Q4	111.5	107.0	75.4
AMNH23008a Q1	100.0	89.7	67.7
AMNHnnA Q1	106.0	96.4	71.0
AMNHnnB Q1	102.0	93.0	64.2
AMNH95122 Q1	108.1	92.3	68.5
AMNH nn Q5	107.7	94.7	74.0
PIM A	100.3	90.0	69.5
PIM B	105.0	93.6	74.0
PIM C	106.0	95.8	74.5
PIM D	104.0	93.5	66.7
PIM E	105.5	93.5	70.0
PIM F	98.2	89.3	65.6
MGL S236	107.7	96.5	74.5
MGL S530	97.7	88.0	62.3
MGL S329	102.5	91.7	67.0
MGL S383	107.0	93.2	70.0
MGL S565	107.0	95.5	70.4
MGL S1066		90.0	63.7
MGL S598	94.0		65.0
MGL S592	99.5	87.5	62.6
MGL S231	101.0	93.0	67.2
MGL S531	105.8	92.1	65.0
MGL S330	102.0	90.0	64.4
MGL S594	100.8	92.6	70.0
MNHNP SMS3	110.9	97.1	74.3
Helladotherium duvernoyi			
MTLA23	110.2	93.0	74.9

Table 13: Astragalus measurements of *Samotherium* and *Helladotherium* from Samos.

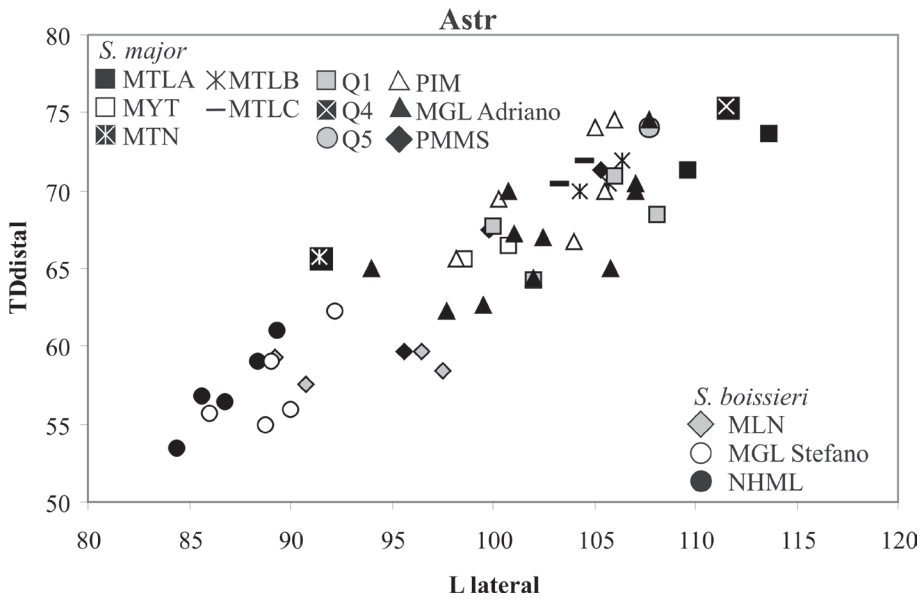

Figure 17: Scatter diagram comparing the astragalus proportions of *Samotherium* from various Samos sites and collections (sources: pers. data). *S. boissieri*: MLN, NHML, MGL-Stefano; *S. major*: MYT, MTN, MTLA, MTLB, MTLC, PMMS, Q4, Q1, Q5, PIM, MGL-Adriano.

the femur is stronger in *H. duvernoyi* than in *S. major*. The minor trochanter is less developed in *H. duvernoyi* and the trochantic fossa is narrower than in *S. major*. The distal trochlea of *S. major* has a more upright position (~70°) than in *H. duvernoyi* (~60°) and the condyles are more posteriorly shifted. The intercondyloid fossa is deeper and narrower in *S. major* than in *H. duvernoyi*. The medial and lateral epicondyles are barely recognizable in *S. major* but strong in *H. duvernoyi*. In cranial view, the supracondyloid fossa faces laterally in *S. major*, but

Table 14: Calcaneum measurements of *Samotherium* from Samos.

	Hmax	Hmin	TDst	APDst	TDmin	APDmin
Samotherium boissieri						
MLN10		100.3	57.5		23.9	55.8
MLN69	173.0	94.3	57.8	75.3	22.3	54.4
MLN70	170.0	93.2	62.6	77.5	22.6	56.7
MLN72	192.7	105.5		84.1	28.1	58.0
NHML M4282a	175.7	100.3	59.0	67.7		
NHML M4282b	173.9	97.9	51.0	71.3		
NHML M4282c	174.1	99.9	52.3	73.4		
NHML M4282d	169.4	97.6	48.6	73.5		
NHML M4282e	163.0	92.2	44.6	68.3		
Samotherium major						
MYT42	191.9	105.2	59.1	83.9	30.0	54.5
MTLA268	221.7	133.5	65.2	98.2	33.5	74.0
MTLA547b	209.4	117.7	67.0	91.3	31.3	71.6
MTLA341	203.0	114.0	67.0	89.0	30.5	69.6
MTLA406		122.0			35.7	
MTLA548	208.9	121.6	64.0	90.8	29.3	69.3
MTLB379			53.6	81.0	26.6	50.8
MTLB386	205.4	116.3	59.7	89.9	31.4	62.9
MTLB405					29.6	64.8
MTLC13			62.3	86.5	32.0	62.4
MTLC31			47.0	78.8		
PMMS76	202.2	111.4	62.9	88.1	35.4	67.5
PMMS77			59.0	89.8		
AMNH20753 Q4	208.7	134.8		90.3		
AMNHnn Q5	209.0	129.3	65.6	90.9		
MGL S563	200.0	128.0	54.5	83.2		

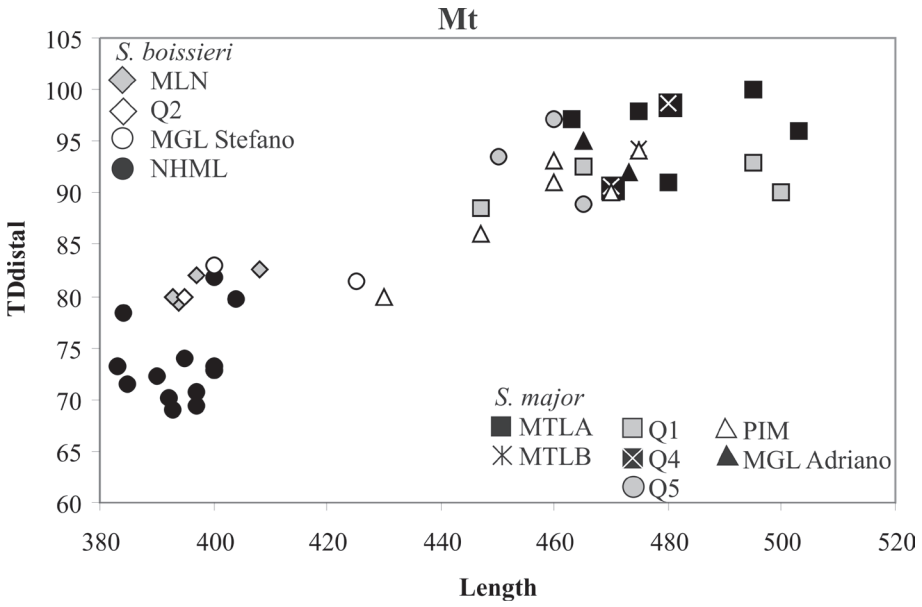

Figure 18: Scatter diagram comparing the metatarsal proportions of *Samotherium* from various Samos sites and collections (sources: pers. data). *S. boissieri*: MLN, Q2, NHML, MGL-Stefano, PIM; *S. major*: MTLA, MTLB, Q4, Q1, Q5, PIM, MGL-Adriano.

is placed more posteriorly in *H. duvernoyi*, in which the medial supracondyloid crest is much better-marked. The increase of tibia length between *S. boissieri* and *S. major* reaches on average 14% but morphology remains stable (Table 12). The *S. major* tibias are shorter and more slender than those of *H. duvernoyi* (MTLA74, 313; Pl. 3, fig. 6). The tibial crest is well developed with a blunt distal part; it appears to be shorter in *S. major* than in *S. boissieri*. The tibial tuberosity strongly curves laterally and is shorter in *S. major* than in *H. duvernoyi*. The tibial sulcus is narrower and deeper than in *H. duvernoyi* and its diaphyseal part is significantly depressed. Different from *S. boissieri*, the medial condyle of the proximal epiphysis prolongs caudally by an eminence; the lateral condyle is not preserved, but according to Iliopoulos (2003) it also shows a caudal projection forming a "V"-shaped popliteal notch with the medial one. In *H. duvernoyi* only the lateral condyle bears a strong and rather distally oriented projection (Pl.

Table 15: Metatarsal measurements of *Samotherium* and *Helladotherium* from Samos.

	L	TDprox	APDprox	TDdia	APDdia	TDdis	APDdis
Samotherium boissieri							
MLN31	394.0	72.0		44.7	41.0	79.4	45.3
MLN33	397.0	68.1	68.4	42.1	41.7	82.0	44.8
MLN43				40.5	44.0		
MLN77	393.0	74.4	62.3	42.0	40.0	79.9	
MLN79	408.0		64.7	43.3	45.5	82.6	43.8
AMNH(M4289A)	400.0	62.0	64.5	40.1	42.0	73.3	43.0
AMNH(M4289B)	375.0		65.8	38.0	46.5	71.6	45.7
NHML M4289a	393.0	65.0	65.0	44.0	43.6	69.0	44.0
NHML M4289b	383.0	70.0	62.0	40.5	39.0	73.2	42.3
NHML M4289c	397.0		64.9	38.0	44.0	70.7	42.0
NHML M4289d	404.0					79.8	46.5
NHML M4289e	384.0		62.0			78.3	42.0
NHML M4289f	400.0	70.1				72.9	40.5
NHML M4289g	397.0	62.0	64.5	39.3	42.0	69.4	43.1
NHML M4289h	390.0	64.0	63.4			72.2	40.5
NHML M4289i	385.0	60.5	68.5			71.5	46.2
NHML M4289j	392.0	65.0	64.7			70.1	41.7
NHML M4289k	400.0	71.8	64.5			81.8	40.0
NHML M4289l	395.0	65.5	65.0	43.1		74.0	45.0
MGL S458	425.0	71.0	73.0	44.5	53.0	81.5	49.0
MGL S382	400.0	75.0	65.0	50.0	47.0	83.0	46.0
AMNH22828b Q2	395.0					80.0	44.6
Samotherium major							
MYT5		78.7					
MTLA72	480.0	86.4		52.0	47.4	91.0	
MTLA84						92.8	54.2
MTLA247	495.0	87.7	84.1	59.3	49.5	100.0	58.0
MTLA342		82.6	82.1	56.4	47.0		
MTLA352		68.8	79.0				
MTLA386				53.6		92.7	53.6
MTLA387	463.0	82.0	87.6	57.6	48.3	97.2	55.5
MTLA400		83.2	82.4				
MTLA401						90.0	50.6
MTLA550						93.5	50.0
MTLA470	475.0	87.6	82.3	52.1	56.0	98.0	52.6
MTLA279	503.0	88.0	86.5	55.0	58.3	96.0	55.8
MTLA210						98.0	52.6
MTLB249		92.7					
MTLB345		83.2	80.7	51.0	51.4		
MTLB401	475.0	83.6	83.0	50.0	51.0	94.3	53.7
AMNH28845A Q4	470.0	81.3	89.1	53.1	50.5	90.7	57.3
AMNH28845B Q4	480.0	79.5	81.5	55.1	53.0	98.7	56.0
AMNH20595 Q1	465.0	80.5	80.1	53.5	53.9	92.5	50.0
AMNH20633 Q1	500.0	85.5		56.4	57.7	90.0	52.4
AMNH20615 Q1	447.0	76.3	74.0	49.7	47.6	88.5	50.5
AMNH20636 Q1	495.0	79.7	79.1	48.0	52.7	93.0	52.0
AMNH22698 Q5	460.0	83.0		51.0		97.2	54.0
AMNH22966 Q5	450.0	83.6	85.5	54.6	49.3	93.6	55.3
AMNH22697 Q5	465.0	80.0	78.0	56.2	48.0	89.0	50.5
MGL S94	465.0	75.0	73.3	51.0	50.4	95.0	53.0
MGL S95	473.0	75.7	77.0	48.7	53.3	92.0	52.3
MGL S382b		79.0	76.0	47.0	50.0		
MGL S1063		73.0	52.0				
PIM344	460.0	71.5	83.4	49.0	52.3	93.1	52.5
PIM355	447.0	85.0	86.0	49.5	58.8	86.0	55.3
PIM352	430.0					80.0	
PIM48	460.0	84.0		54.0		91.0	
PIM346	475.0	85.0	77.5	57.7	52.0	94.0	50.0
PIM350	465.0			50.0			
PIM359	460.0	79.0					
PIM360	470.0	80.0		48.0		90.0	
Helladotherium duvernoyi							
MTLA85	480.0	93.0	84.0	52.0		91.6	53.3

3, fig. 6). On the distal epiphysis, the cranial end of the intertrochlear crest is high and narrow, distally exceeding the tip of the medial malleolus; the notch between them is narrow and certainly deeper than in *H. duvernoyi*, whose intertrochlear end is low and wide. The medial tubercle at the base of the medial malleolus is stronger in *S. major* than in *H. duvernoyi*. The furrow for the long flexor digitorum muscle is rather short and deep. The posterior profile of the distal epiphysis is more undulated in *S. major* since the hunch of the lateral cochlea emerges at the same level with that of the medial one. As in *S. boissieri*, the lateral malleolus has a strong posterior part, a very reduced to absent anterior part and a wide fibular furrow; in *H. duvernoyi* the anterior part of the malleolus is clear and the fibular furrow is narrow and well localized.

The astragalus of *S. major* (Pl. 2, fig. 7) is morphologically similar to that of *S. boissieri* but about 16% longer and 19% wider (Fig. 17, Table 13). The proximal intertrochlear groove is asymmetrical with thick lateral and medial ridges. The lateral ridge does not, however, elevate so much as in *H. duvernoyi* (MTLA23). The medial crest of the calcanear facet is not interrupted by a vertical notch as in *H. duvernoyi* and is oblique instead of vertical in the Pikermi and Perivolaki samples; as a result the posterior part of the medial side faces plantarly. The lateral crest of the calcanear facet has a concave profile and continues downwards to the lowermost point of the lateral condyle of the distal trochlea. In *H. duvernoyi* from Pikermi and Perivolaki the same crest curves laterally below the middle of the bone and forms the external rim of the lateral condyle. Just above the distal trochlea and in lateral position a semicircular depression is always present in *S. boissieri* and *S. major*, while missing from the astragalus of *H. duvernoyi*. In cranial aspect, the lateral ridge of the proximal trochlea bends stronger than in *H. duvernoyi* and forms an acute projection just above the distal trochlea. In lateral aspect, the cuboid facet is larger than in *H. duvernoyi* and the middle tuberosity is strong, reaching the middle of the lateral side.

The mean length difference between the calcaneum of *S. boissieri* and *S. major* reaches 18.5% (Pl. 2, figs. 3-5; Table 14). In both *Samotherium* species the dorsal and plantar edges of the body weakly converge, whereas they are parallel in *H. duvernoyi* from Pikermi and Perivolaki. The calcanear tuber is more developed laterally than medially and has a well-marked caudal groove for the flexor digitorum superficialis. The astragalar facet is concave in cranio-caudal view and symmetrically divided in the same way by a blunt crest. In *H. duvernoyi* the medial part of the same articulation facet is less developed. The sustentaculum tali is narrower than in *H. duvernoyi*. The surface for the scaphocuboid is wider than in *H. duvernoyi* and less twisted distally. In distinction from *H. duvernoyi*,

	L	TDprox	APDprox	TDdis
Samotherium boissieri				
NHML M4290	73.1	24.1	35.2	25.2
	69.0	29.6	37.3	24.5
NHML M4299	77.0	28.8	37.3	26.3
	83.3	29.1	36.9	
	93.0	33.2	45.6	32.6
	86.8	35.7	42.6	32.7
	83.0		37.5	29.7
	90.1	28.6	44.5	27.3
	82.7	35.6	39.2	33.0
	86.8	33.5	42.9	30.6
	86.5		41.8	30.8
NHML M4300	90.0	41.2		38.5
	89.2	37.0	39.7	33.5
	87.0	40.5	44.0	37.5
	83.0	37.1	40.3	38.7
	80.5	33.5	40.5	32.5
MGL S1074	94.0	42.5	44.5	35.0
Samotherium major				
MYT60	104.7	48.8	50.9	45.9
MTLA377	110.4	50.3	56.0	42.3
MTLA551	116.4	49.6	53.7	42.6
MTLB103		47.9	51.5	
MTLB378	112.8	50.4	50.3	47.0
MGL S217	104.8	44.0		43.6
MGL S566	102.5	47.5	47.7	41.3
MGL S335	100.0	47.9	45.7	40.5
MGL S1261	104.5	46.0		41.0
Helladotherium duvernoyi				
MTLA427d	113.0			
MTLA427s	116.0	57.6	52.6	57.3
PIM411	110.8	59.0	62.0	55.5
PIM412	117.0	57.5	62.0	56.0
SMFnn*	[92]	[50]	[54]	[50]

Table 16: First Phalanx measurements of *Samotherium* and *Helladotherium* from Samos. *: data from Bohlin (1926).

Fossil Site	Museum Collections	Genus	Species
Q5	AMNH	*Samotherium*	*major*
MTLA, MTLB, MTLC, Q1, Adriano	NHMA, AMNH, PIM, SMF, MGL,WNNS, NHMB, NHMW		
MYT, Q4, Q6	NHMA, AMNH		
MLN, Q2, Stefana	NHMA, AMNH, MGL, NHML, NHMP		*boissieri*
Qx, Vrysoula	NHML, SPGM, AMNH		

Table 17: *Samotherium boissieri* and *S. major* from Samos; stratigraphic occurrence and linked museum collections.

Measurement	*Samotherium boissieri*					*Samotherium major*				
	females		%dif	males		females		%dif	males	
Rad length	465.7	n=6	9	507.5	n=2	530.0	n=7	8	572.8	n=4
Mc Length	342.6		8.5	372.4		406.6		5	427.3	
Mc TDprox	73.5	n=10	8	79.2	n=11	88.9	n=12	6	94.3	n=21
Mc TDdis	75.8		10.5	83.9		96.1		6	101.7	
Astr Llal	87.2		5	91.6		97.8		8	105.9	
Astr Lmed	76.0	n=7	5	79.8	n=8	88.2	n=14	8	95.1	n=29
Astr TDdis	56.0		6	59.4		64.9		8	70.3	
Mt Length	390.9		3	401.8		459.4		6	487.8	
Mt TDprox	64.9	n=12	11	72.0	n=9	78.9	n=23	8.5	85.6	n=10
Mt TDdis	72.2		12	81.2		91.2		4.5	95.4	

Table 18: Postcranial sexual bimodality of *Samotherium boissieri* and *S. major* from Samos. Rad: radius; Mc: metacarpal; Mt: metatarsal; Astr: astragalus; % dif: % size-difference between sexes.

Measurement	*S. boissieri*	*S. major*	% mean increase		
L P2-M3	174.4	197.9	13.5		
L p2-m3	182.9	206.2	13	females	males
p/m ratio	63.5	57.8	-9		
L Humerus	428 (min406)	442.5 (max465)	3.4 (14)	—	
L Radius	476.1	548.8	15.2	14	13
L Metacarpal	354.9	419.6	18.2	18.6	15
L Femur	—	530.0	—	—	
L Tibia	458.8	524.6	14.3	—	
Llat Astragalus	89.6	103.6	15.7	12	15
Lmax Calcaneus	173.9	206.0	18.5	—	
TD Scaphocuboid	76.4	95.4	25	—	
L Metatarsal	395.6	469.1	18.6	17.5	21.4
L Phalanx I	84.4	107.0	26.7	—	

Table 19: Mean values of several dental and postcranial metrical characters of *S. boissieri* and *S. major* from Samos and estimated average increase (%) from the first to the second species, independent and according to the sex.

the malleolar facet is low and at the same level with the coronoid process; its lower part forms a wide and short concave facet. No important morphological differences between the scaphocuboid of *S. boissieri* and *S. major* (Pl. 2, fig. 8) are traced; the *S. major* scaphocuboid appears to be 23% longer and 25% wider than that of the type-species. The medial astragalar facet is narrower than the lateral one, while in *H. duvernoyi* (MTLA85) the medial facet is longer and wider than in *S. major*. The peak of the medial astragalar facet is much more elevated in *H. duvernoyi* than in *S. major*, whereas the peak of the lateral astragalar facet is much wider and higher in *S. major*. The notch between the two peaks is wide and shallow in *H. duvernoyi*, instead of narrow and deep in *S. major*. In *H. duvernoyi* the calcanear facet prolongs behind the lateral peak, while in *S. major* it stops at its side and extends posteriorly. In plantar aspect, the lateral tuberosity is strong in *S. major* instead of weak and higher placed in *H. duvernoyi* from Pikermi and Perivolaki. The furrow for the long peroneal muscle is located more posteriorly in *S. major* than in *H. duvernoyi*; the distal expression of the same furrow separates the IV metatarsal facet from a posterior and smaller one in *H. duvernoyi*, whereas in *S. major* the small facet is replaced by a protuberance. In medial view and close to the proximal articulation, the scaphocuboid of *H. duvernoyi* shows a protuberance that extends postero-distally as a crest; in *S. major* the same construction appears as a low swelling. In anterior view, the frontal end of the calcanear facet is deeper in *H. duvernoyi* than in *S. major*, which, on the other hand, shows a much more developed and round frontal end of the lateral astragalar facet.

On average, the metatarsals of *S. major* are about 19% longer and 21% wider than those of *S. boissieri* (Fig. 18, Table 15; Pl. 2, figs. 16-17). The robusticity index is rather stable ranging from 9.5 to 12.5 in *S. boissieri* (mean=10.7; n=20) and from 9.7 to 12.5 in *S. major* (mean=11.2; n=24). In contrast to the metacarpal, the metatarsal dimensions of *S. major* and *H. duvernoyi* (MTLA85, Perivolaki, Pikermi) are very close prohibiting a proportional distinction, even though the *S. major* metatarsals are somewhat more

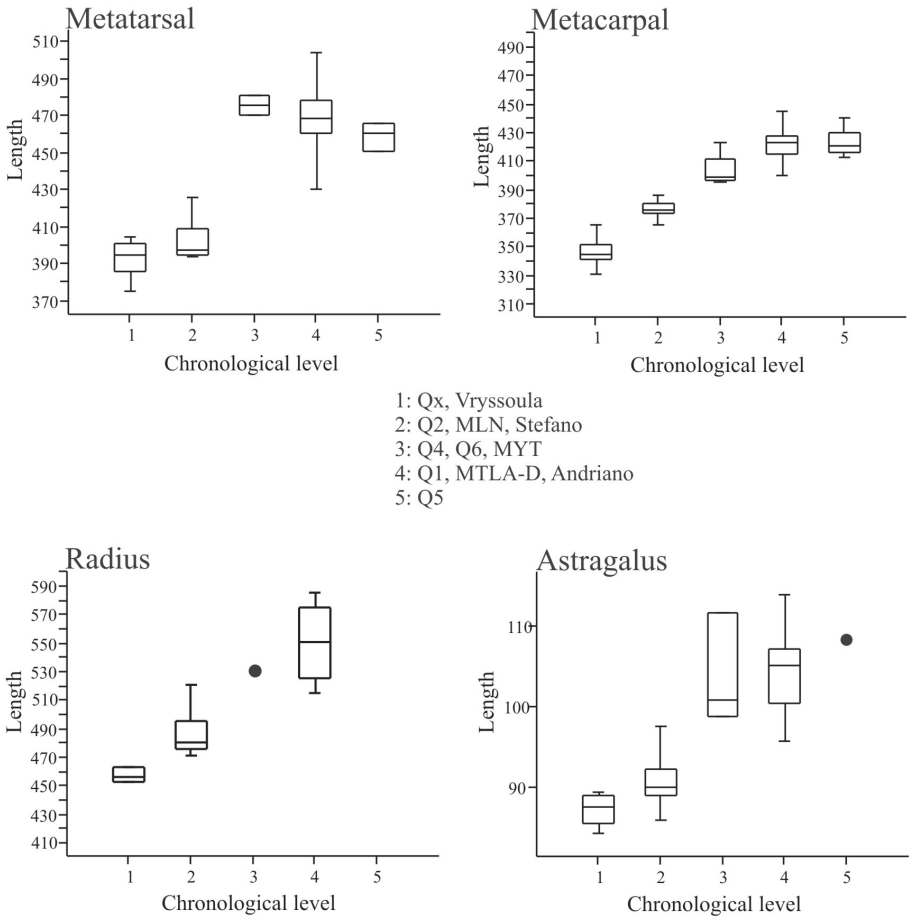

Figure 19: Box-plots demonstrating the chronological distribution of the length of most abundant *Samotherium* postcranial elements.

slender. Nevertheless, as in *S. boissieri* and differing from *H. duvernoyi,* the medial tubercle on the plantar side of the proximal epiphysis of *S. major* is strong, associated with another well developed and acute obelisk-like tubercle in the middle of the plantar side that exceeds the articular surface level (Pl. 2, fig. 13; see also Iliopoulos, 2003). The same tubercle is less developed in *S. boissieri* and absent from *H. duvernoyi*. An additional tubercle is sometimes present in the middle of the lateral side of the proximal epiphysis, while a medial protuberance is shown just in front of the medial tubercle. The plantar crests of the diaphysis are less developed in *S. major* than in *H. duvernoyi*.

The first phalanx of *S. major* appears 26% longer and 41% wider than that of *S. boissieri* (Table 16). In comparison with metapodial growth these numbers indicate that phalanges are proportionally much more elongated in the younger species. The first phalanx of *H. duvernoyi* (MTLA427, PIM411) is longer and wider than that of *S. major* and the plantar tuberosities of the proximal epiphysis are longer.

The postero-lateral tubercle of the proximal epiphysis of the second phalanx is longer in *H. duvernoyi* from Pikermi and Perivolaki than in *S. major* and points postero-dorsally. In lateral view, the third phalanx of *S. major* has straight ventral and dorsal rims and the latter is interrupted by a central hump. In *H. duvernoyi* from Perivolaki the ventral rim is rather concave and the dorsal one clearly convex. The lateral profile of the articular surface is strongly concave in *S. major* instead of weakly concave in *H. duvernoyi*. The dorsal crest that divides the medial from the lateral surface of the third phalanx bends stronger medially in *H. duvernoyi* than in *S. major*. The postero-medial tubercle appears stronger and more elongated in *S. major* than in *H. duvernoyi*.

Discussion:

The genus *Samotherium*, instituted in 1888 by Forsyth-Major based on Samos material, today includes an important variety of late Miocene palaeotragines, sharing the large size, the long-pointed frontal appendages, the reduction of the posterior lobe of p4, the relatively elongate p2, the short premolar row and the large and rather massive limbs (Hamilton, 1978; Geraads, 1986). Apart from the Samos species, the Turolian record includes *S. sinense* Bohlin, 1926 and *S. decipiens* (Bohlin, 1926 but see also Solounias, 2007) from China, *S. neumayri* (Rodler & Weithoffer, 1890) from Maragheh, *S. eminens* (Alexejev, 1915) and *S. maeoticum* Korotkevich, 1978 from the North Pontic region. Godina (2002) set up two more species, *S. korotkevichae* and *S. borissiaki* which, however, seem to be insufficiently documented. Adopting Schlosser's (1921) ideas on the overestimation of '*Samotherium* local racial dissimilarities', Bosccha-Erdbrink (1977) proposed synonymizing most species, which they could provisionally distinguish at subspecific level. Less drastically, Gentry et al. (1999) suggest that *S. major* probably includes *S. eminens* and *S. neumayri*, while *S. maeoticum* might be synonymized with *S. boissieri* or *S.*

major. *Samotherium* is recorded in almost every fossil site known from Samos and it is certainly the most common faunal element after *Hipparion* and caprine-like bovids. The combination of old and new data supports Geraads' (1994) taxonomy and produces adequate evidence for the presence of two well-distinct and non-overlapping species; the smaller *S. boissieri* that occurs in the lower to middle fossil-levels and the larger *S. major* that appears in the middle to upper fossil-levels (Table 17).

Both *S. boissieri* and *S. major* appear to be sexually bimodal, with males of the type species marginally reaching the dimensions of *S. major* females (Table 18). Apart from differences on frontal appendages, the sexual dimorphism within each single species is well documented in several postcranials such as the radius, metacarpal, astragalus and metatarsal (Table 18). Analysis of the mean values shows that size differences between the male and female astragalus of *S. boissieri* are lower than those recorded in *S. major*, while the transverse diameter of the metapodials shows the opposite trend (Table 18). In *S. boissieri*, sex differences are better expressed in the length of the metacarpal than that of the metatarsal, whereas *S. major* does not show such a disparity. The degree and pattern of sexual dimorphism recorded in both *Samotherium* species is certainly lower than that observed in some recent *Giraffa* but comparable to other late Miocene giraffids such as *Helladotherium* or *Bohlinia* (Roussiakis & Iliopoulos, 2004).

Furthermore, and in contrast to the generic disparity suggested by Solounias (2007), all available data points to a rather gradual shifting from *S. boissieri* to *S. major* (Fig. 19, Table 19), forming a clear chronocline and implying direct ancestor-descendant relationships between them. The overall body reconstruction is realized by an increase in height (~15%) and a greater increase in massiveness (~30%), but limb proportions and robusticity remain practically unchanged. Thus, for example, the mean metacarpal/radius length ratio is 74.5 in *S. boissieri* and 76.5 in *S. major*, the metacarpal/metatarsal mean length ratio is 88.7 in the first and 89.5 in the second species and the metatarsal/tibia mean length ratio is 86.2 and 89.4 respectively. From *S. boissieri* to *S. major* the skull becomes larger with a longer face and probably less specialized muzzle, the frontal pneumatisation increasing significantly, the male ossicones enlarging and diverging from the sagittal axis of the skull and the lower premolars being reduced (Table 19) and becoming fully molarized. This model roughly fits Godina's et al. (1993) hypothesis concerning the evolution within giraffid lineages: increase of the animal's height is associated with the development of air cavities on the skull roof, whereas increase in weight allows the widening of the metapodial ends. The pattern of overall body enlargement from *S. boissieri* to *S. major* recalls phyletic growth procedures (Kurtén, 1953; Hone & Benton, 2005) which might benefit later *Samotherium* species with increased potential longevity and resistance to the harsher environmental conditions established during middle-late Turolian together with success in interspecific competition from new arrivals such as *Helladotherium*. Obviously, there is a lack of information concerning the intermediate stages between *S. boissieri* and *S. major*. *S. neumayri* from Maragheh is central to this discussion. Unfortunately, the species is known only by one partially preserved female skull (NHMW A4903) and a few toothrows, but enough postcranials. Judging from the figure of Rodler & Weithoffer (1890: Pl. I, fig. 1), it seems that the *S. neumayri* cranium is closer to *S. boissieri* in the development of the lachrymal depression and the forward placement of the orbit, but it looks more like *S. major* by losing of the periscopic position of the eye. Nevertheless, the orbit is placed much lower than in the Samos species and the choane is wide and opens more or less at the same level with the lateral indentations (at the middle of M3). The *S. neumayri* dentition (P2-M3 = 182.8; P2-P4 = 76.3; M1-M3 = 116.5 mm; p2-m3 = 194.1; p2-p4 = 70.2; m1-m3 = 122.4 mm) is larger than that of *S. boissieri* and smaller than *S. major*, while the lower premolar/molar ratio (57.4) certainly falls within the range of *S. major*. The p2 is rather primitive and more alike to *S. boissieri,* while the p3 is comparable to that of *S. major*. On the other hand, *S. neumayri* limbs are always in between the ranges of *S. boissieri* and *S. major*, sealing their dimensional gap. Although several authors suggest synonymizing *S. neumayri* with *S. boissieri* or *S. major*, it seems that such a decision is still premature and needs further argumentation. The rather well-defined metrical limits of *S. neumayri* in combination with its particularities in skull and dental features and proportions might allow its distinction at species level, simultaneously suggesting a deviation from the *S. boissieri* - *S. major* lineage from which it possibly originates.

Two more *Samotherium* species from the peri-Pontic region are usually involved in the intrageneric discussion (e.g., Gentry & Heizmann, 1996). *S. eminens* is originally known from Nova Elisavetovka and *S. maeoticum* from Nova Emetovka 2. Both sites are placed in the so called "Nova Elizavetovka faunal complex" of Maeotian age, corresponding to the early-middle Turolian of the European land mammal ages. Krakhmalnaya (1996) considers Nova Emetovka 2 as the final stage in the development of the early Maeotian mammal fauna, which is mostly characterized by the Nova Elizavetovka mammal association. *S. eminens* is dimensionally placed between *S. boissieri* and *S. major,* but its skull structure deviates from this lineage. Hence, the cranium follows the general pattern seen in *S. boissieri* but it is characterized by a relatively lower and longer face, longer naso-maxillary contact, backwardly placed orbit, strong orbital crest descending from the anterodorsal corner of the orbit, absence of an ethmoidal fissure, larger and longer paroccipital processes curved backwards, more closely settled and convergent parietal crests, strong lateral wings of the occiput, a posteriorly shifted ossicone and deeper mandible. Most of these features can be also traced on the larger *S. sinense* from China, indicating close relationships between them. On the other hand, metrical and morphological comparison of the *S. maeoticum* type-skull with *S. major* indicates great similarity, especially with the 'horned' female specimen MTLA540 and, therefore, the synonymy suggested by previous authors seems reasonable.

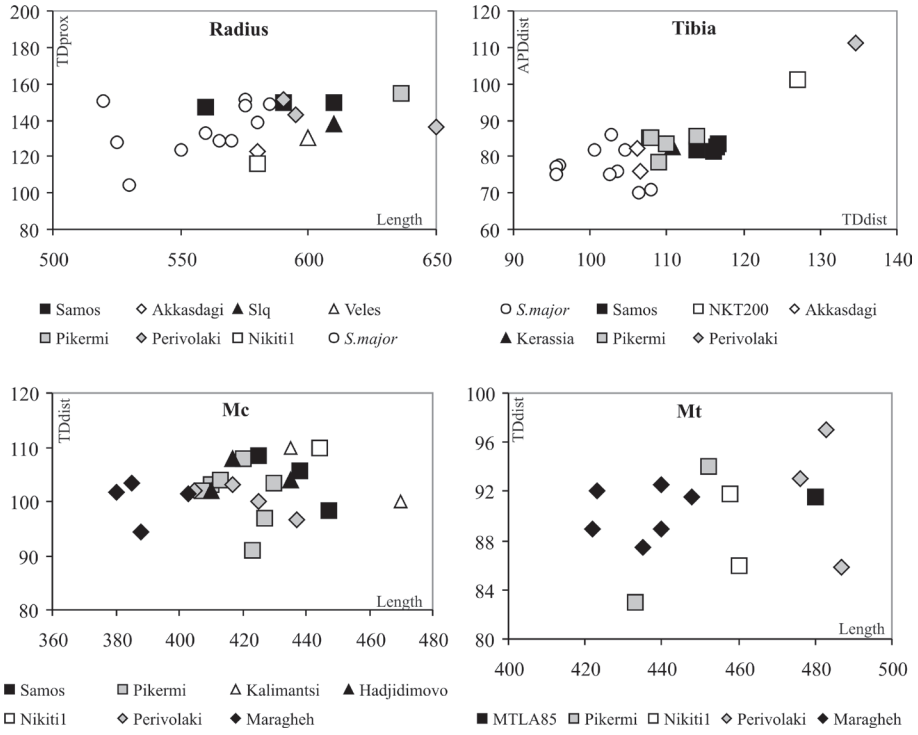

Figure 20: Scatter diagrams comparing limb proportions of *Helladotherium duvernoyi* from several sites (Samos, Pikermi, Akkaşdağı, Perivolaki, Kerassia, Salonique-Axios, Nikiti-1, Titov-Veles, Kalimantsi, Hadjidimovo, Maragheh) and *S. major* from Samos.

Sources: Bohlin, 1926; Geraads et al., 2005; Melentis 1969b, Iliopoulos, 2003; Kostopoulos et al., 1996; Kostopoulos & Saraç, 2005; Kostopoulos & Koufos, 2006 and pers. data).

Sivatheriini Zittel, 1893

Genus *Helladotherium* Gaudry, 1860

Helladotherium duvernoyi Gaudry, 1860

(Plate 3; Tables 7, 9-13, 15-16)

Localities & Ages:
Mytilinii-1A (MTLA), Adrianos ravine; middle Turolian (MN12), 7.1-7.0 My
PMMS, Adrianos ravine; middle Turolian (MN12), 7.1-7.0 My
Quarry 1 (Q1), Adrianos ravine; middle Turolian (MN12), 7.1-7.0 My
Quarry 5 (Q5), Limitzis; early late Turolian (MN13), 6.9-6.7 My
MGLS-Adriano, Adrianos ravine, middle Turolian (MN12), 7.1-7.0 My

The material from the NHMW, PIM, SMF has no locality indication.

Studied Material:
NHMA:
MTLA: MTLA312, 315, 462, distal part of humerus; MTLA534, 535b, radius; MTLA278, proximal part of radius; MTLA461, distal part of radius; MTLA292, magnum; MTLA248, 249, metacarpal; MTLA469 part of pelvis; MTLA73, femur; MTLA320, distal part of femur; MTLA 74, 313, tibia; MTLA83, 254, distal part of tibia; MTLA23, astragalus; MTLA85, metatarsal and scaphocuboid; MTLA427 dex and sin first phalanx.
PMMS (Adrianos): PMMS88, left D4-M2; PMMS82, atlas; PMMS103, femur.
AMNH: AMNH22795b, left D2-M2, Q5; AMNH 95120, left d2-d4, nl; AMNH20610, metacarpal, Q1.
MGL (all specimens from Adrianos): MGL S570, humerus; MGL S834, distal humerus; MGL S322, proximal part of metacarpal.
PIM: PIM469, D3-D4, nl; PIM400, distal humerus; nn radius (from Bohlin, 1926); PIM339, proximal metacarpal; PIM398, distal metacarpal; PIM411, 412, phalanx I.

Reference Material:
NHMW (from Bohlin, 1926): NHMW nn, d2-m1, nl.
SMF (from Bohlin, 1926): SMF2440-2442, D2-D4; SMF2443, D2-M1; SMF2436, metacarpal; first phalanx, nn.

Description & Discussion:
The presence of *Helladotherium*, a quite common late Miocene large sivatheriine, in the faunal assemblages of Samos is rather confused and underestimated. The species is known here only by a few milk dentitions and several postcranials, whereas skull specimens and permanent dentitions are missing from both the old and new collections. According to the available data, all Samos records of *H. duvernoyi* originate from the upper fossil-levels (MTLA, Q1-Q5), where the species coexists, though it is much less frequent, with the similar-sized *S. major*.
The length D2-D4 ranges from 94-108 mm. The strong hypocone and the well-developed metastyle on D2, the long and trapezoidal-shaped anterior lobe of D3 with bifurcated parastyle and quite strong antero-lingual cingulum, the straight posterior flange of the paracone and the presence of a hypoconal spur on D3 and D4 (Pl. 3, fig. 1), the labial cingulum that associates the metastyle

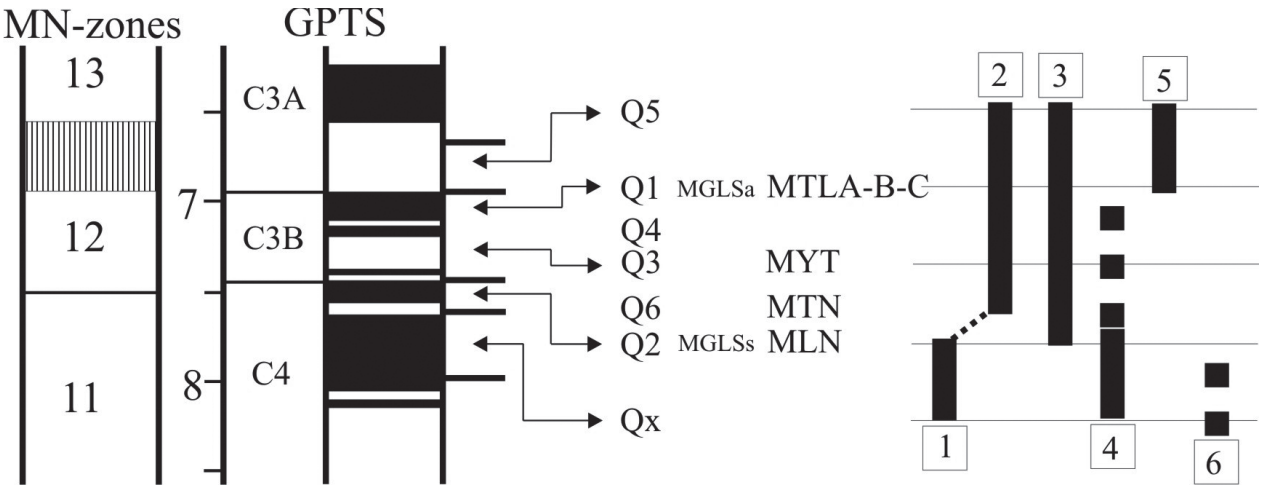

Figure 21: Revised chronological arrangement of old and new Samos fossil sites (modified from Kostopoulos et al., 2003) and time-distribution of Samos giraffids. 1: *Samotherium boissieri*; 2: *S. major*; 3: *Palaeotragus rouenii*; 4: *Palaeotragus quadricornis*/sp.; 5: *Helladotherium duvernoyi*; 6: *Bohlinia attica*. For locality abbreviations see text.

on D3, the bifurcated anterior hypoconal flange of D3 and D4 (Pl. 3, fig. 1) and their strong parastyle, paracone and mesostyle, the presence of a hypoconal spur on the molars (Pl. 3, fig. 1), the comparatively posterior position of the mesostyle to the lingual valley between the molar lobes, the division of the anterior flange of the protocone (Pl. 3, fig. 1: M2) and the rather strong labial cingulum are features characterizing sivatheriines and particularly *H. duvernoyi* (Kostopoulos & Koufos, 2006 and literature therein). Although the molars of *H. duvernoyi* are equally high as those of *S. major* in respect to their length, they appear to be much less prismatic because of their greater width; M1's relative hypsodonty (height/width) exceeds 100 in *H. duvernoyi* whereas it is usually lower than this value in *S. major* from Samos.

The d2-d4 length is 92 mm in the SMF specimen and 101.2 mm in AMNH95120 (Pl. 3, fig. 2). In distinction from *Samotherium*, the d3 is unmolarized with a strong and thin parastylid, a strong paraconid perpendicular to the longitudinal axis of the tooth, a weak to moderate metaconid rather parallel to the paraconid, a widely open anterior valley, an oblique and long entoconid in contact with the metaconid at its base and a strong entostylid. Additionally, the anterior lobe of the d4 is square-shaped and the basal pillars are strong. Theis feature combination is identical to that of *H. duvernoyi* from Pikermi (MNHNP PIK1502,1503; NHML M11496; Gaudry, 1862-67) and similar to *H. duvernoyi* from Perivolaki (Greece) and Kalimatsi (Bulgaria) (Geraads et al., 2005; Kostopoulos & Koufos, 2006). It is worth mentioning that in the d3 from Perivolaki and Kalimatsi the metaconid descends directly from the main labial crest without having any contact with the entoconid, whereas in the Samos and Pikermi samples it originates from the base of the entoconid and is thinner and less developed (Pl. 3, fig. 2). The basic morphological limb characters, proportions, as well as their distinguishing features from *S. major* have already been discussed in the previous chapter (Tables 7, 9-13, 15-16). A metrical comparison with other records of *Helladotherium* (Fig. 20) shows primarily that the size variability in *H. duvernoyi* is much greater than one would expect. Minimum and maximum length values might diverge up to 20%, while differences on transverse diameters might attain 50%, as for example in the proximal epiphysis of the radius. Roussiakis & Iliopoulos (2004) presume a relatively high sexual dimorphism for the species, a reason that could justify such a kind of metrical disparity. The limb proportions of the Samos sample fall well within the known variation range of *H. duvernoyi* from Pikermi, Perivolaki, Nikiti-1, as well as from Bulgaria and Turkey, being somewhat larger than that from Maragheh (Fig. 20). Geraads et al. (2005) imply a growth with time that, however, needs further documentation. Excluding the latest Vallesian sample from Nikiti-1 that clusters with the largest known morphotypes, the available metacarpal sample of a Turolian *Helladotherium* shows a rather gradual increase from Maragheh to Perivolaki-Pikermi-Hadjidimovo to Samos-Kalimantsi (Fig. 20). Other data fails, however, to support this scenario.

3. Conclusion

The revision of the Samos giraffid remains allows the recognition of five species: *Palaeotragus rouenii*, *Palaeotragus quadricornis*, *Samotherium boissieri*, *Samotherium major* and *Helladotherium duvernoyi*. Another set of specimens referred to as *Palaeotragus* sp. appears to be better affiliated with *P. quadricornis* than with *P. coelophrys* from Maragheh, although the distinction between these two species remains problematic. Bernor et al. (1996) also mention ?*Bohlinia* "*speciosa*" from the Main Bone Beds member and ?*Bohlinia attica* from the White Bone Beds member of Samos, but their data seems to be based on old and rather doubtful information. Nevertheless, Iliopoulos (2003) also observes that one calcaneum from the *Samotherium* collection in London, labeled NHML M4283(311), has a much larger anteroposterior diameter of the calcanear

tuber than that of *S. boissieri*, a condition that fits better with *Bohlinia attica*. Present or not, the species is certainly of minor importance for the structure of the Samos giraffid association and it is quite possible that if present, it is restricted to the lower fossil-levels.

Kostopoulos et al. (2003) update the chronological arrangement of old and new fossil sites from Samos based on magnetostratigraphic and biochronological data, suggesting the presence of four to five successive fossil-levels. Some additions and corrections should be made. The Brown's Q6 site is usually placed together with Qx into the lowermost fossil-level (Bernor et al., 1996) correlated weakly with the radiometric samples SK3 (8.26±0.8 My) and SK6 (7.8±0.4 My) of Weidman et al. (1984) (see also Swisher III, 1996). Nevertheless, the poor collected fauna from this site undoubtedly includes *Samotherium major,* which suggests a quite younger age than Qx and even Q2, MLN and Stefano, implying a date no older than 7.4 My. Topographic indications on old quarries given by Solounias (1981) allow Kostopoulos et al. (2003) to correlate Q4 directly with MLN. This is, however, misleading, as the first site bears *S. major* while the second yields *S. boissieri*. Supposing that Solounias data regarding the presence of one of Brown's sites at the very specific place of the basin is correct, one could assume that for inexplicable reasons the Q4 location has been confused with that of Q2 and vice versa. In any case Q2 is certainly older than Q4 and on the same fossil-level with Forsyth-Major's Stefano and MLN. They are both dated between 7.45 and 7.65 My. The site Q3/ MYT is slightly younger indicating an age of about 7.3 My. According to the giraffid, bovid and hipparionine assemblages, Q4 is most probably even younger, placed between Q3/MYT and Q1-level. A revised version of the chronological arrangement of the Samos sites is given in Fig. 21.

Palaeotragus rouenii is well-known from several SE European sites ranging from late Vallesian to late Turolian. The species first appears on Samos in the MLN-Q2-Stefano fossil-level and it is still present in the younger known site Q5 (Fig. 21). The presence of another *Palaeotragus* species in Samos is certainly more difficult to be appreciated biochronologically. The original material of *P. quadricornis* comes most probably from the Qx fossil-level but evidence for its presence also exists in MLN and MTLB suggesting a quite vast occurrence (Fig. 21).

Samotherium boissieri is known from Qx and MLN-Q2-Stefano fossil-level while *Samotherium major* is already present in Q6, as well as in Q4, MYT, Q1-MTLA/B and Q5 fossil-levels (Fig. 21). The replacement of the one species by the other should take place at about 7.4 My, i.e. close to the MN11/MN12 boundary (Kostopoulos et al., 2003). A very similar situation is already recognized in the neighboring Kemiklitepe site (Turkey), where *S. major* replaces *S. boissieri* between 7.6 and 7.2 My (Geraads, 1994; Sen et al., 1994). *Helladotherium duvernoyi* first appears on Samos at Q1-MTLA/B level, i.e., at 7.0-7.1 My and it is still present at Q5 (~6.7-6.9 My) (Fig. 21). Similarly to Samos, *H. duvernoyi* is not recorded in the Kemiklitepe A/B level (~7.2 My) but it does occur at Akkasdağı (~7.0 My; Kostopoulos & Saraç, 2005), suggesting a later arrival time in the East Aegean area.

Indeed, the chrono-spatial distribution of *Samotherium* and *Helladotherium* across the Aegean region shows some interesting particularities. *Samotherium boissieri*, a rather typical early Turolian species, never occurs in the western part of this area. The genus is first recorded in N Greece during early Middle Turolian (Vathylakkos 3) with the large species *S. major*, which reappears later at Kerassia (middle Turolian). Its arrival time roughly coincides with the time of the first emergence of *S. major* in the East. Yet, *S. major* failed to be established in the West, as the rich middle Turolian record from Greece and Bulgaria shows; its two occurrences are rather occasional and might represent either its very marginal occidental limits or paroxysmal distribution phases. On the other hand, *Helladotherium duvernoyi* appears to be a stable faunal element of the West faunas of the Aegean area even from latest Vallesian, documented in numerous sites from Hungary to Southern Greece. In the East and apart from a couple of early problematic records in Middle Sinap-Loc. 63 and Gülpinar, Turkey (Gentry, 2003) the species does not appear until late Middle Turolian (~7.2 My). At that time *H. duvernoyi* seems to expand eastwards, documented in several sites from Ukraine, Moldova, Turkey and SE Greece.

4. Acknowledgements

The excavations on Samos have been supported by the Prefecture of Samos and the "Konstantinos and Maria Zimalis" Foundation. The Municipality of Mytilinii provided generous help too. The Natural History Museum of the Aegean offered us the premises for the preparation and storage of the fossils. Thanks are due to Prof. A. Baud from the University of Lausanne; Dr. A. Currant and Dr. A. Gentry from the Natural History Museum in London; Dr. G. Daxner-Höck from the Naturhistorisches Museum Wien; Dr. E. Delson and S. Bell from the American Museum of Natural History; Dr. S. Sen, Dr. P. Tassy, and Dr. C. Sagne from the Muséum National d' Histoire Naturelle de Paris; Dr. M. Bertling from the Paleontologisches Institut Münster; Dr. A. Ziems and Dr. W. Etter from the Museum of Natural History in Basel, for granting me access to the Samos collections in their care and photographic material. I also thank Dr. S. Roussiakis (Athens), Dr. N. Solounias (NY), Dr. G. Iliopoulos (Crete) and Dr. D. Geraads (Paris) for interesting information on Samos giraffids. The Zimalis Foundation and all colleagues who worked in the field and in the laboratory are sincerely thanked for their assistance. I am especially indebted to Dr. E. Heizmann from the Staatliches Museum für Naturkunde in Stuttgart for providing photographic material and valuable remarks on the original manuscript.

5. References

Alexejev, A.,1915. Animaux fossiles du village Novo-Elizavetovka. — Tipografiya „Technik":1–453, Odessa.

Arambourg, G. & Piveteau, J., 1929. Les vertébrés du Pontien de Salonique. — Annales de Paléontologie, **18**:1–82, Paris.

Bernor, R.L., Solounias, N., Swisher III, C.C., van Couvering, J.A., 1996. The correlation of the classical "Pikermian" mammal faunas - Maragheh, Samos and Pikermi, with the European MN unit system. — [in:] Bernor, R.L., Fahlbusch, V. & Mittmann, H.-W. (eds.). The Evolution of the Western Eurasian Neogene Mammal Faunas. – 137–154, New York (Columbia University Press)

Bohlin, B., 1926. Die Familie Giraffidae. — Palaeontologica Sinica, ser. C, **4**(**1**):1–178, Beijing.

Borissiak, A., 1914. Mammifères fossiles de Sebastopol. — Mémoires du Comité Géologique, II, **87**:105–154, St. Petersburg.

Borissiak, A., 1915. Mammifères fossiles de Sebastopol. — Mémoires du Comité Géologique, II, **137**:27–47, St. Petersburg.

Bosscha-Erdbrink, D.P., 1977. On the distribution in time and space of three giraffid genera with Turolian representatives at Maragheh in N.W. Iran. — Proceedings of the Koninklijke Nederlandse Akademie van Wetenschappen, B, **80**(**5**):337–355, Amsterdam.

Churcher, C.S., 1970. Two new upper Miocene giraffids from Fort Ternan, Kenya, East Africa: *Palaeotragus primaevus* and *Samotherium africanum*. — Fossil Vertebrates of Africa, **2**:1–15, London.

de Mequenem, R., 1924. Contribution à l'étude des fossiles de Maragha. — Annales de Paléontologie, **13-14**:1–62, Paris

Forsyth-Major, C.J., 1888. Sur un gisement d'osséments fossiles dans l'île de Samos, contemporain de l'age de Pikermi. — Comptes Rendus de l'Académie des Sciences, **107**:1178–1182, Paris.

Forsyth-Major, C.J., 1891. On the fossil remains of species of the family Giraffidae. — Proceedings of the Zoological Society of London:315–326, London.

Forsyth-Major, C.J., 1901. On the reported occurrence of the camel and nilgai in the upper Miocene of Samos. — The Geological Magazine, NS, (**4**)**7**:354–355, London.

Forsyth-Major, C.J., 1902. On the okapi. — Proceedings of the Zoological Society of London:73–79, London.

Gaudry, A., 1860. Résultats des fouilles exécutées en Grèce sous les auspices de l'Académie. — Comptes Rendus de l'Académie des Sciences, **51**:802–804, Paris.

Gaudry, A., 1861. Note sur la giraffe et l' *Helladotherium* trouvées à Pikermi (Grèce). — Bulletin de la Societée Géologique de France, 2eme serie, **5**: 587–597, Paris.

Gaudry, A., 1862-1867. Animaux fossiles et géologie de l'Attique. — Savi, F. (ed). – 1–474, Paris.

Gentry, A.W., 2003. Ruminantia (Artiodactyla). — [in:] Fortelius, M., Kappelmann, J., Sen, S. & Bernor, R. (eds.). Geology and Paleontology of the Miocene Sinap Formation, Turkey. – 332–379, New York (Columbia University Press).

Gentry, A. & Heizmann, E.P.J., 1996. Miocene Ruminants of central and eastern Tethys and Paratethys. — [in:] Bernor, R., Fahlbush, V., Mittmann H.-W. (eds.). The evolution of western Eurasian Neogene mammal faunas. – 378–391, New York (Columbia University Press).

Gentry, A.W., Rössner, G.E., Heizmann, P.J., 1999. Suborder Ruminantia. — [in:] Rössner, G. & Heissig, K. (eds.). The Miocene land mammals of Europe. – 225-258, Munich (Verlag Dr F. Pfeil).

Geraads, D., 1974. Les giraffidés du Miocène supérieur de la région de Thessalonique (Grèce). These, 3eme cycle, Université Paris VI – 1–102 (unpublished), Paris.

Geraads, D., 1978. Les Palaeotraginae (Giraffidae, Mammalia) du Miocène supérieur de la région de Thessalonique (Grèce). — Géologie Mediterranéenne, **5**(**2**):269–276, Provence.

Geraads, D., 1979. Les Giraffinae (Giraffidae, Mammalia) du Miocène supérieur de la région de Thessalonique (Grèce). — Bulletin du Muséum National d'Histoire Naturelle Paris, 4eme sér., C, **4**:377–389, Paris.

Geraads, D., 1986. Rémarques sur la systématique et la phylogénie des Giraffidae (Artiodactyla, Mammalia). — Géobios, **19**(**4**):465–477, Villeurbanne.

Geraads, D., 1994. Les gisements de mammifères du Miocène supérieur de Kemiklitepe, Turquie: 8. Giraffidae. — Bulletin du Muséum National d'Histoire Naturelle, 4eme sér., C, **16**:159–173, Paris.

Geraads, D., Spassov, N., Kovachev, D., 2005. Giraffidae (Artiodactyla, Mammalia) from the late Miocene of Kalimantsi and Hadjidimovo, Southwestern Bulgaria. — Geologica Balcanica, **35**:11–18, Sofia.

Godina, A.Ya., 1979. [History of fossil giraffes of the genus Palaeotragus]. — Trudy. Paleontological Institut Akademia Nauk SSSR, **177**:1–114, Moscow (in Russian).

Godina, A.Ya., 2002. On the taxonomy and evolution of *Samotherium* (Giraffidae, Artiodactyla). — Paleontological Journal, **36**:395–402, Moscow.

Godina, A.Ya., Vislobokova, I., Abdrachmanova, L.T., 1993. A new Giraffidae representative from the lower Miocene of Kazakhstan. — Paleontological Journal, **27**:91–105, Moscow.

Hamilton, W. R., 1978. Fossil giraffes from the Miocene of Africa and a revision of the phylogeny of Girafoidea. — Philosophical Transactions of the Royal Society of London, B, **283**:165–229, London.

Hone, D. & Benton, M.J., 2005. The evolution of large size: how does Cope's Rule work? — Trends in Ecology and Evolution, **20**(**1**):4– 6, London.

Iliopoulos, G., 2003. The Giraffidae (Mammalia, Artiodactyla) and the study of the history and chemistry of fossil mammal bone from the late Miocene of Kerassia (Euboea Island, Greece). — PhD Thesis, University of Leicester, 1–144, Leicester.

Killgus, H., 1922. Unterpliozäne Säuger aus China. — Paläontologische Zeitschrift, **5**:251–253, Berlin.

Korotkevitch, E. L., 1978. [A new *Samotherium* species from the Meotian of the Northern part of the Black Sea region]. — Vestnik Zoologii, **4**:9–18, Kiev (in Russian)

Korotkevitch, E.L., 1988. [History of the formation of the Hipparion fauna in Eastern Europe] – 1–160, Naukova Dumka, Kiev (in Russian)

Kostopoulos, D.S. & Koufos, G.D., 2006. The late Miocene vertebrate fauna from Perivolaki (Thessaly, Greece). Giraffidae. — Palaeontographica, Abt. A, **276**:135–149, Stuttgart.

Kostopoulos, D.S. & Saraç, G., 2005. The Late Miocene mammal locality of Akkaşdaği (Central Anatolia, Turkey). Giraffidae. — Geodiversitas, **27**(**4**):735–745, Paris.

Kostopoulos, D.S., Koliadimou, K.K. & Koufos, G.D., 1996, The giraffids (Mammalia, Artiodactyla) from the late Miocene mammalian localities of Nikiti (Macedonia, Greece). — Palaeontographica, Abt. A, **239**:61–88, Stuttgart.

Kostopoulos, D.S., Sen, S., Koufos, G.D., 2003. Magnetostratigraphy and revised chronology of the late Miocene mammal localities of Samos, Greece. — International Journal of Earth Sciences, **92**:779–794, Berlin-Heidelberg.

Kostopoulos, D.S., Koufos, G.D., Sylvestrou, I.A., Syrides, G., Tsombachidou, E., this volume. The Late Miocene Mammal Faunas of the Mytilinii Basin, Samos Island, Greece: New Collection. 2. Lithostratigraphy and Fossiliferous Sites. — Beiträge zur Paläontologie, **31**:13–26, Wien.

Koufos, G.D., Syrides, G., Kostopoulos, D. S., Koliadimou, K., Sylvestrou, I., Seitanidis, G., Vlachou, Th., 1997. New excavations in the Neogene mammalian localities of Mytilinii, Samos island, Greece. — Geodiversitas, **19**(**4**):877–885, Paris.

Krakhmalnaya, T.V., 1996, [The Hipparion fauna from the Meotian of the Northern part of the Black Sea region]. – 1-225, Naukova Dumka, Kiev (in Russian).

Kurtén, B., 1953. On the variation and population dynamics of fossil and recent mammal populations. — Acta Zoologica Fennica, **76**:1–122, Helsinki.

Lydekker, R., 1890. A new fossil mammalian fauna. — Nature, **43**:85–87, London.

Melentis, J., 1969a. Paläontologische Ausgrabungen auf der Insel Samos. — Annals of the Academy of Athens, **43**:344–349, Athens.

Melentis, J., 1969b. Studien über fossile Vertebraten Griechenlands. 28. Die Pikermifauna von Halmyropotamos (Euböa, Griechenland), Teil 2: Osteologie. — Annales Géologiques des Pays Hélleniques, **21**: 217–306, Athens.

Ozansoy, F., 1965. Ètudes des gisements continentaux et des mammifères du Cénozoique de Turquie. — Mémoires de la Societé géologique de France, N.S., **44**(**1**):1–92, Paris.

Pavlow, M., 1913. Mammifères tertiaires de la nouvelle Russie. — Nouvelles Mémoires de la Societée Impériale des Naturalistes de Moscou, **17**(**3**):1–67, Moscow.

Pilgrim, G.E., 1911. The fossil Giraffidae of India. — Palaeontologica Indica, n.s., **4**:1–29, Calcutta.

Rodler, A. & Weithoffer, K.A., 1890. Die Wiederkäuer der Fauna von Maragha. — Denkschriften der Kaiserlichen Akademie der Wissenschaften, Mathematisch-Naturwissenschaftliche Klasse, **57**:753–771, Wien.

Roussiakis, S. & Iliopoulos, G., 2004. Preliminary observations on the metrical variation of *Helladotherium duvernoyi* and *Bohlinia attica*. — Proceedings of the 5th International Symposium on Eastern Mediterranean Geology, **1**:343–346, Thessaloniki.

Schlosser, M., 1921. Die Hipparionenfauna von Veles in Mazedonien. — Abhandlungen der Bayerischen Akademie der Wissenschaften, **29**:1–55, Munich.

Sen, S., de Bonis, L., Dalfes, N., Geraads, G., Koufos, G., 1994. Les gisements de mammifères du Miocène supérieur de Kemiklitepe, Turquie: 1. Stratigraphie et magnétostratigraphie. — Bulletin du Muséum National d'Histoire Naturelle, 4eme ser., **16**:5–17, Paris.

Senyürek, M.S., 1954. A study of the remains of *Samotherium* found at Taskinpaşa: Ankara. — Universitesi Dil ve Tahir-Cografya Fakiltesi Dergisi, **12**(**1-2**):1–32, Ankara.

Solounias, N., 1981. The Turolian fauna from the island of Samos, Greece. — [in:] Hecht, M. & Szalay, F.S. (eds.). Contribution to Vertebrate Evolution. – 1–232, Basel (Karger AG Publ. House).

Solounias, N., 1988. Prevalence of ossicones in Giraffidae (Artiodactyla, Mammalia). — Journal of Mammalogy, **69**:845–848, Lawrence.

Solounias, N., 2007. Family Giraffidae. — [in:] Prothero, D.R. & Foss, S.E. (eds.). The Evolution of Artiodactyls. – 257– 277, Baltimore (John Hopkins University Press).

Swisher III, C.C., 1996. New $^{40}Ar/^{39}Ar$ Dates and their contribution toward a revised chronology for the late Miocene nonmarine of Europe and West Asia. — [in:] Bernor, R.L., Fahlbusch, V. & Mittmann, H.-W. (eds.). The Evolution of the Western Eurasian Neogene Mammal Faunas. – 64– 77, New York (Columbia University Press).

Weidmann, M., Solounias, N., Drake, R.E., Curtis, J., 1984. Neogene stratigraphy of the Mytilini Basin, Samos island, Greece. — Geobios, **17**(**4**):477–490, Villeurbanne.

Zittel, K.A. von, 1893. Handbuch der Paläontologie, Abteilung I. Paläozoologie. IV Band, 1ste Lief. Vertebrata (Mammalia). Oldenbourg R. (ed.) – 1–779, Munich and Leipzig.

PLATE 1

***Palaeotragus rouenii* from Samos**

Fig. 1 AMNH22944, Q5, part of right mandible with p2-m3 in lingual view.

Fig. 2 AMNH86373, Q5, left p3-m3 in occlusal view.

Fig. 3 AMNH86507, nl, right D2-M1 in occlusal view.

Fig. 4 NHMA MTLB128, left P2-M3 in occlusal view.

Fig. 5 NHMA MTLB226, left p2-m3 in occlusal view.

Fig. 6 NHMA MTLA261, right ossicone in lateral view.

Fig. 7 NHMA MTLB155 right metacarpal, in proximal and anterior view.

Fig. 8 NHMA MTLB165, right scapula in dorsal view.

Fig. 9 NHMA MTLB156, right radius in anterior and distal view.

Fig. 10 NHMA MLN75, right scaphocuboid in proximal and medial views.

Fig. 11 NHMA MLN75, right metatarsal in proximal view.

Figs. 1-5, scale-bar 3 cm (black); Figs. 6-11, scale-bar 6 cm (black & white).

PLATE 1

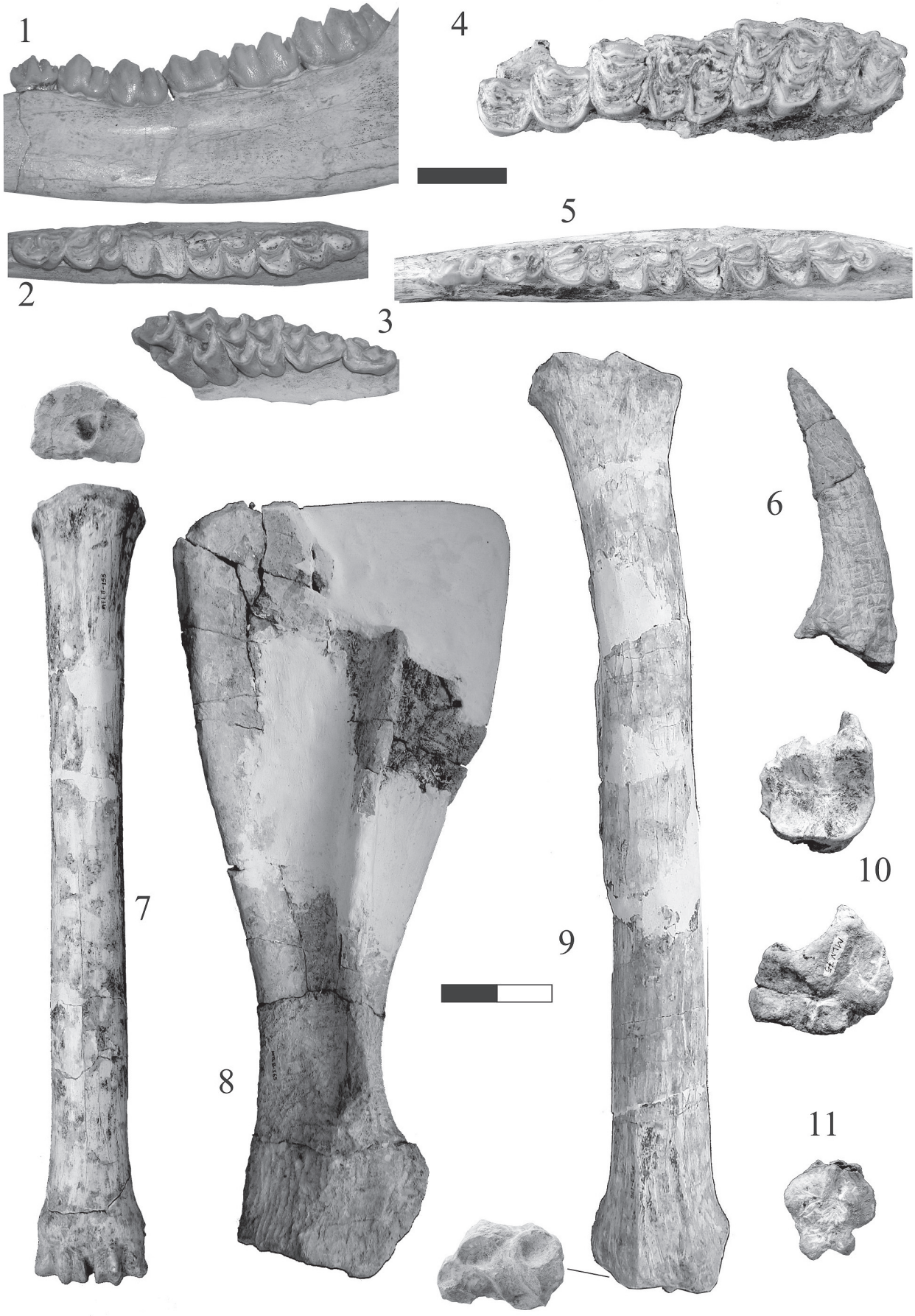

PLATE 2

***Samotherium* from Samos.**

Fig. 1. *Samotherium major*, AMNH20596, Q1, atlas in ventral and dorsal view.

Fig. 2. *Samotherium major*, NHMA MTLA291, left magnum in proximal view.

Fig. 3. *Samotherium boissieri*, NHMA MLN72, left calcaneum in medial view.

Fig. 4. *Samotherium major*, NHMA MYT42, left calcaneum in medial view.

Fig. 5. *Samotherium major*, NHMA MTLB386, left calcaneum in medial view.

Fig. 6. *Samotherium major*, NHMA MTLA255, left femur in medial view.

Fig. 7. *Samotherium major*, NHMA MTLB400, left astragalus in caudal view.

Fig. 8. *Samotherium major*, NHMA MTLA279, left scaphocuboid in proximal view.

Fig. 9. *Samotherium major*, NHMA MTLA75, right metacarpal in anterior view.

Fig. 10. *Samotherium major*, NHMA MYT41, right metacarpal in anterior view.

Fig. 11. *Samotherium boissieri*, NHMA MLN9, left metacarpal in anterior view.

Fig. 12. *Samotherium major*, NHMA MTLD nn, left metacarpal in proximal view.

Fig. 13. *Samotherium major*, NHMA MTLB249, left metatarsal in proximal view.

Fig. 14. *Samotherium major*, NHMA MTLA256, left pelvis in dorsal view.

Fig. 15. *Samotherium major*, PIM364, right humerus in anterior view

Fig. 16. *Samotherium boissieri*, NHMA MLN33, left metatarsal in anterior view

Fig. 17. *Samotherium major*, NHMA MTLB249, left metatarsal in anterior view

Fig. 18. *Samotherium major*, NHMA MTLA468, right radiocubitus in posterior view.

All figures in 10 cm scale-bar.

PLATE 2

PLATE 3

***Helladotherium duvernoyi* from Samos**

Fig. 1. PMMS88, left D4-M2, buccal and occlusal view.

Fig. 2. AMNH95120, left d2-d4 in occlusal and lingual view.

Fig. 3. NHMA MTLA534, right radiocubitus in posterior view.

Fig. 4. NHMA MTLA469, right pelvis, detail of acetabulum.

Fig. 5. NHMA MTLA249, left metacarpal in posterior and proximal view.

Fig. 6. NHMA MTLA74, left tibia in posterior view

Fig. 7. PMMS103, right femur in anterior view (a) and comparison of the femoral head (MTLA73) with that of *Samotherium major* (MTLA255) (b).

Fig. 8. NHMA MTLA420, atlas in dorsal view

Figs. 1-2, scale-bar 5 cm (black); Figs. 3-8, scale-bar 10 cm (black & white).

PLATE 3